Robust Control Design for Vehicle Steer-by-Wire Systems

Submitted in total fulfilment of the requirements of the degree of Doctor of Philosophy

Zhe Sun

Faculty of Science, Engineering and Technology

Swinburne University of Technology

Melbourne, Australia

2017

Declaration

This is to certify that:

1. This thesis contains no material which has been accepted for the award to the candidate of any other degree or diploma, except where due reference is made in the text of the examinable outcome.

2. To the best of the candidate's knowledge, this thesis contains no material previously published or written by another person except where due reference is made in the text of the examinable outcome.

3. The work is based on the journal research and publications; the relative contributions of the respective authors are disclosed.

_____

Zhe Sun, 2017

Acknowledgements

At the moment when the thesis is to be accomplished and submitted, nearly four years have been spent during my PhD study. During this period, I have confronted a lot of troubles and difficulties. For instance, I must overcome the loneliness in an unfamiliar foreign country at the beginning of the PhD study. I must overcome getting bored when monotonously reading scientific papers one after another for the aim of finding innovative ideas and effective schemes to solve my problems in research. I must overcome the depression when a seemingly ideal methodology with perfect simulation results cannot lead to satisfactory experimental results. However, after I experience these hardships and try my best to solve them, I find that my abilities have been improved to a large extent in terms of stronger confidence, patience and persistence in dealing with difficulties for achieving my goals. I really want to thank this period of PhD study, not only because it offers me a Doctoral degree, but more importantly, it makes me to become a better person.

There are a lot of people to whom I would like to express my sincere appreciation. Firstly, I would like to thank my principal supervisor Dr. Jinchuan Zheng, and my co-supervisor Professor Zhihong Man. They both offer me vigorous support and insightful suggestions in the improvement of my research work during my PhD study. I get inspired a lot and benefit a lot from their high academic attainments. Especially, I would like to present my deep gratitude to my principal supervisor Dr. Zheng. Before I knew him, I had no ambition and confidence in PhD research. I was not so confident that I was capable of accomplishing the PhD study and obtaining the Doctoral degree abroad. However, Dr. Zheng encouraged me patiently and

promised that he would help me as much as he could. During my PhD study, whenever I come across difficulties beyond my own capability, I ask help from Dr. Zheng. And he always discusses about the problems with me, and guides me to find solutions to solve them. The difficulties are not only restricted to academic ones, but also contain the ones in life. Therefore, I think Dr. Zheng is not only a supervisor in my academic research, but also a mentor in my life.

I would like to express my sincere appreciation to other professors and lecturers in the Robotics and Mechatronics Laboratory, Professor Weixiang Shen, Professor Zhenwei Cao, Dr. Songhe Zhao and Dr. Jiong Jin, who give tremendous help and support to me not only in research, but also in tutoring. I also want to thank my predecessors, Hai Wang, Wenjie Ye, Fengxian He and Xiudong Cui. Especially Hai Wang, who is a professor now, helps me a lot in experiments and paper revision. I also would like to express my appreciation to my friends in Melbourne including Mingyue Jiang, Kai Zhu, Boda Ning, Ali Al-Ghanimi, Zhenzhen Chen, Mengqiu Tao, Lingkai Xing, Hong Du, Pengcheng Wang and Weiduo Zhang. I also want to specifically thank my flatmates Linxian Zhi and Lanjun Wei. I enjoy the time when having dinner and chatting together in the apartment we live in.

I also would like to thank Swinburne University of Technology for offering me the valuable opportunity of PhD study, the scholarship to alleviate my economic pressures, the comfortable environment and the advanced facilities.

Finally, I would like to express my heartfelt gratitude to my parents, who care me the most in the world. As the only child of you, I know that you must be anxious about my safety and life when I study abroad. However, you offered me your total understanding and support when I made the decision to start the

PhD study. During this period, you always keep in contact with me and offer me your suggestions to solve any problem I come across. The thesis would not be accomplished without your love and support.

Abstract

Steer-by-Wire (SbW) technology is an innovation for automobiles, whose idea is to utilize electromechanical actuators and electronic control devices to replace the conventional linkages in a vehicle steering system. In an SbW system, the steering column is removed and replaced by electromechanical actuators. A steering motor is utilized to generate steering torques for the steering system instead of the driver of a vehicle. And a feedback motor is utilized to provide feedback torques for the driver such that the driver can feel the interaction between the front wheels and road surface. The SbW technology possesses several remarkable advantages such as the elimination of injury to a driver under a front-end automobile collision due to the removal of the steering column and the reduction of weight, noises and vibrations owing to the replacement of conventional mechanical linkages and hydraulic systems. The outstanding merits of SbW systems motivate us to investigate the control design for SbW systems.

In this thesis, the background and research about SbW technologies and the contributions of the author are elaborated at first. Then, the dynamic model of a SbW system is identified as a second-order system from the steering motor input voltage to the front wheel steering angle. Specifically, the self-aligning torque and the tyre-road frictions are treated as external disturbances. Afterwards, an adaptive sliding mode (ASM) control method, an adaptive fast non-singular terminal sliding mode (AFNTSM) control method, a sliding mode-based active disturbance rejection control (SMADRC) method and an iterative learning control (ILC) method are proposed for the SbW system. The stability of the control systems under these

control schemes is verified in the sense of Lyapunov and Nyquist plot, respectively. Simulation and experimental results of these control schemes are obtained and analyzed. Finally, the thesis is concluded and several future works are elaborated.

The main contributions of this thesis are indicated in several aspects. First, a mathematical plant model is proposed to identify the dynamics of a vehicle SbW system, which is the basis of effective control design. Then, an ASM controller with an adaptive estimation law to estimate the self-aligning torque is designed for the SbW system. The ASM control can achieve high tracking accuracy due to the effective compensation of the self-aligning torque disturbance, and strong robustness against parametric uncertainties and varying road conditions due to the sliding mode. Based on that, an AFNTSM controller is designed to achieve faster convergence rate without weakening the merits of the ASM control. However, the proposed ASM and AFNTSM controllers both require an accurate plant model. To overcome this shortage, an SMADRC scheme is proposed for the SbW system, which not only possesses high tracking precision, strong robustness and fast convergence rate, but also is less dependent on the accuracy of plant models. Finally, an ILC methodology is proposed to testify the theoretically highest tracking accuracy of the SbW control system, which can be treated as a benchmark for other control designs.

The results of this thesis may contribute to the next generation of intelligent vehicles. With the development of modern transportation technologies, travel will become more and more convenient.

Contents

List of Figures

List of Tables

Chapter 1

Introduction

1.1 Steering technologies

A vehicle steering system is a set of devices utilized to change or maintain the direction of a vehicle during running or reversing. The function of vehicle steering systems is to control the running direction of vehicles according to drivers' command. The steering performance of a steering system is very significant for a vehicle's maneuverability and safety. Thus, the development of vehicle steering system has attracted a great deal of attention from the industry and academia about automobile manufacturing. The development of vehicle steering systems has experienced the following stages.

1. Conventional mechanical steering system

In a conventional mechanical steering system, drivers' physical strength is utilized as the steering energy, and all linkages in the system are mechanical [1]. Figure 1.1 shows the structure of a typical mechanical steering system using rack-and-pinion steering mechanisms. In this steering system, drivers maneuver the

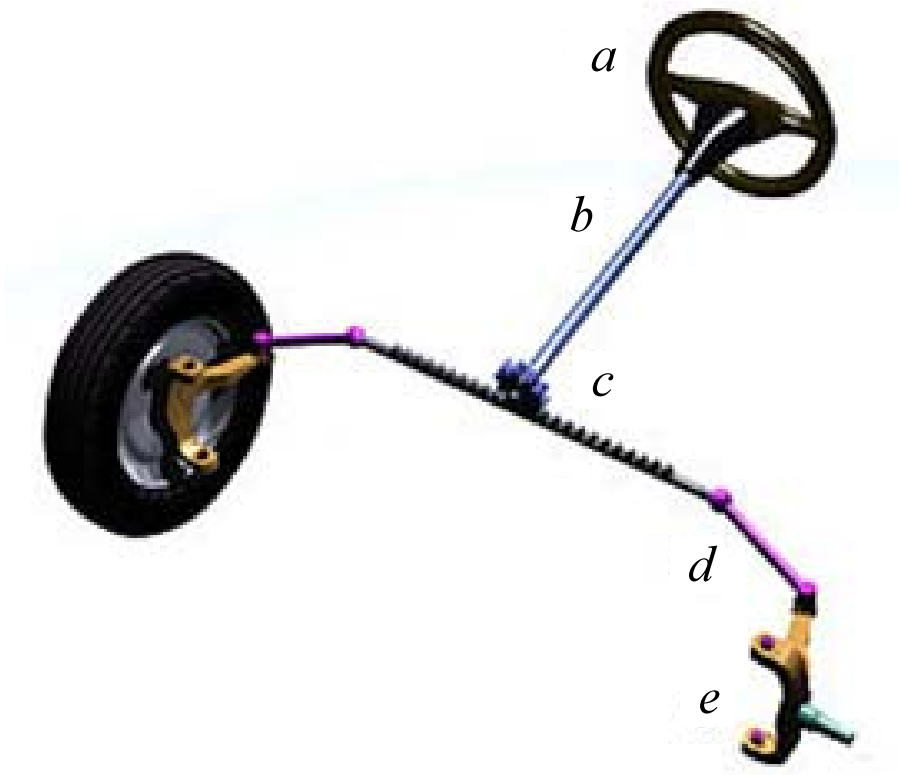

Figure 1.1: Structure of a conventional mechanical steering system. a. Steering wheel. b. Steering column. c. Rack-and-pinion d. Tie rod. e. Kingpin.

steering wheel and exert a steering torque to the steering wheel. Through the transfer of the steering column, the steering torque turns the pinion gear, and the pinion moves the rack which is a linear gear meshing with the pinion. Then, the linear motion of the rack applies steering torque to the kingpins of the steered wheels via tie rods and a short lever arm called the steering arm. Thus, the front wheels of a vehicle is then steered.

2. Hydraulic-power-assisted steering system

Compared with the conventional mechanical steering system, the hydraulic-power-assisted steering system can add controlled energy to the steering mechanisms such that drivers can provide less efforts to turn the steered wheels when driving at specific speeds [2]–[9]. The basic structure of a hydraulic-power-assisted

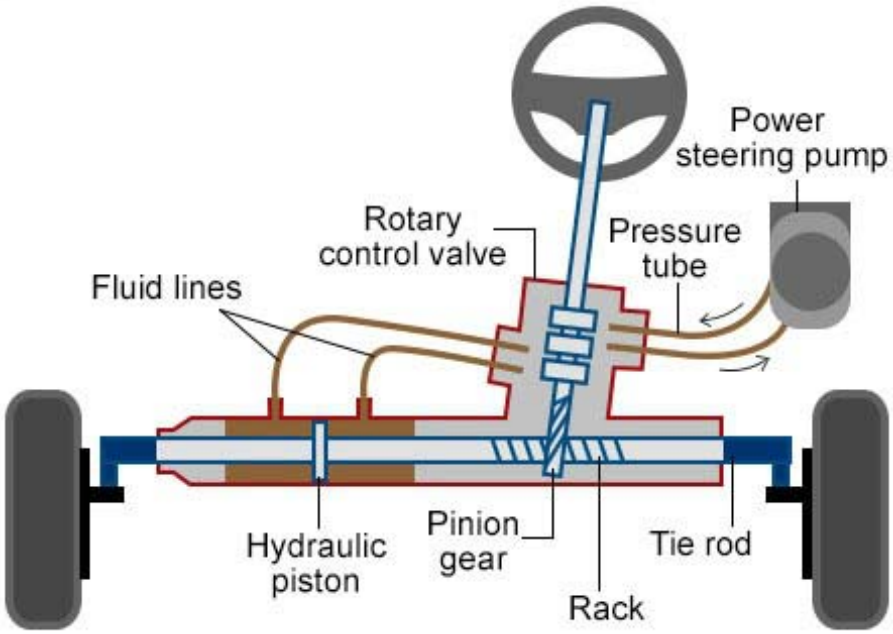

Figure 1.2: Structure of a hydraulic-power-assisted steering system.

steering system is shown in Figure 1.2. By utilizing a hydraulic system, a hydraulic-power-assisted steering system can multiply the steering torques acting on the front wheels. Usually, a power steering pump that is driven by the vehicle's engine is utilized to generate the hydraulic pressure. The rotary control valve is operated to control the fluid flows to the cylinder. The larger the steering torque acting on the steering wheel and the steering column, the more fluid is allowed to flow to the cylinder by the valve, which leads to a larger steering torque utilized to steer the front wheels.

3. Electric-power-assisted steering system

Electric-power-assisted steering is the third stage in the development of vehicle steering systems. The basic structure of an electric-power-assisted steering system is shown in Figure 1.3. In an electric-power-assisted steering system, sensors are utilized to detect the position and torque of the steering column, and an elec-

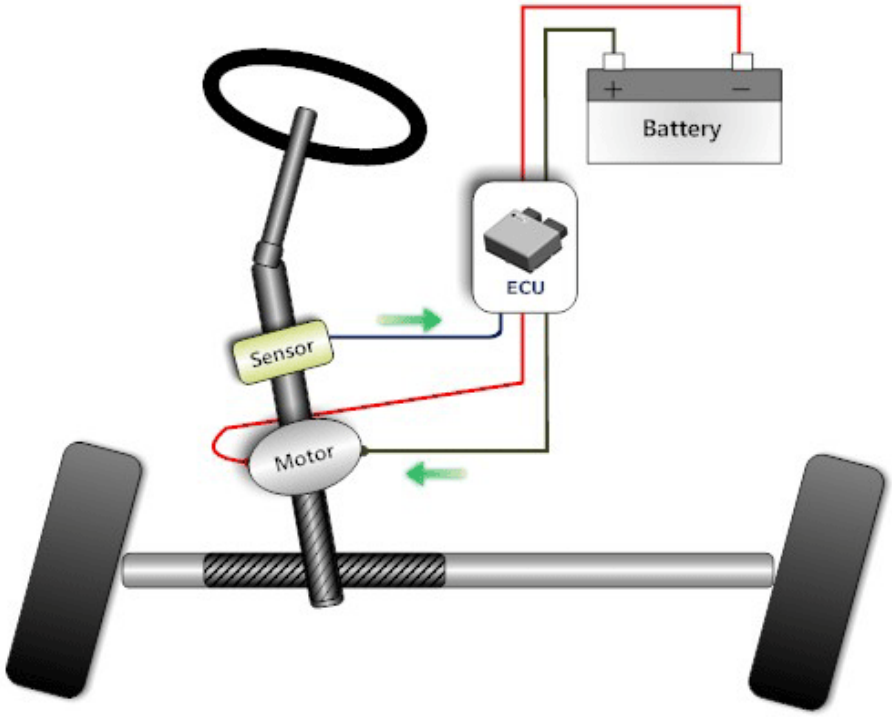

Figure 1.3: Structure of an electric-power-assisted steering system.

tric motor usually connected to the steering gear or steering column is utilized to generate assisting torque to assist the driver of a vehicle [10]–[14]. The electric-power-assisted steering system can allow varying amounts of assisting torque depending on different driving conditions. Usually, conventional mechanical linkages between the steering wheel and the pinion-and-rack system is retained in electric-power-assisted steering systems. If component failure or power failure leads to the disability of providing assistance, the mechanical linkages can serve as a back-up, and it requires heavier efforts provided by the driver of a vehicle to steer. Compared with hydraulic-power-assisted steering systems, the electric-power-assisted steering system has the advantages in less noises and less fuel consumptions due to the elimination of the constantly running hydraulic pumps despite whether assistance is required or not [15]–[19].

4. Steer-by-Wire system

As a newly developed technology, drive-by-wire technology has been playing a significant role in the automotive industry. The main idea of drive-by-wire is to use electromechanical actuators and electronic control systems to replace the conventional mechanical linkages [20]–[23]. Different components of a vehicle constitute different parts of the by-wire technology such as steer-by-wire (SbW) [24]–[30], brake-by-wire [31]–[35], shift-by-wire [36]–[38] and throttle-by-wire [39], [40] technologies. As one part of the drive-by-wire systems, SbW system is an innovative technology for automobile steering applications. The basic structure of an SbW system is shown in Figure 1.4. In an SbW system, the steering column is removed and replaced by electromechanical actuators. A steering motor is utilized to generate steering torques for the steering system instead of the driver of a vehicle. And a feedback motor is utilized to provide feedback torques for the driver such that the driver can feel the interactions between front wheels and road surface.

The SbW technology possesses several remarkable advantages. Firstly, the removal of the steering column can eliminate the injury to a driver when there is a front-end collision to a large extent. Secondly, in a SbW system, the traditional mechanical linkages and hydraulic systems between the steering wheel and front wheels are replaced by electromechanical actuators and human-machine interfaces, which not only reduce weight, noises, vibrations and energy consumptions, but also increase the freedom and capability for a driver to tune the steering command such that the stability and maneuverability of a vehicle are improved [41]. Finally, a feedback motor is typically coupled to the steering wheel and provides the driver with mimic haptic feedbacks of the interaction forces between front wheels and

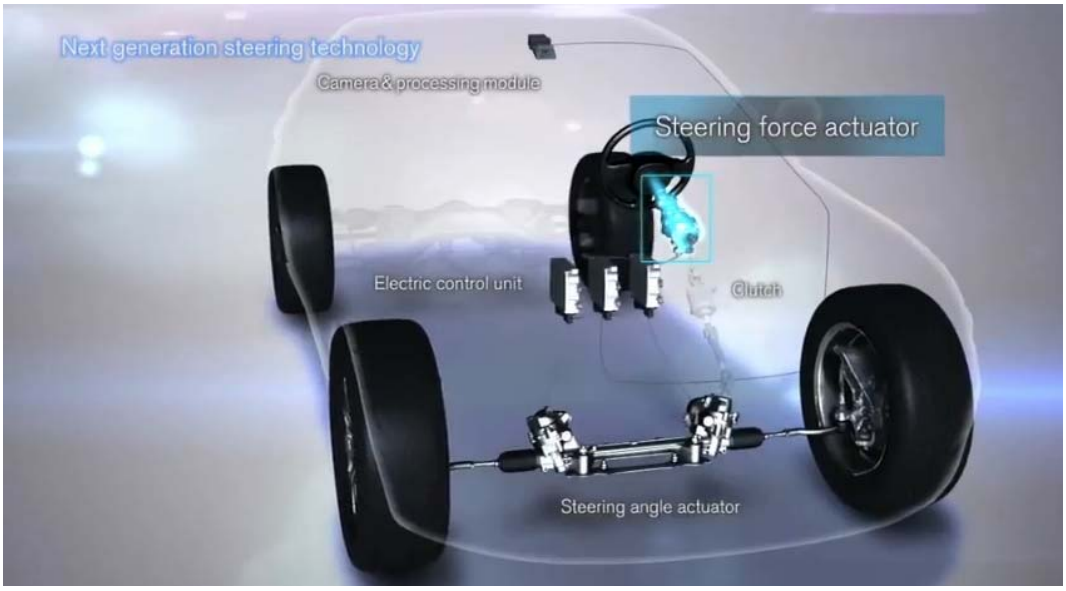

Figure 1.4: Structure of a steer-by-wire system.

road surface.

Since the SbW technique has so many prominent advantages, more and more researchers and engineers have focused on the research and development of the SbW system. Nissan has developed a fully electric steering system to replace the mechanical steering linkages of today's cars with a 'wired' steering column that uses driver's inputs to steer the front wheels via electronic controllers. A model-based estimation method which utilizes pneumatic trail information in steering torque to estimate tire slip angle is proposed by J. C. Gerdes, etc. [42]. The estimation method is validated on an experimental Steer-by-Wire research vehicle as shown in Figure 1.5.

1.2 Control technologies

In conventional vehicle steering systems, the steering torque is entirely generated by the driver. The front wheels are steered by the steering torque transfered

Figure 1.5: A Steer-by-Wire research vehicle [42].

through conventional mechanical linkages without electronic control systems. However, with the development of automobile industry, the proportion of electric-drive technologies has been increased significantly. In an electric-power-assisted steering (EPAS) or SbW system, a steering motor is utilized to generate auxiliary steering torque or entire steering torque to steer the pinion in the pinion-and-rack system. Thus, how to effectively control the steering motor to generate specific steering torque to steer front wheels plays a pivotal role in modern vehicle steering systems. A great deal of research has been carried out about the dynamic modeling and control of vehicle steering systems.

1.2.1 System modeling

For an EPAS equipped vehicle, the steering torque is detected by a torque sensor when a driver steers. Then, the measured torque is approximated as the torque that the driver applies to the steering wheel to determine the amount of

the assisting torque to be generated by the steering motor. The amount of assisting torque is calculated based on the speed of the vehicle and the steering torque applied to the steering wheel. The combination of this assisting torque and the driver's torque provides the total steering torque. Numerous studies have been carried out about the dynamic modeling of EPAS systems [43]–[45]. In [46], based on the relationship between the steering mechanism, the motor's electrical dynamics and the tire/road contact forces, two second-order differential equations are utilized to express the dynamics of an EPAS system.

In SbW systems, the conventional mechanical linkages between the steering wheel and the front wheels are removed and the whole system is operated by electric actuators. A lot of studies about the mechanical modeling of SbW systems have been carried out in recent years. In [47], a second-order mathematical model of SbW systems is shown and a force reflection bilateral control scheme using disturbance observer is outlined. Yih and Gerdes utilize a simple second-order model to represent the dynamics of SbW systems [48], where the tire forces acting on the steering system are treated as disturbances that restrict the steering motion away from the straight-ahead position. In both the front wheels side and the steering wheel side, two second-order differential equations are utilized to describe the effect of tire forces and the dynamics of the driver-interaction part [49]. Baviskar reports an adjustable steer-by-wire haptic-interface tracking controller for ground vehicles based on two simplified second-order models which describe the dynamics of the driver interface subsystem and the directional control subsystem [50], respectively. In [51], the dynamics of the Electro-Hydraulic steer-by-wire system for the articulated vehicle are composed of three different dynamic models, namely, the dynamic

model of the variable-displacement axial piston pump, the dynamic model of the pilot spool of the two-stage proportional electro-hydraulic valve and the dynamic model of the cylinder in the electro-hydraulic steer-by-wire system, which are described by three different second-order differential equations, respectively. The steer-by-wire system is comprised of the driver interface and the directional control assembly. The dynamics of the haptic interface is described by a second-order differential equation, and the motor shaft rotational dynamics are also expressed as a second-order model in [52]. Anwar and Chen also use a second-order equation to approximate the dynamics of the steering system [53].

1.2.2 Linear control

One of the most traditional and classical control techniques is the proportional-integral-derivative (PID) control, which offers the simplest and the most efficient solution to many real-world control problems [54]. The popularity of PID control has grown tremendously since the invention of the PID control methodology in 1990 and the Ziegler-Nichols' straightforward tuning methods in 1942. A behavior-based steering controller consists of a position controller and a kinematic constraint controller which are both PID controllers with their own PID gains is proposed by Lam, Qian and Xu to control the omnidirectional steering interface of a four-wheel independent steering vehicle [55].

H_∞ robust control is widely used in motor control because it can be effective to deal with tasks with parameter or load variations by finding linear control feedback laws that guarantee stability for almost all possible uncertainty variations or by using a modified algebraic Riccati equation to derive linear control laws for

stabilizing linear uncertain systems [56], [57]. In H_∞ control systems, the control problem is normally expressed as a mathematical optimization problem. The H_∞ controller is found to be the solution to the optimization problem, which possesses advantages over classical control techniques, such as strong robustness and high applicability to multivariate systems [58]–[67]. In [68], an H_∞ optimal control theory is utilized to minimize the worst-case gain of an unknown disturbance input and insulin injection for blood glucose regulation, which can correct the blood glucose deviation effectively by using clinically acceptable insulin delivery rates. In [69], Oritz et. al. presents a robust H_∞ controller for an experimental platform of an unmanned aerial vehicle quadrotor, which demonstrates satisfactory control performance compared with a conventional PID controller. In [70], a robust weighted gain-scheduling H_∞ control scheme is proposed for ground vehicles in terms of steer-by-wire and brake-by-wire systems, which is capable of dealing with the effects of steering system backlash-type hysteresis and the time-varying parameters.

1.2.3 Robust nonlinear control

As an important part of robust nonlinear control, sliding mode control is a powerful control methodology known as its high tracking accuracy and strong robustness in dealing with system parametric uncertainties [71]–[80]. In [81], a sliding mode-based control methodology with a novel sliding surface and a nonlinear disturbance observer is developed for systems with mismatched uncertainties, which can substantially alleviate the chattering problem and retain its nominal performance. In [82], a fast current-based maximum power point tracking strategy

employing sliding mode control is proposed to maximize the power produced by photovoltaic systems, which can lead to a very prompt tracking of the variations in the irradiance value and guarantee the rejection of the low-frequency voltage oscillations affecting the photovoltaic array. Since sliding mode control has the remarkable merit of strong robustness to handle the problems of parametric uncertainties existing in plant models, it is also implemented in vehicle SbW systems. In [83], Wang etc. utilized a nominal feedback controller to stabilize the nominal part of the plant model and augmented a sliding mode compensator to cope with the influence of both the unknown system dynamics and uncertain road conditions for a vehicle steering system. In [49], a sliding mode controller was designed based on the bounded information of uncertain system parameters, self-aligning torque and torque pulsation disturbances.

Adaptive control is a significant control strategy in motion control implementations due to its effectiveness in learning time-varying parameters or dynamics in a plant model [84]–[98]. In [99], an adaptive backstepping control methodology is proposed for hydraulic systems to cope with parametric uncertainties along with nonlinear friction compensation, which can guarantee asymptotic tracking performance in the presence of parametric uncertainties, and the robustness against unconsidered dynamics and external disturbances. In [100], Kim *et. al.* proposes an adaptive speed tracking control scheme for an uncertain surface-mounted permanent magnet synchronous motor without the need for the upper and lower bounds of the parameters of the permanent magnet synchronous motor, which can avoid the singularity problem and achieve good control performances.

Due to its outstanding advantages and effectiveness, adaptive control is also

widely used in vehicle steering control applications. In [101], an adaptive controller was reported which intervenes only when the front tire cornering stiffness undergoes a number of changes to realize the desired steering characteristics on a vehicle. In [102], an adaptive steering-control system for the SbW system was developed, which used an adaptive online estimation method to identify the dynamic parameters of the vehicle directional-control unit and the driver-interaction unit. In [103], an adaptive steering wheel haptic feedback control strategy is provided to increase the driver's knowledge of the roadway and driving conditions, which enables the driver to avoid obstacles presented in the roadway earlier than without any feedback.

It is also quite common for researchers to combine adaptive control with other control schemes to obtain more comprehensive advantages , such as adaptive fuzzy control [104], adaptive sliding mode control [105]–[109], adaptive robust H_∞ control [110], and adaptive neural network control [111]. In order to attain accurate positioning, Sencer etc. presented a robust adaptive sliding-mode control method to reject harmonic disturbances in servo systems [112]. The merits of combining adaptive control with conventional sliding mode control motivate us to present an adaptive sliding mode (ASM) control methodology for the SbW system, where the adaptive control is utilized to estimate the coefficient of the self-aligning torque acting on the steering system. Then, feedforward control inputs equivalent to the estimated self-aligning torques are generated to compensate for the effect of the self-aligning torques. Furthermore, a feedback controller based on sliding mode is adopted to cope with the system parametric uncertainties.

As a newly proposed control methodology, fast non-singular terminal sliding

mode (FNTSM) control has no switching elements in the control input, which implies that the control chattering commonly existing in conventional sliding mode control (SMC) and non-singular terminal sliding mode control (NTSMC) can be essentially avoided in the FNTSM control [113]. Furthermore, the fast-TSM-type model [114] contained in the FNTSM control law can guarantee the exponential stability of the control system, which leads to a faster convergence rate of the tracking error in comparison with the conventional SMC and NTSMC. In [115], Zheng *et al.* presented an FNTSM controller for a linear motor positioner, which can guarantee a much shorter convergence time of the tracking error in the presence of system uncertainties and external disturbances with an inherently continuous control input. Though adaptive control and FNTSM control both have remarkable benefits, the combination of them is still rare, especially in the implementation on vehicle SbW systems. Thus, it motivates us to combine adaptive control with the FNTSM control for the SbW system to integrate their merits. The adaptive estimation law in the AFNTSM controller can be utilized to estimate the self-aligning torque acting on front wheels. The estimated self-aligning torque can not only be provided to the steering wheel feedback motor to generate corresponding 'road feels' for the driver, but also be contributed to a feedforward control input to compensate for the effect of the self-aligning torque disturbance. The FNTSM control law in the AFNTSM controller can be used to guarantee a fast convergence rate of the tracking errors especially in the case of shock disturbance rejection, and the controller's robustness in dealing with system uncertainties, unmodeled dynamics and other external disturbances.

As an effective control methodology which has been widely used in numerous as-

pects in industry, active disturbance rejection control (ADRC) plays a pivotal role in nonlinear control, especially for the plant models with unknown or unmodeled disturbance dynamics. With ADRC, the unknown disturbances can be estimated and compensated actively, which enhances the robustness of the feedback control loop, and makes the controller less dependent on accurate mathematical models of the physical dynamics. In [116], L. Zhao *et al.* present an active disturbance rejection position control scheme for a magnetic rodless cylinder in servo systems without pressure states, from which both control precision and response speed are guaranteed. In [117], an active disturbance rejection control method is proposed for an accurate position tracking of an ionic polymer-metal composite actuator, which can substantially improve the control performance in the tracking of various reference motions including step, sinusoidal, trapezoidal and sawtooth wave profiles. In the SbW system control issue, the self-aligning torque is the main disturbance existing in the plant model. However, the self-aligning torque mathematical model we used is a simplified one on the basis of small slip angle assumption. In reality, the self-aligning torque model is much more complicated with respect to many factors such as vehicle speed and yaw rate. Hence, a control methodology that is less dependent on the accurate mathematical models of self-aligning torque and other frictions is necessary in our case, which motivates us to design an active disturbance rejection controller for our SbW system.

1.2.4 Intelligent control

Neural network control is one of the newest developed intelligent control methodologies, which is effective in control complex, nonlinear and uncertain sys-

tems [118]–[127]. In [128], an observer-based cooperative control is presented with the aid of graph tools, self-structuring neural networks, Lyapunov-based design method and separation principle for a group of nonlinear multiagent systems under a directed graph characterizing the interaction between the leader and the followers. The proposed control method verifies that each agent can follow the active leader only if the communication graph contains a spanning tree. In [129], Chen et. al. proposed an adaptive neural network consensus control method for a class of nonlinear multiagent systems with state time-delay and utilized the approximation property of radial basis function neural networks to neutralize the uncertain nonlinear dynamics in agents, which is able to guarantee the convergence on the basis of Lyapunov stability theory and achieve effective control performance.

Iterative learning control (ILC) is a newly developed intelligent control methodology, which was originally introduced by Arimoto [130]. ILC is essentially a feedforward control scheme which is able to overcome the drawbacks of feedback control algorithms by changing the control input iteratively from trial to trial. The objective of ILC is to utilize the repetitive nature of the process and the past control information to alter the shape of demand profile such that the high-precision motion tracking can be achieved. ILC has been successfully applied to many industrial areas, such as robot manipulators [131], computer numerical controller machine tools [132], chain conveyors [133], agricultural tractors [134] and antilock braking systems of hybrid electric vehicles [135]. However, the application of ILC to SbW systems is still rare, which accordingly motivates us to investigate the ILC technique for a SbW system under the condition that the reference command is periodic to achieve possible highest steering tracking accuracy.

1.3 Contribution of the thesis

In this thesis, the basic objective is to propose robust and effective control methodologies for vehicle SbW systems. For the vehicle SbW system, we require satisfactory control performance such that the actual front wheel steering angle can follow the reference command fast and accurately regardless of external disturbances like varying self-aligning torques caused by different road conditions. To achieve this objective, we identify a plant model to describe the dynamics of the vehicle SbW system including a simplified model to describe the main disturbance of the control system, i.e., the self-aligning torque. Then, we propose several controllers for the vehicle SbW system, including an adaptive sliding mode controller, an adaptive fast non-singular terminal sliding mode controller, a sliding mode-based active disturbance rejection controller and an iterative learning controller. These controllers all have their own advantages and drawbacks. The contributions of the thesis are listed as follows.

1. A mathematical plant model is proposed to identify the dynamics of the vehicle SbW system from the steering motor input voltage to the front wheel steering angle, in which the Coulomb frictions between vehicle front wheels and road surface and the self-aligning torques are treated as external disturbances of the control system. Specifically, the generation process and complete dynamic model of the self-aligning torque are described in detail. Considering the difficulty of control design and implementation , a simplified model of the self-aligning torque is proposed.

2. An adaptive sliding mode controller is designed for the vehicle SbW system.

In the proposed adaptive sliding mode control methodology, an adaptive estimation law is utilized to adaptively estimate the coefficient of the self-aligning torque such that a corresponding feedforward control component can be generated to compensate for the effect of the self-aligning torque disturbance to improve the tracking accuracy of the control system; the sliding mode control component is used to guarantee the controller's robustness against the parametric uncertainties existing in the plant model, unmodeled dynamics and normal frictions. Simulation and experimental results indicate that the designed adaptive sliding mode controller can be successfully implemented on the actual SbW system and achieve high tracking precision and strong robustness.

3. On the basis of the adaptive sliding mode control, we further design an adaptive fast non-singular terminal sliding mode controller for the vehicle SbW system. In the proposed adaptive fast non-singular terminal sliding mode control methodology, we utilize an adaptive estimation law to estimate the self-aligning torque acting on the steering system, and a fast non-singular terminal sliding mode control component to handle the parametric uncertainties and the unmodeled dynamics. Simulation and experimental results verify that the designed adaptive fast non-singular terminal sliding mode controller possesses high tracking accuracy due to the effective estimation and compensation of the self-aligning disturbance, strong robustness and fast convergence rate owing to the fast non-singular terminal sliding mode control component.

4. The designed adaptive sliding mode controller and the adaptive fast non-singular terminal sliding mode controller both have a high requirement for the accuracy of the dynamic model of the SbW system. However, the proposed plant

model may have a difference from the actual one, and may be lack of some unmodeled dynamics. Thus, it is very important for a designed controller to be less dependent on the accuracy of the plant model but still robust and effective. In order to achieve this objective, a sliding mode-based active disturbance rejection control methodology is proposed for the SbW system, in which a nonlinear extended state observer is utilized to estimate the states of the SbW system. The designed sliding mode-based active disturbance rejection controller is successfully implemented on the SbW experimental setup. Both simulation and experimental results evidently demonstrate that the designed sliding mode-based active disturbance rejection controller can achieve high tracking accuracy, strong robustness against parametric uncertainties and varying road conditions, fast convergence rate for tracking errors, and less dependency on the accuracy of the plant model.

5. The designed adaptive sliding mode controller, the adaptive fast non-singular terminal sliding mode controller and the sliding mode-based active disturbance rejection controller are all effective and possess their own advantages. However, the tracking precision of them still have room for improvement. Iterative learning control is a control methodology known as high tracking accuracy due to its iterative learning property. Thus, we propose an iterative learning controller for the SbW system and verify the stability of the control system by using Nyquist plots. Simulation results demonstrate that the designed iterative learning controller can achieve very high tracking accuracy after several iterations' learning. The experimental implementation of the iterative learning controller and how to overcome the restrictions of the periodic reference commands still need to be investigated.

1.4 Thesis organization

This thesis is organized as follows.

Chapter 2 introduces the basic structure of the SbW experimental platform. The mathematical dynamic model of the SbW system from the steering motor input voltage to the front wheel steering angle is identified, in which the self-aligning torque and the Coulomb frictions acting on the steering system are treated as main external disturbances of the SbW control system, and the generation of the self-aligning torque is elaborated in detail.

Chapter 3 introduces the design of an adaptive sliding mode controller. The stability of the control system is verified in the sense of Lyapunov. Simulation and experiments of the designed adaptive sliding mode controller are carried out, the simulation and experimental results are analyzed.

In Chapter 4, we design an adaptive fast non-singular terminal sliding mode controller for the vehicle SbW system. The stability of the control system is proved in the sense of Lyapunov. Both simulation and experiments of the proposed adaptive fast non-singular terminal sliding mode controller are carried out. Through the analysis of the simulation and experimental results, we conclude the advantages and disadvantages of the designed adaptive fast non-singular terminal sliding mode controller.

In Chapter 5, a sliding mode-based active disturbance rejection controller is designed for the vehicle SbW system. In the sense of Lyapunov, we verify the stability of the control system. Through the simulation and experiments of the sliding mode-based active disturbance rejection controller, we obtain and analyze the sim-

ulation and experimental results. The control performance and characteristics of the sliding mode-based active disturbance rejection controller are also concluded.

A novel iterative learning controller is designed for the vehicle SbW system in Chapter 6. The stability of the control system is verified by using Nyquist plot. Simulation of the presented iterative learning controller is carried out. The advantages and disadvantages of the iterative learning controller are analyzed through the simulation results.

Chapter 7 concludes the thesis and shows a few future works on the SbW systems.

Chapter 2

Modeling of Steer-by-Wire Systems

This chapter not only describes the main components of our experimental platform and the fundamental working principles of the SbW system, but also elaborates the mathematical model of the SbW system from the steering motor to front wheels and the model of the self-aligning torque acting on the steering system. This mathematical model will be used for the control design in the following chapters.

2.1 Experimental platform

Our experimental platform of a SbW system is shown in Figure 2.1. The conventional mechanical linkages between the steering wheel and the front wheels are removed and the whole system is operated by electric actuators. The main compo-

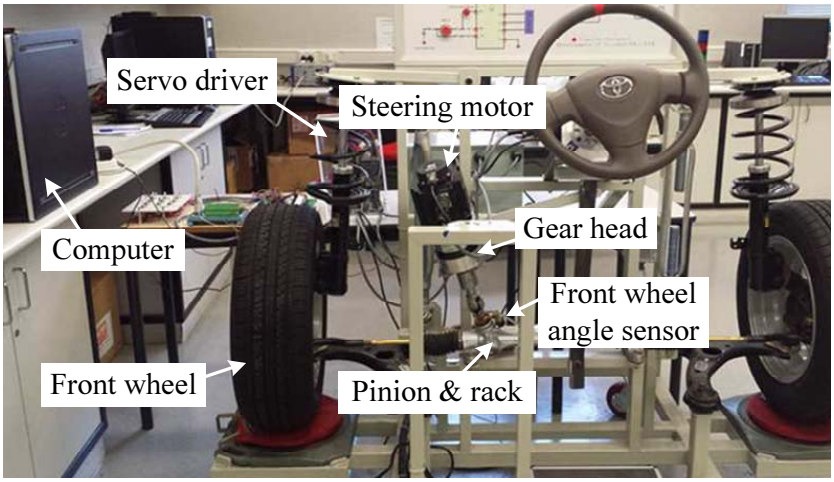

(a)

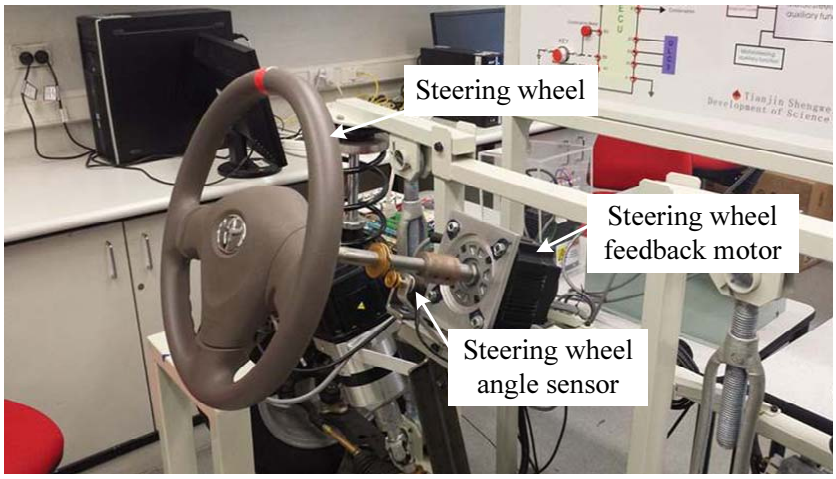

(b)

Figure 2.1: Experimental setup of a SbW system.

nents of the experimental platform are also shown by white arrow lines in Figure 2.1. The controller will be designed and implemented through MATLAB installed on a personal computer (PC). The steering motor is chosen as a Mitsubishi HF-SP102 AC motor and is connected with a gear head. The servo driver is selected as a Mitsubishi MR-J3100A servo driver. There is an angle sensor installed on the pinion, of which the type is 59006-10 turn, MoTec. The function of the angle sensor is to measure the front wheel steering angle indirectly [49].

Being provided with an input current by the servo driver, the steering motor

can generate a steering torque to the gear head. Because the steering motor is a three phases permanent magnet AC motor, whose power amplifier has a much higher bandwidth than that of the transmission mechanism on the SbW system, the steering torque generated by the steering motor can be simply treated as proportional to the input current provided by the servo driver. As the input current is linearly proportional to the input voltage, we can assume that the steering torque is linearly proportional to the input voltage. An advantech PCI 1716 multifunction card [49] is used for real-time A/D, D/A converter. The Euler method is adopted for the discretization of the controller.

2.2 Modeling of the steer-by-wire system and disturbances

In this section, we first elaborate the SbW system dynamics from the steering motor input voltage to the front wheel steering angle in detail. Then we expound the model of the self-aligning torque acting on the steering system of the vehicle which is turning on the ground.

2.2.1 Steer-by-wire system dynamics

The mechanical structure of the SbW system [49] is shown in Figure 2.2, where we can see that the SbW system can be divided into two separate blocks: the steering wheel block and the front wheel block. The steering wheel block consists of a steering wheel, a steering wheel angle sensor, and a steering wheel feedback motor. The front wheel block is made up of an assembly of a steering motor and a gear head, a pinion angle sensor, a rack and pinion gearbox, and two front wheels.

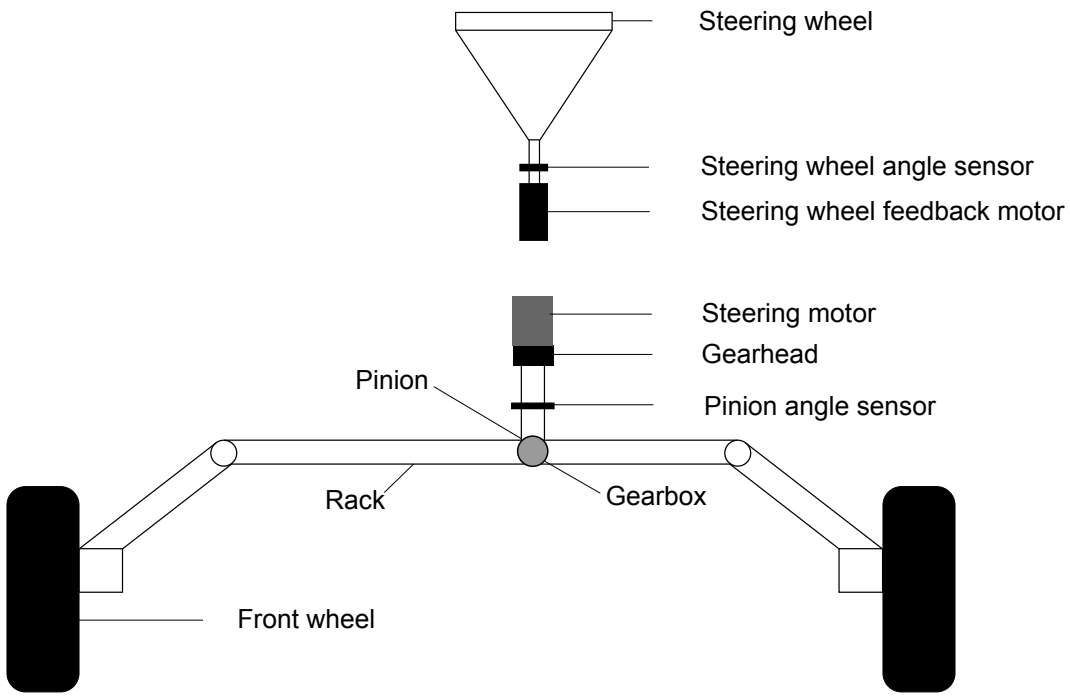

Figure 2.2: The structure of the SbW system.

The function of the steering wheel feedback motor is to provide a feedback torque to the driver such that the driver can have the feeling of the interactions between the front wheels and the various road surfaces during driving. On the other hand, the steering motor produces a steering torque to steer the front wheels through the gear head, the rack and pinion gearbox, and the steering arm, thus ensuring the steering of the front wheels can track the rotation of the steering wheel closely. In this research, our interest is focused on the modeling and control of the front wheel steering motor, and thus control of the steering wheel block is omitted for simplicity.

In what follows, we shall derive the SbW system model defined from the steering motor input voltage to the front wheel angle. The description of the SbW model parameters are listed in Table 2.1. For simplicity, we can neglect the backlash between the gear teeth of the steering motor shaft and the gear head. Meanwhile,

Table 2.1: Description of SbW system model parameters

Symbols	**Description**
J_{mg}	Moment of inertia of the whole assembly composed of the steering motor and the gear head
J_{fw}	Moment of inertia of front wheels
c_{mg}	Moment of viscous frictions of the whole assembly composed of the steering motor and the gear head
c_{fw}	Moment of viscous frictions of front wheels
δ_g, δ_{fw}	Rotational angle of the gear head shaft and steering angle of front wheels
τ_{sm}/τ_g	Torques generated by the steering motor/the gear head
τ	Self-aligning torque
τ_{cf}	Torque of Coulomb friction in SbW system
τ_{gtf}	Torque applied on the steering arm by the steering motor through the gear head and the rack and pinion gearbox
τ_{ftg}	Torque exerted on the shaft of the gear head by the front wheels
u	Steering motor input voltage
b_1	Gear ratio of the rack and pinion system
b_2	Scale factor to account for the transition from the linear motion of the rack to the steering of front wheels
b_3	Gear ratio of the gear head
b_4	Scale factor accounting for the conversion from the steering motor input voltage to the steering motor output torque

the steering motor and the gear head are considered as one unit. Then the dynamic equation of the assembly can be described by the following second-order differential equation [49], [136]:

$$J_{mg}\ddot{\delta}_g + c_{mg}\dot{\delta}_g + \tau_{ftg} = \tau_g. \tag{2.1}$$

In addition, we can use the following second-order differential equation to describe the rotation of the steered front wheels about their vertical axes crossing the wheel centers [48], [49], [137]:

$$J_{fw}\ddot{\delta}_{fw} + c_{fw}\dot{\delta}_{fw} + \tau_{cf} + \tau = \tau_{gtf} \tag{2.2}$$

where τ_{cf} is the Coulomb friction. The definition of τ_{cf} is given by

$$\tau_{cf} = \rho \text{sign}(\dot{\delta}_{fw}) \tag{2.3}$$

with ρ indicating the Coulomb friction constant, and sign( ) denoting the standard signum function.

Assuming that the backlash between the rack and pinion gear teeth is negligible, we have the following relationship:

$$\frac{\ddot{\delta}_{fw}}{\ddot{\delta}_g} = \frac{\dot{\delta}_{fw}}{\dot{\delta}_g} = \frac{\delta_{fw}}{\delta_g} = \frac{1}{b_1 b_2} = \frac{\tau_{ftg}}{\tau_{gtf}}. \tag{2.4}$$

From (2.4), we obtain

$$\tau_{gtf} = b_1 b_2 \tau_{ftg} \tag{2.5}$$

and

$$\begin{aligned} \ddot{\delta}_g &= b_1 b_2 \ddot{\delta}_{fw} \\ \dot{\delta}_g &= b_1 b_2 \dot{\delta}_{fw}. \end{aligned} \tag{2.6}$$

Substituting (2.1), (2.3), (2.5) into (2.2), we have

$$\begin{aligned} &J_{fw}\ddot{\delta}_{fw} + c_{fw}\dot{\delta}_{fw} + \rho \text{sign}(\dot{\delta}_{fw}) + \tau \\ &= b_1 b_2 (\tau_g - J_{mg}\ddot{\delta}_g - c_{mg}\dot{\delta}_g). \end{aligned} \tag{2.7}$$

Substituting (2.6) into (2.7) leads to

$$\begin{aligned} &J_{fw}\ddot{\delta}_{fw} + c_{fw}\dot{\delta}_{fw} + \rho \text{sign}(\dot{\delta}_{fw}) + \tau \\ &= b_1 b_2 (\tau_g - J_{mg} b_1 b_2 \ddot{\delta}_{fw} - c_{mg} b_1 b_2 \dot{\delta}_{fw}). \end{aligned} \tag{2.8}$$

Re-arranging (2.8), we obtain

$$J\ddot{\delta}_{fw} + c\dot{\delta}_{fw} + \rho \text{sign}(\dot{\delta}_{fw}) + \tau = \tau_{equ} \tag{2.9}$$

where

$$\begin{aligned} J &= J_{fw} + (b_1 b_2)^2 J_{mg} \\ c &= c_{fw} + (b_1 b_2)^2 c_{mg} \\ \tau_{equ} &= b_1 b_2 \tau_{mg} \\ \tau_{mg} &= b_3 \tau_{sm}. \end{aligned} \tag{2.10}$$

In our experiment setup [49], the steering motor is a three phase permanent magnet AC motor, whose power amplifier has a much higher bandwidth than that of the transmission mechanism on the SbW system. Thus, we simply use a scaling factor b_4 to approximate the model from the steering motor input voltage to the

steering motor output torque. That is,

$$\tau_{sm} = b_4 u \tag{2.11}$$

where u indicates the steering motor input voltage. The control-oriented plant model from the steering motor input voltage u to the steering angle of front wheels δ_{fw} can be rewritten as:

$$J\ddot{\delta}_{fw} + c\dot{\delta}_{fw} + \rho \text{sign}(\dot{\delta}_{fw}) + \tau = b_1 b_2 b_3 b_4 u \tag{2.12}$$

where u is the control input to be designed. For simplicity, we use parameter b to represent the product of b_1, b_2, b_3 and b_4, namely, $b = b_1 b_2 b_3 b_4$. Then, we can rewrite (2.12) into

$$J\ddot{\delta}_{fw} + c\dot{\delta}_{fw} + \rho \text{sign}(\dot{\delta}_{fw}) + \tau = bu \tag{2.13}$$

Now, we can see that the self-aligning torque τ has a great influence on the steering accuracy. Thus, the model of τ will be discussed next.

2.2.2 Friction and self-aligning torque

When a driver is driving a vehicle over the road, the influence of tire forces exerted on the whole steering system is non-ignorable. As a matter of fact, when the front wheels of a moving vehicle are being steered, the forces acting on the steering system will tend to resist this kind of motion which deviates from the right ahead position. These forces can be treated as external disturbances imposed on the steering system which are essentially the main contributions to the self-aligning torque τ. The self-aligning torque is usually expressed as an equation

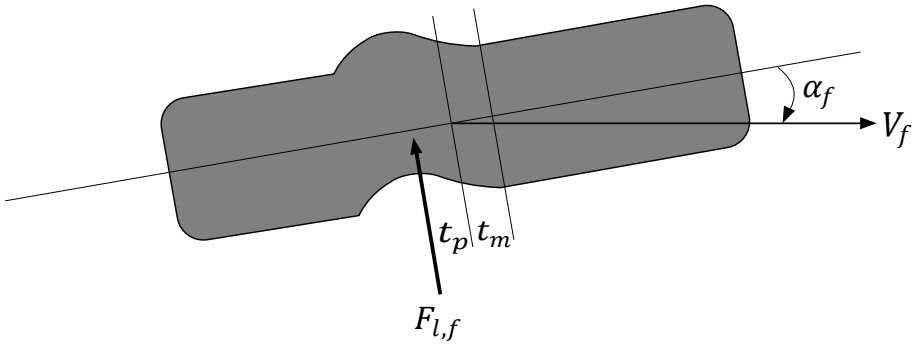

Figure 2.3: Generation of self-aligning torque [48].

about steering geometry, especially about the kingpin angles and how the tires deform to generate lateral forces. In Figure 2.3 [48], $F_{l,f}$ is the lateral force exerted on the tire; α_f is the tire slip angle; V_f is the velocity of the tire at the point of the center of the area where the tire touches the ground; t_p is the pneumatic trail, namely, the distance between the position where the lateral force acting on the tire and the center of the area where the tire touches the ground; t_m is the mechanical trail, which means the distance between the center of the area where the tire touches the ground and the point of intersection of the tire's steering axis and the ground as shown in Figure 2.4. From Figure 2.4, it is also seen that the turning of the vehicle is implemented through the steering of the tire along an inclined axis. The reason why the axis is not vertical to the ground can be attributed to the existence of the caster angle. The total self-aligning torque can be obtained as follows:

$$\tau = (t_p + t_m)F_{l,f}(\alpha_f). \tag{2.14}$$

At a small slip angle, the lateral force is linearly related to the tire slip angle α_f as shown in Figure 2.4 and can be modeled as follows:

$$F_{l,f} = -C_f \cdot \alpha_f \tag{2.15}$$

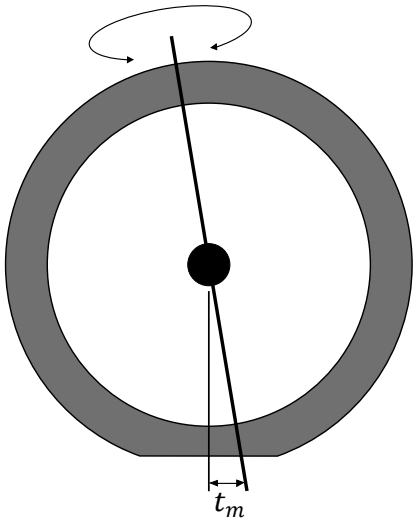

Figure 2.4: Mechanical trail [48].

where C_f is the front tire cornering stiffness coefficient, a parameter closely related to the tire-road friction. Assuming that the vehicle body slip angle is close to zero as shown in Figure 2.5, we can approximate the front-wheel sideslip angle α_f as follows [11], [12]:

$$\alpha_f \approx \beta + \frac{\gamma \cdot d_f}{V_{CG}} - \delta_f. \tag{2.16}$$

Thus, the front tire lateral force $F_{l,f}$ and the self-aligning torque τ can be expressed as:

$$\begin{aligned} F_{l,f} &= -C_f \cdot \big(\beta + \frac{\gamma \cdot d_f}{V_{CG}} - \delta_f\big), \\ \tau &= -C_f(l_p + l_m)\big(\beta + \frac{\gamma \cdot d_f}{V_{CG}} - \delta_f\big). \end{aligned} \tag{2.17}$$

The steering angle of the steered front wheel δ_f and the yaw rate γ are measured by using the pinion angle sensor and the yaw rate sensor, respectively. The vehicle body slip angle β can be estimated from the bicycle model of the road vehicle as [1], [12]:

$$\beta = \tan^{-1}\big(\frac{d_r \tan\delta_f}{d_r + d_f}\big). \tag{2.18}$$

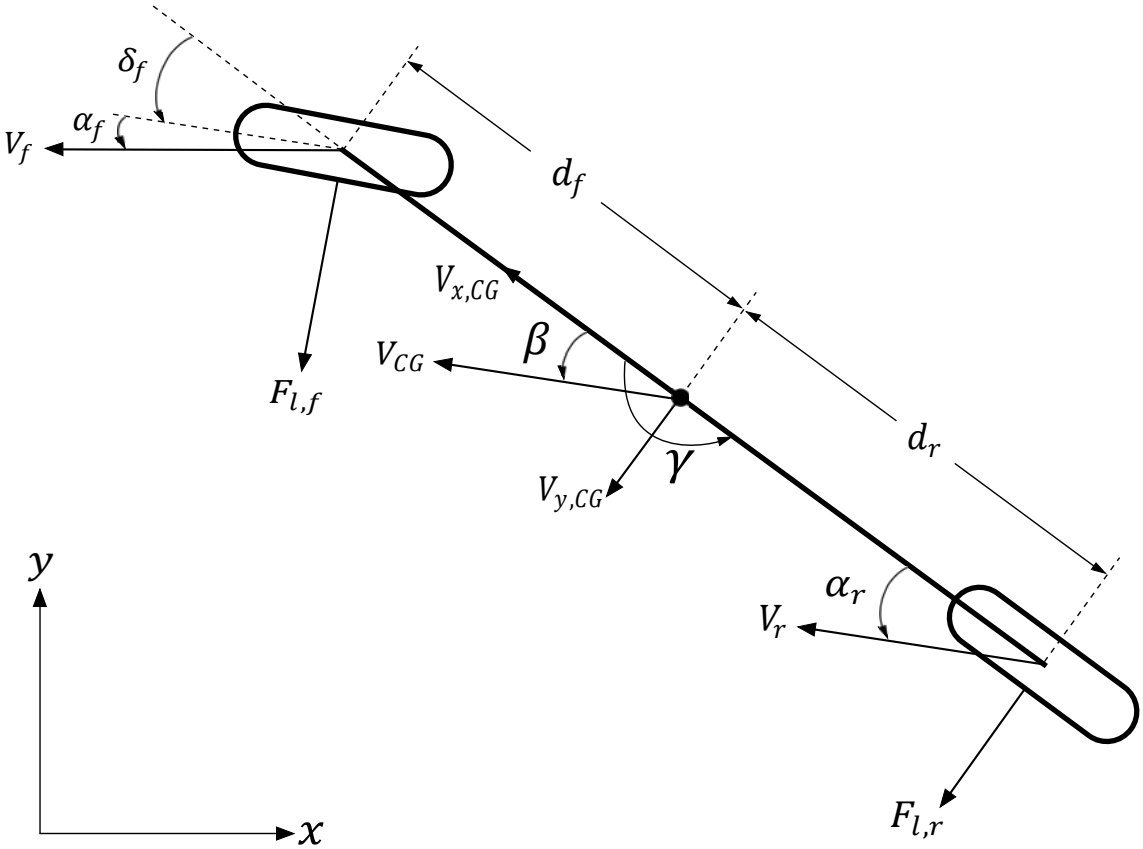

Figure 2.5: Bicycle model of vehicle in which β is the sideslip angle at the center of gravity (CG), γ is the yaw rate at CG, V_{CG} is the velocity of the vehicle at CG, $V_{x,CG}$ and $V_{y,CG}$ are the longitudinal and lateral components of V_{CG}, δ_f is the steering angle of the front wheel in this bicycle model, $F_{l,f}$ and $F_{l,r}$ are the lateral tire forces of the front wheel and the rear wheel, respectively, α_f and α_r are the tire slip angle front and rear, d_f and d_r are the distances of the front and rear wheel axles from CG [48].

Therefore, the final equation of the self-aligning torque τ can be expressed as:

$$\tau = -C_f(d_r + d_f)\big[\tan^{-1}\big(\frac{d_r \tan\delta_f}{d_r + d_f}\big) + \frac{\gamma \cdot d_f}{V_{CG}} - \delta_f\big]. \tag{2.19}$$

In our SbW experimental platform, the tires have no contact with the ground due to experimental equipment limitation. Hence, during the experiments, the tires are not exerted by real self-aligning torque. However, we can utilize a hyperbolic tangent signal to mimic the self-aligning torque imposed on the steering system:

$$\tau = \xi \cdot \tanh(\delta_{fw}) \tag{2.20}$$

where ξ is a scaling constant. Different values of ξ can represent different amount of self-aligning torque generated under various road conditions.

As aforementioned, the steering motor is a three phases permanent magnet AC motor, whose power amplifier has a much higher bandwidth than that of the transmission mechanism on the SbW system. Thus, we can use the scaling factor b_4 to approximate the model from the steering motor input voltage to the steering motor output torque as shown in (2.11). Consequently, we artificially generate the following voltage signal:

$$u_{sel} = \frac{\tau}{b} + n_s = \frac{\xi}{b} \cdot \tanh(\delta_{fw}) + n_s \tag{2.21}$$

which is injected to the steering motor to produce a mimic self-aligning torque physically acting on the SbW system. Note that n_s is added here as white noise signals to account for the unmodeled dynamics of the self-aligning torque.

2.3 Plant model and system uncertainties

For simplicity, we utilize parameter x to represent δ_{fw}. Thus, the plant model can be written as

$$\begin{aligned} J\ddot{x} + c\dot{x} &= bu - \rho \text{sign}(\dot{x}) - \tau \\ \tau &= \xi \tanh(x) \end{aligned} \tag{2.22}$$

where x is the system output, namely, the steering angle of the front wheels, u is the control input of the steering motor; J and c are the equivalent moment of inertia and the equivalent viscous friction of the steering system, respectively; ρ is the Coulomb friction constant and sign( ) denotes the standard signum function;

τ denotes the self-aligning torque exerted on the front wheels, in which ξ is the coefficient of the self-aligning torque with respect to road conditions and tanh() is the hyperbolic tangent function; b is the scaling factor which is the product of four components, namely, the scale factor accounting for the conversion from the steering motor input voltage to the steering motor output torques, the gear ratio of the gear head, the gear ratio of the pinion-and-rack system, and the transmission gain from the linear motion of the rack to the steering angle of front wheels. The value of the scale factor b is given by

$$b = 273.5 \text{ Nm/V}. \tag{2.23}$$

The value of b is regarded as a constant as it is slightly varying in our experimental setup. Nevertheless, for the other parameters, we consider the parametric uncertainties with the bounds as follows:

$$\begin{aligned} \frac{1}{h} \leq & \frac{J}{J_0} \leq h \quad (J_0 = 85.5 \text{ kgm}^2,\ h = 1.6) \\ |\Delta_J| = & |J - J_0| \leq \bar{\Delta}_J = |(h-1)J_0| = 51.3 \text{ kgm}^2 \\ |\Delta_c| = & |c - c_0| \leq \bar{\Delta}_c \quad (c_0 = 218.8 \text{ Nms/rad},\ \bar{\Delta}_c = 22 \text{ Nms/rad}) \\ |\Delta_\rho| = & |\rho - \rho_0| \leq \bar{\Delta}_\rho \quad (\rho_0 = 42.5 \text{ Nm},\ \bar{\Delta}_\rho = 4.5 \text{ Nm}) \end{aligned} \tag{2.24}$$

where J_0, c_0 and ρ_0 are the nominal parameters in the plant model; Δ_c and Δ_ρ represent the parametric uncertainties; $\bar{\Delta}_c$ and $\bar{\Delta}_\rho$ denote the upper bounds of the corresponding uncertainties; and h is the so-called gain margin of the control system [138]. The values in (2.23) and (2.24) are identified based on physical parameters in our experimental setup. Our control objective in this thesis is to

develop control schemes to achieve decent control performance in the presence of these uncertainties.

2.4 Summary

In this chapter, a dynamic model of SbW systems is given. The SbW system is modeled as a second-order system from the steering motor input voltage to the front-wheel steering angle. In the plant model, the self-aligning torque and friction arising from the tire-to-ground contact are regarded as external disturbance acting on the SbW system. Specifically, we utilize a hyperbolic tangent signal to mimic the self-aligning torque imposed on the steering system, in which different values of the coefficient of the self-aligning torque represents different road conditions. Thus, with a specific plant model of SbW systems, advanced control methodologies can be proposed for the SbW system of our experimental setup. In the following chapters, we will present several robust and innovative control schemes with different characteristics for our SbW system. The merits and shortages of these control methods will also be compared and analyzed based on simulation and experimental results.

Chapter 3

Adaptive Sliding Mode Control

In Chapter 2, the plant model of the SbW system has been identified with a simplified dynamic model of the self-aligning torque acting on the front wheels. Thus, how to design an appropriate and effective control scheme to control the SbW system becomes a pivotal objective. In this chapter, we combine the conventional sliding mode control with an adaptive estimation law and design an adaptive sliding mode (ASM) controller for vehicle SbW systems such that the conventional sliding mode control component can be utilized to cope with the existing parametric uncertainties and unmodeled dynamics, and the adaptive estimation law can be used to accurately estimate the self-aligning torque to improve the control precision. The stability of the control system is verified in the sense of Lyapunov. Experimental results of the ASM control are also shown and analyzed.

3.1 Introduction

Adaptive control is another control method which plays an important role in the area of motion control owing to its effectiveness to deal with time-varying

parameters in a plant model. In [139], with the investigation of simultaneous adaptive positioning and vibration control of a flexible active composite manipulator with two piezoelectric patches and an active strut, an adaptive fuzzy logic control strategy and an independent modal space adaptive control scheme are proposed for the active strut motion control and for the manipulator vibration control, respectively. In [140], M. Hojati *et al.* present a combined direct and indirect adaptive control scheme for adjusting an adaptive fuzzy controllers, and an adaptive fuzzy identification model parameters. And the performance analysis using a Lyapunov synthesis approach proves the superiority of the proposed control scheme in terms of faster and improved tracking and parameter convergence.

It is also quite common for researchers to combine adaptive control with sliding mode control to obtain more comprehensive advantages. In [141], a nonlinear control approach based on adaptive sliding-mode control is employed to tackle the problem of engine torque control during regenerative mode, which incorporates the approximately known inverse dynamic model output of the engine as a model-base component of the controller, and an estimated uncertainty term to compensate for the unmodeled dynamics, external disturbances and time-varying system parameters. In [142], an adaptive sliding-mode control scheme is proposed for piezoelectric actuators with nonlinear uncertainties, in which the sliding-mode part is used to reject dominant uncertainties, and the adaptive component is continuously refined based on prevailing input and output signals only.

In this chapter, we will present an ASM control methodology for the SbW experimental setup, where the adaptive control will be utilized to estimate the coefficient of the self-aligning torque acting on the steering system. Then, feedforward con-

trol inputs equivalent to the estimated self-aligning torques will be generated to compensate for the effect of the self-aligning torques. Furthermore, a feedback controller based on sliding mode will be adopted to cope with the system parametric uncertainties.

3.2 Control design

In this section, an ASM control law is proposed, and the stability of the control system is proved in the sense of Lyapunov. The estimation of the coefficient of self-aligning torques is elaborated in detail. Based on experimental application, the guidelines of the selection of control parameters are also described.

3.2.1 Adaptive sliding mode control law

Considering the SbW plant model in (2.13) and (2.20), define the tracking error e as

$$e = x_r - x \tag{3.1}$$

where x_r is the reference command for the front wheel steering angle to track, which is usually twice differentiable due to the curve of roads. Furthermore, a linear sliding variable s is defined as

$$s = \dot{e} + \lambda e \tag{3.2}$$

where $\lambda > 0$ is to be designed.

Solving the sliding mode dynamics as given by

$$\dot{s} = \lambda\dot{e} + (\ddot{x}_r - \ddot{x}) = 0 \tag{3.3}$$

and neglecting the parametric uncertainties and the self-aligning torque, namely, utilizing the nominal parameters to replace the actual ones in (2.13) and supposing $\tau = 0$, we obtain an expression of u_0 which is also called the equivalent control input [138] as follows

$$u_0 = \frac{1}{b}[J_0\lambda\dot{e} + J_0\ddot{x}_r + c_0\dot{x} + \rho_0\text{sign}(\dot{x})]. \tag{3.4}$$

In order to guarantee the robustness of the controller against the parametric uncertainties and the Coulomb friction, a reaching control input u_1 [115] is introduced as

$$u_1 = \frac{1}{b}[\varpi s + K\text{sign}(s)] \tag{3.5}$$

where $\varpi > 0$ is to be designed, and K is given by

$$K = \bar{\Delta}_J\lambda|\dot{e}| + \bar{\Delta}_J|\ddot{x}_r| + \bar{\Delta}_c|\dot{x}| + \bar{\Delta}_\rho \tag{3.6}$$

where $\bar{\Delta}_J$, $\bar{\Delta}_c$ and $\bar{\Delta}_\rho$ are defined in (2.24).

Lastly, a control input u_2 is proposed to exclusively compensate for the self-aligning torque acting on the SbW system:

$$u_2 = \frac{\hat{\xi}}{b}\tanh(x) \tag{3.7}$$

where $\hat{\xi}$ denotes the estimation of the actual coefficient ξ, whose adaptation law is

given by

$$\dot{\hat{\xi}} = \mu s \tanh(x) \tag{3.8}$$

with $\mu > 0$ denotes the adaptation gain [143] to be designed and s the sliding variable as defined in (3.2). The design of μ will be detailed in the next subsection.

Lemma 3.1: Consider the SbW system (2.13) with the parametric uncertainties (2.24) and under the ASM control law

$$u = \ u_0 + u_1 + u_2 \tag{3.9}$$

with u_0 defined in (3.4), u_1 in (3.5) and u_2 in (3.7), respectively. Then, the tracking error (3.1) of the SbW closed-loop system can asymptotically converge to zero for a given steering wheel reference command.

Proof: Choose the Lyapunov function as

$$V = \frac{1}{2}s^2 + \frac{1}{2\mu J}(\xi - \hat{\xi})^2. \tag{3.10}$$

Evaluating the first-order derivative of V along the system trajectories yields

$$\dot{V} = s\dot{s} + \frac{1}{\mu J}(\xi - \hat{\xi})(\dot{\xi} - \dot{\hat{\xi}}). \tag{3.11}$$

We assume that $\dot{\xi} = 0$ because the switching between different road conditions generally happens in an instant due to the relatively high speed and short length

of a vehicle. Therefore, we have

$$\begin{aligned}\dot{V} =& s\dot{s} + \frac{1}{\mu J}(\xi - \hat{\xi})(-\dot{\hat{\xi}}) \\ =& s\dot{s} - \frac{1}{J}(\xi - \hat{\xi})s\tanh(x) \\ =& s(\lambda\dot{e} + \ddot{x}_r - \ddot{x}) - \frac{1}{J}(\xi - \hat{\xi})s\tanh(x) \\ =& s\big[\lambda\dot{e} + \ddot{x}_r + \frac{c}{J}\dot{x} + \frac{\rho}{J}\text{sign}(\dot{x}) + \frac{\xi}{J}\tanh(x) \\ & - \frac{bu}{J}\big] - \frac{1}{J}(\xi - \hat{\xi})s\tanh(x).\end{aligned} \tag{3.12}$$

Substituting the control input (3.9) into (3.12) yields

$$\begin{aligned}\dot{V} =& s\big\{\lambda\dot{e} + \ddot{x}_r + \frac{c}{J}\dot{x} + \frac{\rho}{J}\text{sign}(\dot{x}) + \frac{\xi}{J}\tanh(x) \\ & - \frac{b}{J}\frac{1}{b}\big[J_0\lambda\dot{e} + J_0\ddot{x}_r + c_0\dot{x} \\ & + \rho_0\text{sign}(\dot{x}) + \varpi s + \hat{\xi}\tanh(x) \\ & + K\text{sign}(s)\big]\big\} - \frac{1}{J}(\xi - \hat{\xi})s\tanh(x) \\ =& s\big[\frac{\Delta_J}{J}\lambda\dot{e} + \frac{\Delta_J}{J}\ddot{x}_r + \frac{\Delta_c}{J}\dot{x} \\ & + \frac{\Delta_\rho}{J}\text{sign}(\dot{x}) - \frac{K}{J}\text{sign}(s) - \frac{\varpi}{J}s\big] \\ =& -\frac{\varpi}{J}s^2 + \frac{K_m s - K|s|}{J}\end{aligned} \tag{3.13}$$

with

$$K_m = \Delta_J\lambda\dot{e} + \Delta_J\ddot{x}_r + \Delta_c\dot{x} + \Delta_\rho\text{sign}(\dot{x}). \tag{3.14}$$

According to the following inequalities

$$\begin{aligned} \Delta_J \lambda \dot{e} s &\leq \bar{\Delta}_J \lambda |\dot{e}||s| \\ \Delta_J \ddot{x}_r s &\leq \bar{\Delta}_J |\ddot{x}_r||s| \\ \Delta_c \dot{x} s &\leq \bar{\Delta}_c |\dot{x}||s| \\ \Delta_\rho \text{sign}(\dot{x}) s &\leq \bar{\Delta}_\rho |s| \end{aligned} \tag{3.15}$$

where $\bar{\Delta}_J$, $\bar{\Delta}_c$ and $\bar{\Delta}_\rho$ are the upper bounds of the parametric uncertainties Δ_J, Δ_c and $\Delta\rho$ as defined in (2.24), we have

$$\begin{aligned} & \Delta_J \lambda \dot{e} s + \Delta_J \ddot{x}_r s + \Delta_c \dot{x} s + \Delta_\rho \text{sign}(\dot{x}) s \\ \leq \; & \bar{\Delta}_J \lambda |\dot{e}||s| + \bar{\Delta}_J |\ddot{x}_r||s| + \bar{\Delta}_c |\dot{x}||s| + \bar{\Delta}_\rho |s| \end{aligned} \tag{3.16}$$

namely,

$$K_m s \leq K|s|. \tag{3.17}$$

Based on the above analysis, we can easily conclude that

$$\dot{V} = -\frac{\varpi}{J} s^2 + \frac{K_m s - K|s|}{J} \leq 0. \tag{3.18}$$

The proof is thus completed.

Remark 1: In the ASM controller, we employ the adaptation law to estimate the coefficient of the self-aligning torque ξ without the need of any prior information for ξ. This is the key benefit of adaptive estimation because the road conditions are typically unknown to the vehicle system in reality. On the other hand, for the uncertain parameters J, c and ρ, their nominal values and bounds can be accurately identified offline. Thus, by using the sliding mode control the effects

of these uncertainties on the system performance can be compensated fast and effectively.

Remark 2: Like the conventional sliding mode controller, the control input u_1 (3.5) contains a discontinuous term $K\text{sign}(s)$ which may induce undesired chattering to the control signal. To alleviate this effect, the boundary layer technique [144], [145] is also adopted, namely, using the following saturation function to replace the signum function in (3.5):

$$\text{sat}(z) = \begin{cases} z/\psi & \text{if } |z| < \psi \\ \text{sign}(z) & \text{if } |z| \geq \psi \end{cases} \tag{3.19}$$

where ψ denotes the boundary layer thickness. However, the adoption of boundary layer is generally at the cost of reduced tracking accuracy.

3.2.2 Estimation of coefficient of self-aligning torque

As aforementioned, the self-aligning torque can be estimated by adaptively estimating its coefficient ξ as shown in (3.8). It is manifest that the accuracy of the estimation of the coefficient of the self-aligning torque by the adaptive estimation law plays a pivotal role in the tracking performance of the proposed adaptive sliding mode controller. The designed adaptive estimation law should guarantee not only the estimation precision of the coefficient of the self-aligning torque, but also a fast convergence rate for the estimated coefficient converging to the actual one. To facilitate the adjustment for either good estimation accuracy or fast estimation

rate, we set the adaptation gain μ as a linear filter [143] as follows:

$$\mu = \mu_1 + \mu_2 p \tag{3.20}$$

where $\mu_1 > 0$, $\mu_2 > 0$, and p is the Laplace operator. Note that the derivative of the sliding variable s is given in (3.14). Substituting $\dot{s}$ and (3.20) into the adaptation law described in (3.8) yields

$$\begin{aligned}
\dot{\hat{\xi}} =& \mu s \tanh(x) \\
=& \mu_1 s \tanh(x) + \mu_2 \dot{s} \tanh(x) \\
=& \mu_1 s \tanh(x) + \mu_2 \Bigg[-\frac{\varpi s}{J} + \frac{\tanh(x)}{J}\xi \\
& - \frac{\tanh(x)}{J}\hat{\xi} + \frac{K_m - K\text{sign}(s)}{J} \Bigg] \tanh(x) \\
=& \mu_1 s \tanh(x) - \frac{\mu_2 \varpi s \tanh(x)}{J} + \frac{\mu_2 \tanh^2(x)}{J}\xi \\
& - \frac{\mu_2 \tanh^2(x)}{J}\hat{\xi} + w
\end{aligned} \tag{3.21}$$

with

$$w = \frac{\mu_2}{J}[K_m - K\text{sign}(s)]\tanh(x). \tag{3.22}$$

Rewrite (3.21) by using the Laplace transform, we have

$$\begin{aligned}
& \left[\frac{\mu_2 \tanh^2(x)}{J} + p\right]\hat{\xi} \\
=& \frac{\mu_2 \tanh^2(x)}{J}\xi + \frac{(\mu_1 J - \mu_2 \varpi) s \tanh(x)}{J} + w.
\end{aligned} \tag{3.23}$$

It can be seen that if there are no parametric uncertainties except the self-aligning torque acting on the SbW system, selecting the design parameter μ_1 as

$$\mu_1^* = \mu_2 \frac{\varpi}{J} \tag{3.24}$$

leads to the term $(\mu_1 J - \mu_2 \varpi) s\tanh(x)/J = 0$ as well as $w = 0$. Thus, the adaptation dynamic equation (3.23) reduces to

$$\hat{\xi}^* = \frac{\mu_2 \tanh^2(x)/J}{\mu_2 \tanh^2(x)/J + p} \xi \tag{3.25}$$

where μ_1^* and $\hat{\xi}^*$ denote the parameters under the ideal condition without uncertainties. However, due to the existing parametric uncertainties in the plant model and also because the equivalent moment of inertia J is not completely known in practice, we simply use the nominal parameter J_0 to replace J in (3.24), that is,

$$\mu_1 = \mu_2 \frac{\varpi}{J_0}. \tag{3.26}$$

Substituting (3.26) into (3.22) yields

$$\hat{\xi} = \frac{\mu_2 \tanh^2(x)/J}{\mu_2 \tanh^2(x)/J + p} \xi + d_a \tag{3.27}$$

with d_a referred to as the adaptation perturbation, which is given by

$$\begin{aligned} d_a = & \frac{\mu_2}{J}[K_m - K\text{sign}(s)]\tanh(x) \\ & + \frac{\Delta_J}{J_0 J} \mu_2 \varpi s \tanh(x). \end{aligned} \tag{3.28}$$

It is noted from (3.28) that the adaptation perturbation d_a is bounded in the presence of uncertainties and actually reduces to zero without parametric uncertainties. This implies that $\hat{\xi}$ will converge to the actual ξ in the case of no parametric uncertainties or approach to a region close to the actual ξ when uncertainties arise according to (3.27). Moreover, we can see that the value of μ_2 affects the convergence rate of the estimation (i.e., the adaptation bandwidth). The selection of μ_2 will be discussed in the next subsection.

3.2.3 Selection of control parameters

To this end, we have presented the ASM control law and the adaptation law for the self-aligning torque. It is clear that the stability of the overall control system can be guaranteed in the sense of Lyapunov. However, for practical implementation the controller parameters should be carefully selected to compromise between the tracking accuracy and robustness against the measurement noises, the system uncertainties and unmodeled system dynamics.

Selection of λ

The parameter λ crucially determines the tracking bandwidth of the sliding mode function as given by (3.2) and the decay rate of tracking errors on the sliding surface [143], [115]. A larger λ leads to a faster response rate and higher tracking accuracy, which, however, may bring excessive high-frequency measurement noises to the system that deteriorate the tracking accuracy inversely. To account for this trade-off we set $\lambda = 15$ in our case.

Selection of ϖ

The term with the parameter ϖ in (3.5) is introduced to enforce the tracking error onto the sliding surface [143]. It is obvious that the control system bandwidth becomes higher by increasing ϖ which leads to a faster response to the reference command as well. Nevertheless, a larger ϖ will similarly amplify the measurement noises from the sliding variable s and meanwhile result in a larger adaptation perturbation d_a that degrades the estimation accuracy. From the actual implementations, we find that $\varpi = 45$ is an acceptable value.

Selection of μ_2

From (3.27) we can see that the parameter μ_2 critically determines the adaptation bandwidth for the estimation of the self-aligning torque. Apparently, a larger μ_2 leads to a higher adaptation bandwidth implying a faster convergence rate for the estimated coefficient $\hat{\xi}$ to track the actual one ξ. However, we also note that the existence of μ_2 reversely augments the undesired adaptation perturbation d_a in (3.28). Hence, a satisfactory $\mu_2 = 2638$ is chosen for implementation.

Selection of ψ

It is well known that a larger value of the boundary layer thickness ψ (3.19) leads to less chattering but at the cost of reducing tracking accuracy [144]. In this chapter, the disturbance of self-aligning torque is compensated by a separate control input (3.7), which means that a smaller value of K in (3.5) would be sufficient to overcome the remaining uncertainties and disturbances. This implies that the chattering effects due to the sign function in (3.5) would be much less

compared to the conventional sliding mode control. In actual implementation, we set $\psi = 0.8$ to obtain a satisfied balance between control smoothness and tracking accuracy.

3.3 Controllers for Comparison

To compare the benefits of the proposed ASM controller, a conventional sliding mode controller and a linear H_∞ controller are also designed based on the methods employed in [49], [146].

3.3.1 Conventional sliding mode control

Define the tracking error e as

$$e = x_r - x \tag{3.29}$$

where x_r is the reference command for the front wheel steering angle to track, which is usually twice differentiable due to the curve of roads. Furthermore, a linear sliding variable s_{csm} is defined as

$$s_{csm} = \dot{e} + \lambda_{csm} e \tag{3.30}$$

where $\lambda_{csm} > 0$ is to be designed.

Then the sliding mode controller is given by

$$u_{csm} = \frac{1}{\bar{b}}(\bar{J}\lambda_{csm}|\dot{e}| + \bar{J}|\ddot{x}_r| + \bar{c}|\dot{x}| + \bar{\rho} + \bar{\tau})\text{sign}(s_{csm}) \tag{3.31}$$

where sign( ) is a standard signum function; $\bar{J}$, $\bar{c}$ and $\bar{\rho}$ denote the upper bounds of the parameters J, c and ρ, respectively; and $\bar{\tau}$ denotes the upper bound of the self-aligning torque acting on the SbW system. The upper bounds of the parameters J, c and ρ are given by

$$\begin{aligned} \bar{J} =& hJ_0 \\ \bar{c} =& c_0 + \bar{\Delta}_c \\ \bar{\rho} =& \rho_0 + \bar{\Delta}_\rho \end{aligned} \tag{3.32}$$

where h, $\bar{\Delta}_c$ and $\bar{\Delta}_\rho$ are given in (2.24).

Though the sliding mode controller u_{csm} is designed for the vehicle SbW system, we need to guarantee the stability of the control system. To prove the stability of the SbW system under the conventional sliding mode control, we choose the Lyapunov function as

$$V_{csm} = \frac{1}{2} {s_{csm}}^2. \tag{3.33}$$

According to (3.30), the first-order derivative of the sliding variable s_{csm} is

$$\dot{s}_{csm} = \ddot{e} + \lambda_{csm}\dot{e}. \tag{3.34}$$

Based on the definition of e shown in (3.29), we have

$$\dot{s}_{csm} = \ddot{x}_r - \ddot{x} + \lambda_{csm}\dot{e}. \tag{3.35}$$

It is deduced from (2.22) that

$$\ddot{x} = -\frac{c}{J}\dot{x} - \frac{\rho}{J}\text{sign}(\dot{x}) - \frac{\tau}{J} + \frac{b}{J}u_{csm}. \tag{3.36}$$

Combining (3.35) and (3.36), we have

$$\dot{s}_{csm} = \ddot{x}_r + \lambda_{csm}\dot{e} + \frac{c}{J}\dot{x} + \frac{\rho}{J}\text{sign}(\dot{x}) + \frac{\tau}{J} - \frac{b}{J}u_{csm}. \tag{3.37}$$

Substituting (3.31) into (3.37)

$$\begin{aligned}\dot{s}_{csm} =& \ddot{x}_r + \lambda_{csm}\dot{e} + \frac{c}{J}\dot{x} + \frac{\rho}{J}\text{sign}(\dot{x}) + \frac{\tau}{J} \\ & - \frac{1}{J}(\bar{J}\lambda_{csm}|\dot{e}| + \bar{J}|\ddot{x}_r| + \bar{c}|\dot{x}| + \bar{\rho} + \bar{\tau})\text{sign}(s_{csm}).\end{aligned} \tag{3.38}$$

Therefore, evaluating the first-order derivative of V_{csm} yields

$$\begin{aligned}\dot{V}_{csm} =& s_{csm}\dot{s}_{csm} \\ =& s_{csm}[\lambda_{csm}\dot{e} + \ddot{x}_r + \frac{c}{J}\dot{x} + \frac{\rho}{J}\text{sign}(\dot{x}) + \frac{\tau}{J} \\ & + (-\frac{\bar{J}}{J}\lambda_{csm}|\dot{e}| - \frac{\bar{J}}{J}|\ddot{x}_r| - \frac{\bar{c}}{J}|\dot{x}| - \frac{\bar{c}}{J} - \frac{\bar{\tau}}{J})\text{sign}(s_{csm})] \\ =& \lambda_{csm}\dot{e}s_{csm} + \ddot{x}_r s_{csm} + \frac{c}{J}\dot{x}s_{csm} + \frac{\rho}{J}\text{sign}(\dot{x})s_{csm} + \frac{\tau}{J}s_{csm} \\ & - \frac{\bar{J}}{J}\lambda_{csm}|\dot{e}||s_{csm}| - \frac{\bar{J}}{J}|\ddot{x}_r||s_{csm}| - \frac{\bar{c}}{J}|\dot{x}||s_{csm}| - \frac{\bar{\rho}}{J}|s_{csm}| - \frac{\bar{\tau}}{J}|s_{csm}| \\ =& (\lambda_{csm}\dot{e}s_{csm} - \frac{\bar{J}}{J}\lambda_{csm}|\dot{e}||s_{csm}|) + (\ddot{x}_r s_{csm} - \frac{\bar{J}}{J}|\ddot{x}_r||s_{csm}|) \\ & + (\frac{c}{J}\dot{x}s_{csm} - \frac{\bar{c}}{J}|\dot{x}||s_{csm}|) + (\frac{\rho}{J}\text{sign}(\dot{x})s_{csm} - \frac{\bar{\rho}}{J}|s_{csm}|) \\ & + (\frac{\tau}{J}s_{csm} - \frac{\bar{\tau}}{J}|s_{csm}|)\end{aligned} \tag{3.39}$$

According to the following inequalities

$$\begin{aligned}&\lambda_{csm}\dot{e}s_{csm} \le \frac{\bar{J}}{J}\lambda_{csm}|\dot{e}||s_{csm}|, \quad \ddot{x}_r s_{csm} \le \frac{\bar{J}}{J}|\ddot{x}_r||s_{csm}|, \\ &\frac{c}{J}\dot{x}s_{csm} \le \frac{\bar{c}}{J}|\dot{x}||s_{csm}|, \quad \frac{\rho}{J}\text{sign}(\dot{x})s_{csm} \le \frac{\bar{\rho}}{J}|s_{csm}|, \quad \frac{\tau}{J}s_{csm} \le \frac{\bar{\tau}}{J}|s_{csm}|\end{aligned} \tag{3.40}$$

we can easily conclude that

$$\dot{V}_{csm} \le 0. \tag{3.41}$$

The proof is completed.

The control input u_{csm} contains a discontinuous term $\text{sign}(s_{csm})$ which may include undesired chattering to the control signal. To alleviate this effect, the boundary layer technique [144], [145] can be adopted. More specific, we use the following saturation function to replace the signum function in (3.31):

$$\text{sat}(z) = \begin{cases} z/\psi_{csm} & \text{if } |z| < \psi_{csm} \\ \text{sign}(z) & \text{if } |z| \geq \psi_{csm} \end{cases} \tag{3.42}$$

where ψ_{csm} denotes the boundary layer thickness.

For a fair comparison, we set the parameters λ_{csm} and ψ_{csm} as the same as the corresponding parameters in the design of the ASM controller, namely,

$$\lambda_{csm} = 15, \quad \psi_{csm} = 0.8. \tag{3.43}$$

Thus, the conventional sliding mode controller for comparison has been designed and the stability of the control system has also been analyzed and verified.

3.3.2 H_∞ control

The H_∞ controller is of the following form

$$u_h = 0.31\ddot{x}_r + 20.66e + 9.06\dot{e} + 0.79\dot{x} \tag{3.44}$$

which is designed based on a small-gain theorem proposed by Zhou in [146].

3.4 Simulation results

Before the experimental implementation of the designed ASM controller, the conventional sliding mode controller and the H_∞ controller, we need to obtain the simulation results at first. In this section, simulation of the ASM controller, the conventional sliding mode controller and the H_∞ controller are carried out by MATLAB Simulink, and the simulation results are analyzed. In order to demonstrate the superiority of the designed ASM controller in terms of high tracking accuracy and strong robustness against varying road conditions, two cases are considered in the simulation.

3.4.1 Case 1: steering for a slalom path following

In this case, the steering wheel as shown in Figure 2.1(b) is maneuvered to generate an approximate sinusoidal waveform which mimics the vehicle following a slalom path. Then, the steering wheel angle sensor collects the corresponding steering angle. By multiplying this angle sensor signal by the corresponding scaling factor from the steering wheel to the front wheels, a steering wheel reference angle is obtained and input to the controllers under test. From [49] we know that setting the values of the coefficient of the self-aligning torque ξ as

$$\xi = \begin{cases} 155, & 0 < t \leq 20\,\text{s}, \quad \text{Snowy road} \\ 585, & 20 < t \leq 40\,\text{s}, \quad \text{Wet asphalt road} \\ 960, & 40 < t \leq 60\,\text{s}, \quad \text{Dry asphalt road} \end{cases} \tag{3.45}$$

can represent the self-aligning torque dynamics in the scenarios of snowy road, wet asphalt road and dry asphalt road, respectively. The simulation results for this

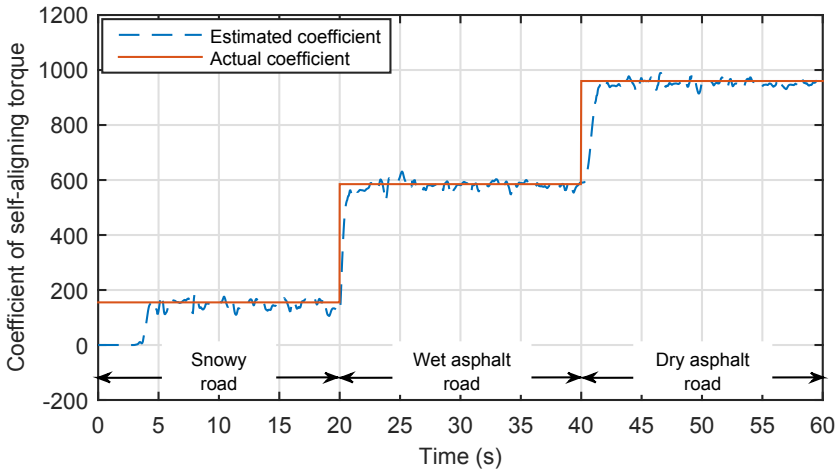

Figure 3.1: Simulated estimation of the coefficient of the self-aligning torque $\hat{\xi}$ under various road conditions in Case 1.

case are shown in Figures 3.1–3.4.

From Figure 3.1 we can clearly see that the adaptive estimation law in the designed ASM controller can estimate the coefficient of the self-aligning torque ξ fast and accurately. There is some slight chattering in the curve of estimated coefficient, which is mainly caused by the sensor measurement noises existing in the reference signal.

Figures 3.2–3.4 indicate the control performances of the ASM controller, the conventional sliding mode controller and the H_∞ controller in simulation, respectively. From Figure 3.2, we can see that the peak tracking errors of the ASM controller are about 0.02 rad, 0.028 rad and 0.03 rad during the three periods, respectively. The peak tracking errors occur at the beginning of the three periods because the adaptive estimation law needs to learn the coefficient of self-aligning torque when the road condition is changed. However, once this short learning procedure is accomplished, the tracking error can converge to a very small region within -0.005 rad to 0.005 rad regardless of the increasing of the self-aligning torque. For the conventional sliding mode controller, the peak tracking errors in the three periods

are 0.02 rad, 0.035 rad and 0.06 rad, respectively as shown in Figure 3.3. And Figure 3.4 indicates the peak tracking errors of the H_∞ controller, which are 0.018 rad, 0.045 rad and 0.07 rad, respectively. Thus, it is manifest that the tracking errors of the ASM controllers are significantly less than those of the conventional sliding mode controller and the H_∞ controller due to the accurate estimation and effective compensation of the self-aligning torque.

3.4.2 Case 2: steering for a circular path following

In this case, we consider a road path being straight and followed by a circular curve which is more common in reality. This is referred to as a circular path in this chapter. Similarly, we maneuver the steering wheel to generate the steering reference command for such a path following as shown in Figure 3.6(a). Simulation with a duration of 15 seconds is carried out and the coefficient of the self-aligning torque ξ is set as 700 to mimic the condition on a wet asphalt road.

From Figure 3.5 it is evidently seen that in the case of circular path following, the adaptive estimation law in the ASM controller can still estimate the coefficient of the self-aligning torque precisely, which is demonstrated by the negligible estimation error. During the 9th second to the 11th second, there is slight chattering existing in the line of 'estimated coefficient' mainly due to the sudden change of vehicle's steering direction.

It is shown in Figure 3.6 that the peak tracking error of the ASM controller in the case of circular path following is 0.06 rad at the beginning of the adaptive estimation. After the coefficient is accurately estimated, the tracking error decreases significantly, and finally converges to zero. However, from Figure 3.7 and

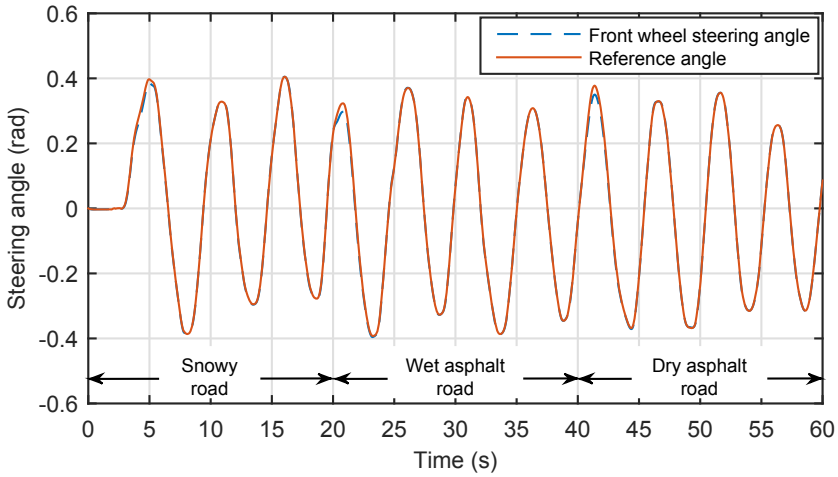

(b) Tracking profiles

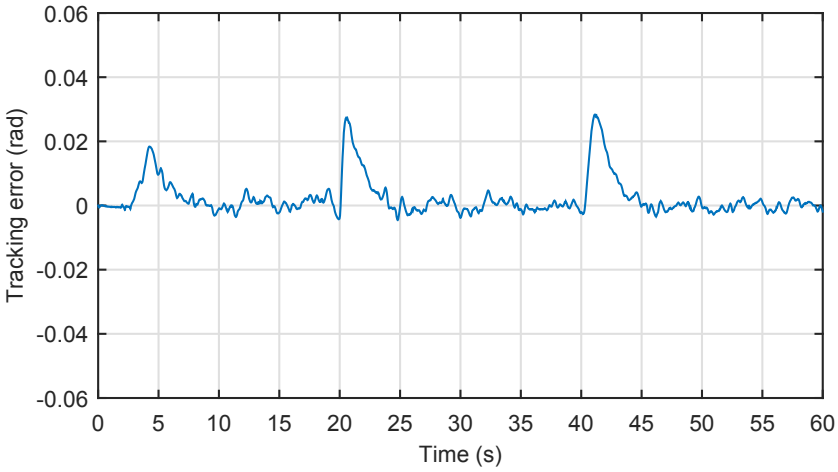

(c) Tracking errors

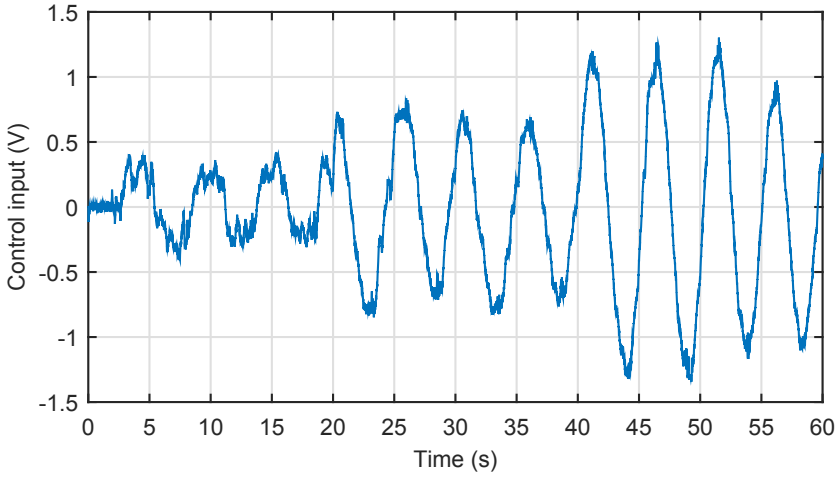

(d) Control inputs

Figure 3.2: Simulated control performance of the ASM controller in Case 1.

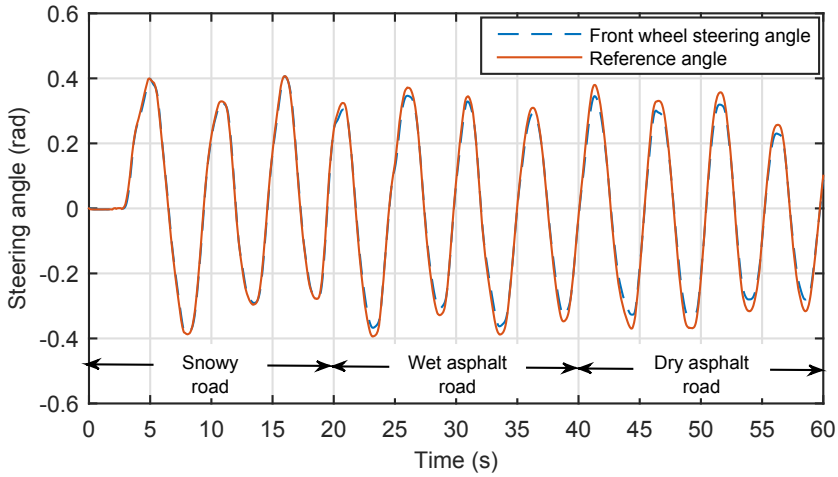

(a) Tracking profiles

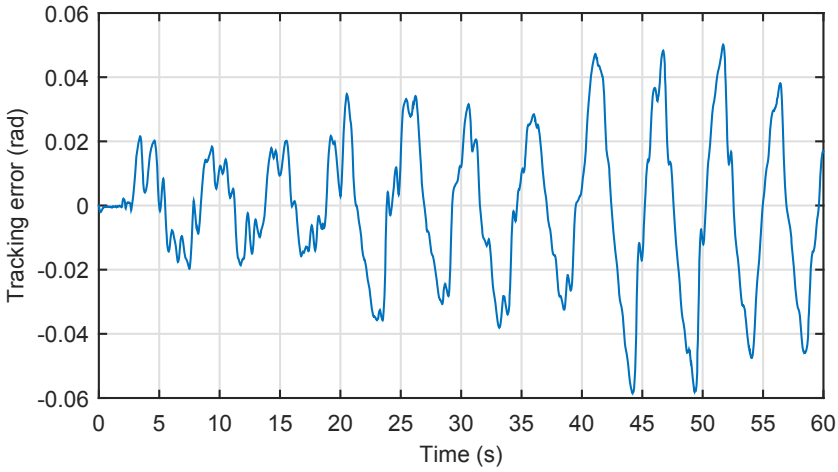

(b) Tracking errors

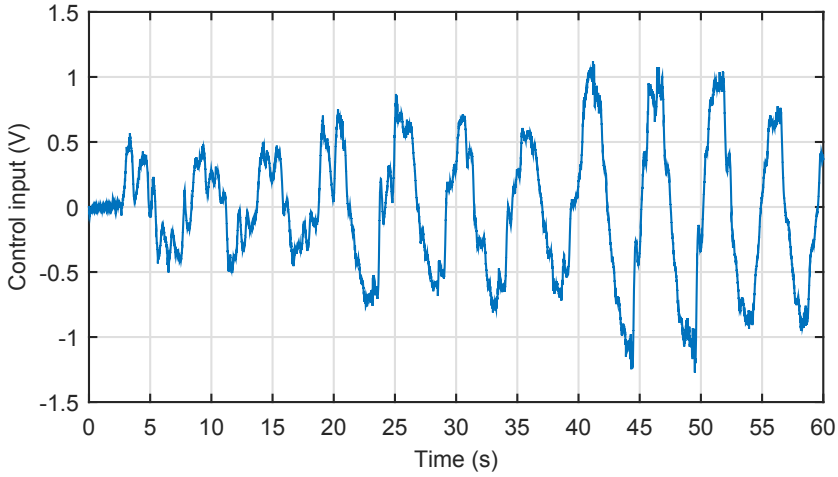

(c) Control inputs

Figure 3.3: Simulated control performance of the conventional sliding mode controller in Case 1.

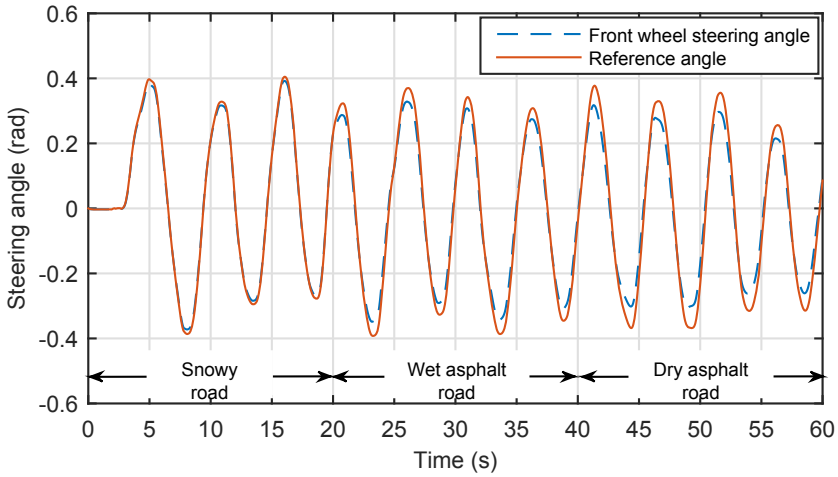

(a) Tracking profiles

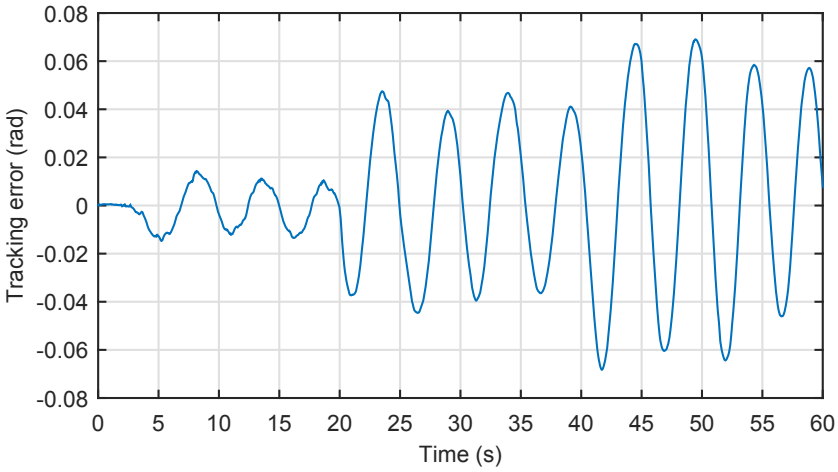

(b) Tracking errors

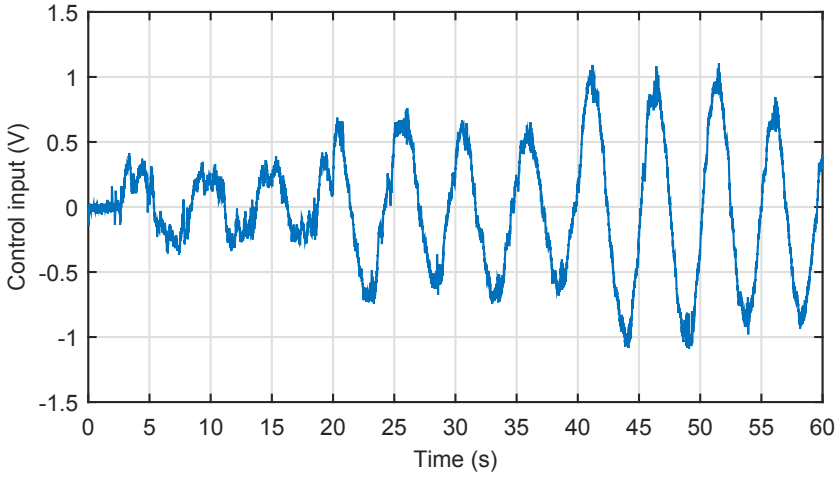

(c) Control inputs

Figure 3.4: Simulated control performance of the H_∞ controller in Case 1.

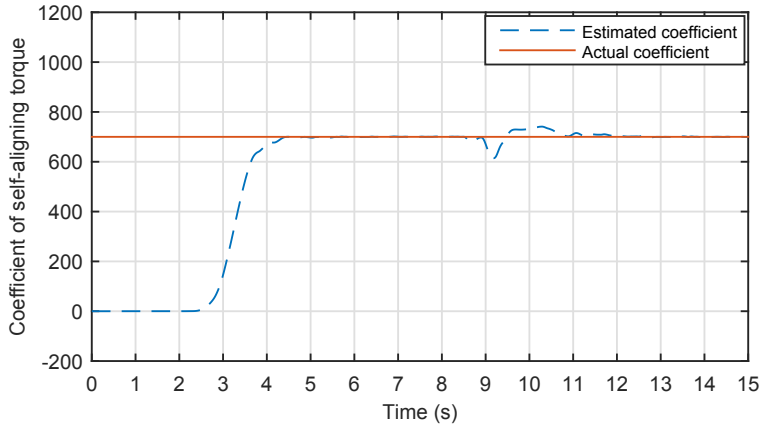

Figure 3.5: Simulated estimation of the coefficient of the self-aligning torque $\hat{\xi}$ in Case 2.

Figure 3.8, we can see that the peak tracking errors of the conventional sliding mode controller and the H_∞ controller are 0.055 rad and -0.06 rad, respectively. Besides, the steady state errors of the conventional sliding mode controller and the H_∞ controller have no tendency to converge to zero or converge to a small bounded region due to the lack of effective estimation and compensation of the self-aligning torque disturbance. Hence, the superiority of the ASM controller to the conventional sliding mode controller and the H_∞ controller is apparently demonstrated in both the cases of slalom path following and circular path following.

3.5 Experimental results

Experiments are carried out on the actual SbW setup to verify the designed controllers with a sampling period of 1 ms. To demonstrate that the designed ASM controller can be effectively implemented on the SbW experimental setup and can also possess similar superiority indicated in the simulation results, identical cases with the same reference commands and road conditions as those in the simulation are considered in this section.

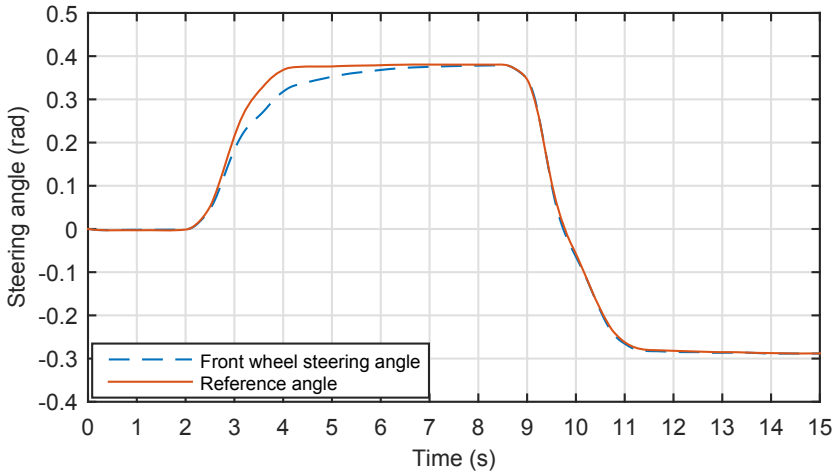

(b) Tracking profiles

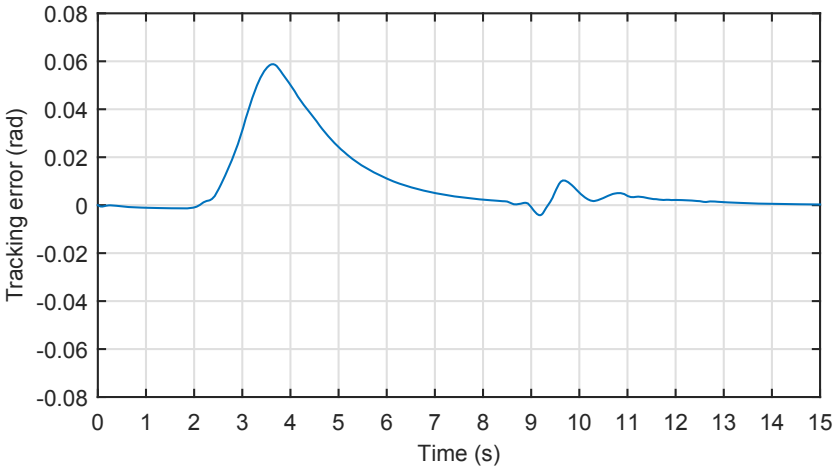

(c) Tracking errors

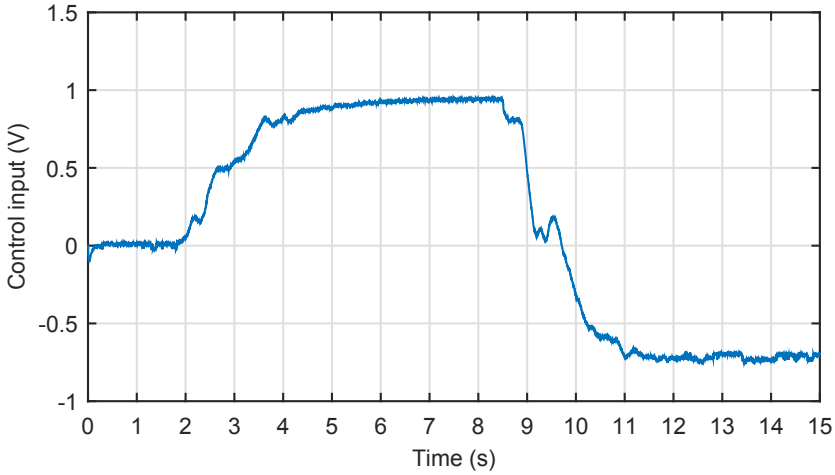

(d) Control inputs

Figure 3.6: Simulated control performance of the ASM controller in Case 2.

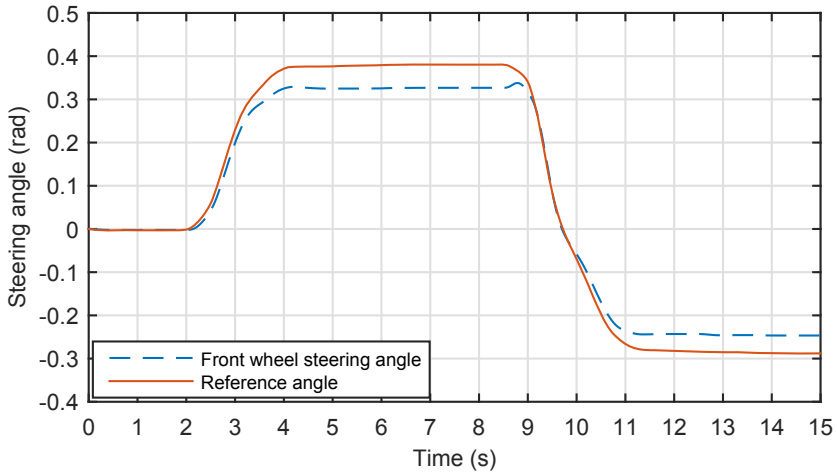

(a) Tracking profiles

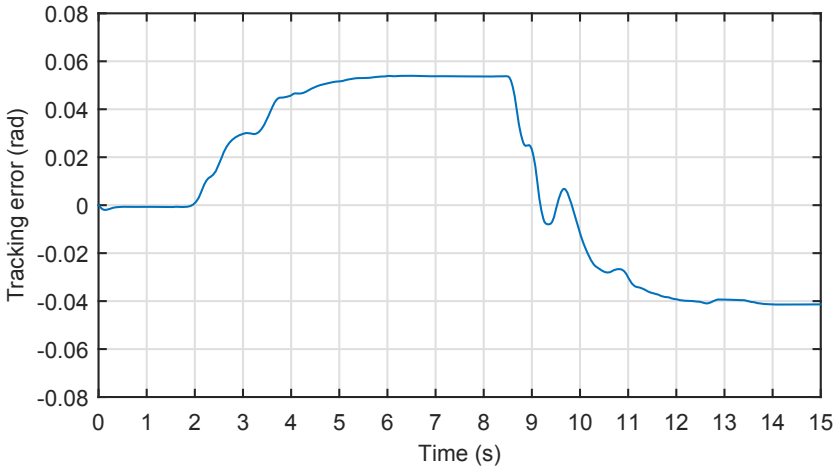

(b) Tracking errors

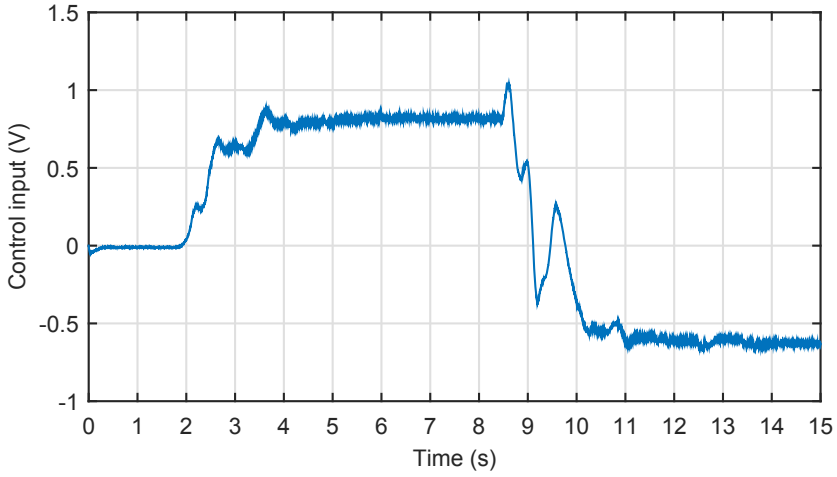

(c) Control inputs

Figure 3.7: Simulated control performance of the conventional sliding mode controller in Case 2.

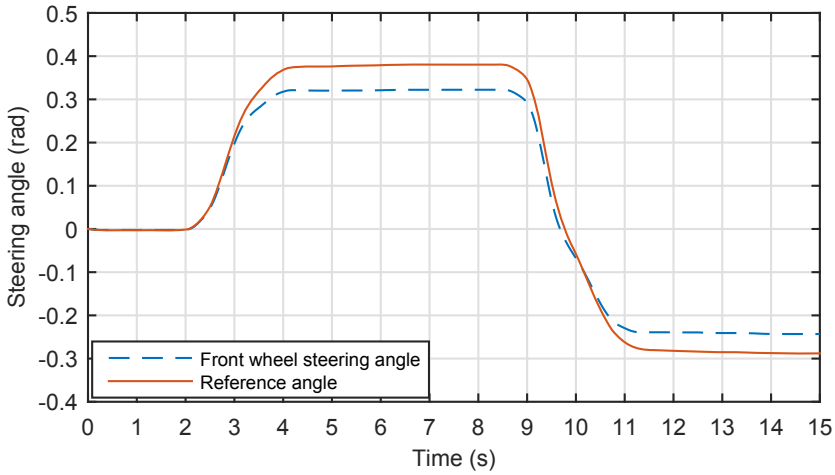

(a) Tracking profiles

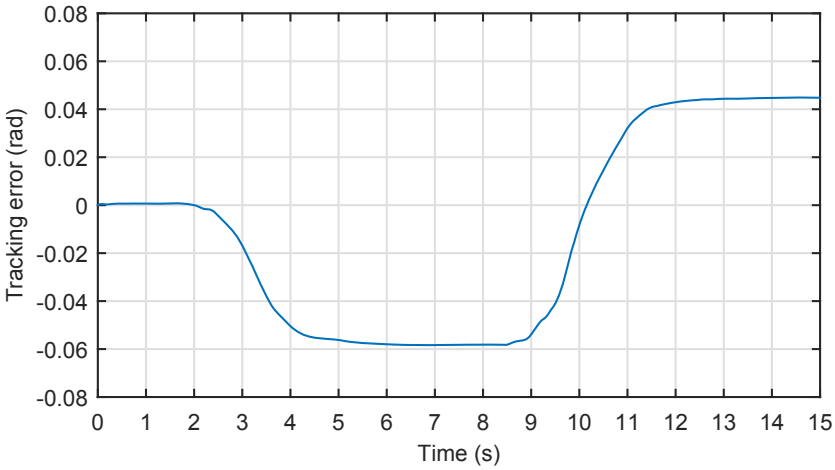

(b) Tracking errors

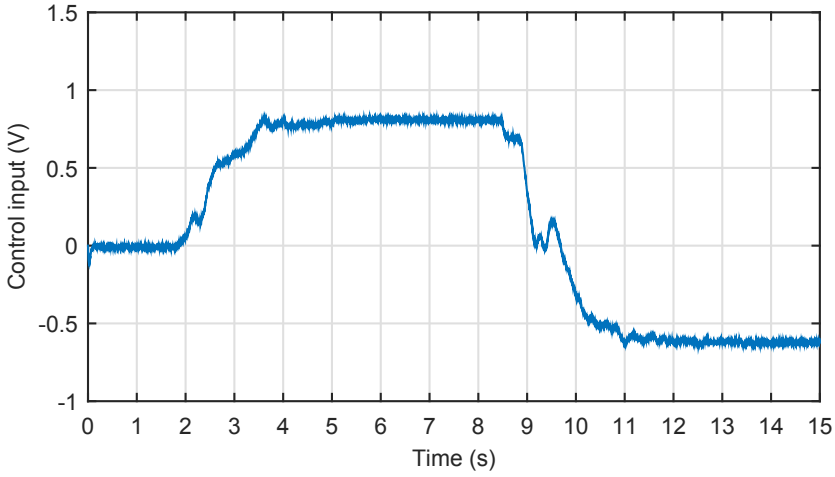

(c) Control inputs

Figure 3.8: Simulated control performance of the H_∞ controller in Case 2.

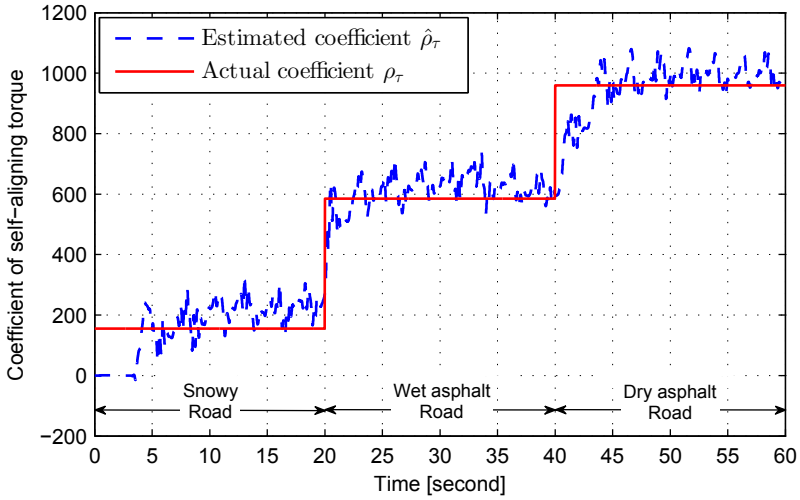

Figure 3.9: Experimental estimation of the coefficient of the self-aligning torque $\hat{\xi}$ under various road conditions in Case 1.

From Figure 3.9 we can see that the designed adaptation law in Case 1 can properly estimate various coefficients of the self-aligning torque ξ with respect to the change of road conditions. Compared with the simulation result as shown in Figure 3.1, there exist more oscillations in the curve of the estimated coefficient $\hat{\xi}$. This is primarily caused by the high frequency measurement noises from the angle sensors on the steering wheel and the front wheel. Though we have low-pass filtered the high frequency noises, the cut-off frequency of the filter cannot be set too low as we also need to guarantee the fidelity of the signals of the measured angles. It is also noted that when the steering angle x is zero at the beginning of the experiment, the estimated coefficient $\hat{\xi}$ is zero as well. This is because that $x = 0$ implies $\hat{\xi} = 0$. To solve this problem, we actually can set the initial value of $\hat{\xi}$ as the last estimated one during the previous driving cycle.

From Figure 3.10 it is seen that the peak tracking errors of the ASM controller under the three road conditions are 0.022 rad, 0.025 rad and 0.028 rad, which are pretty close to those in the simulation results as shown in Figure 3.10. The peak

tracking errors occur at the beginning of each change of the road conditions, at the time of which the adaptation law starts to estimate the new value of ξ. Once the estimated coefficient $\hat{\xi}$ converges to the actual one, the peak tracking errors consistently converge into a small region no matter how large the magnitudes of the self-aligning torque are. However, the steady-state errors are a little larger than those in the simulation results due to the sensor measurement noises. In comparison, the peak tracking errors under the conventional sliding mode controller and the H_∞ controller as shown in Figures 3.11–3.12 are much larger than those under the ASM controller and also become larger with respect to the increasing of the self-aligning torque.

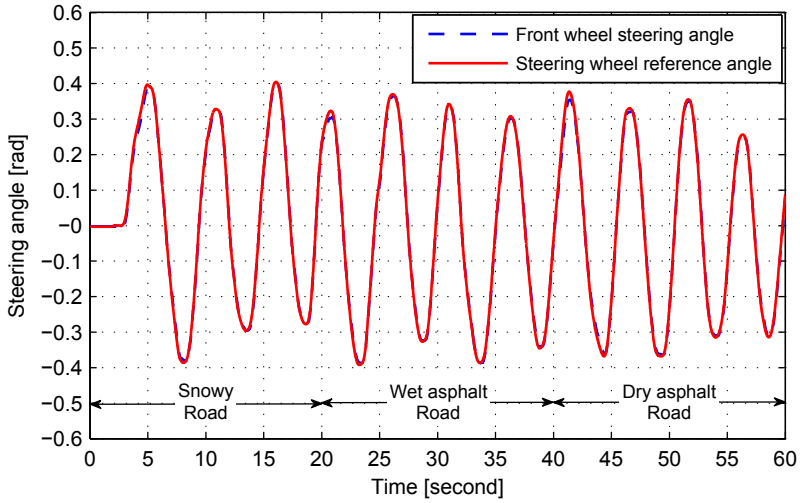

(b) Tracking profiles

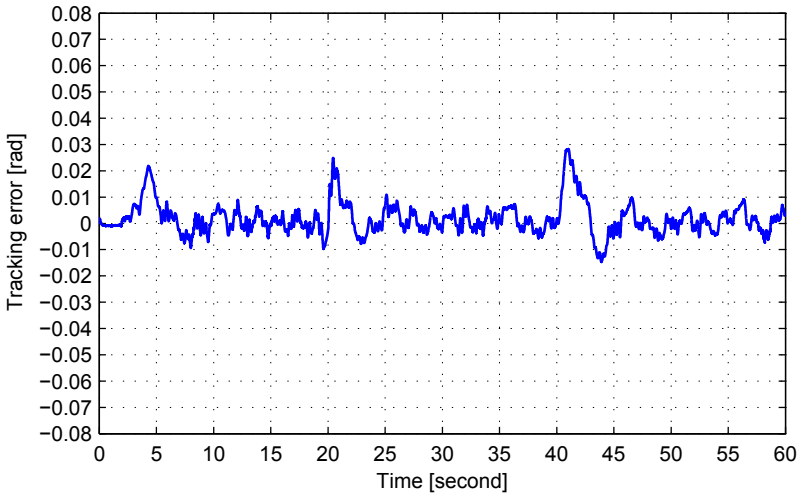

(c) Tracking errors

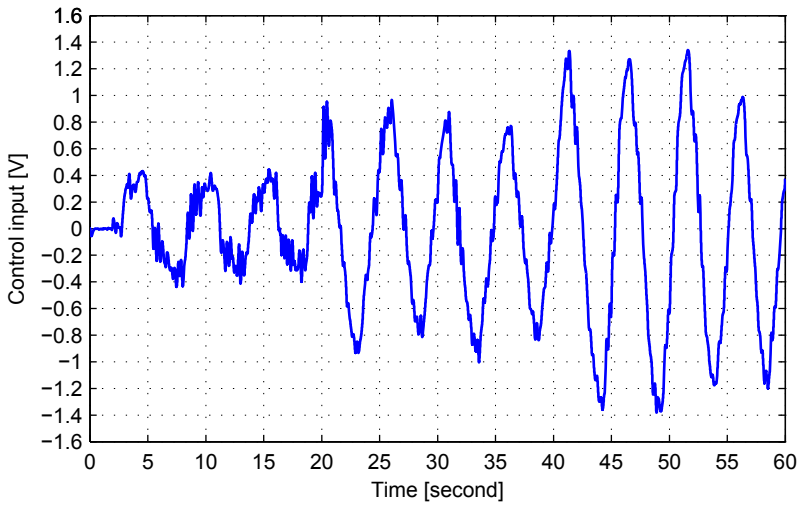

(d) Control inputs

Figure 3.10: Experimental control performance of the ASM controller in Case 1.

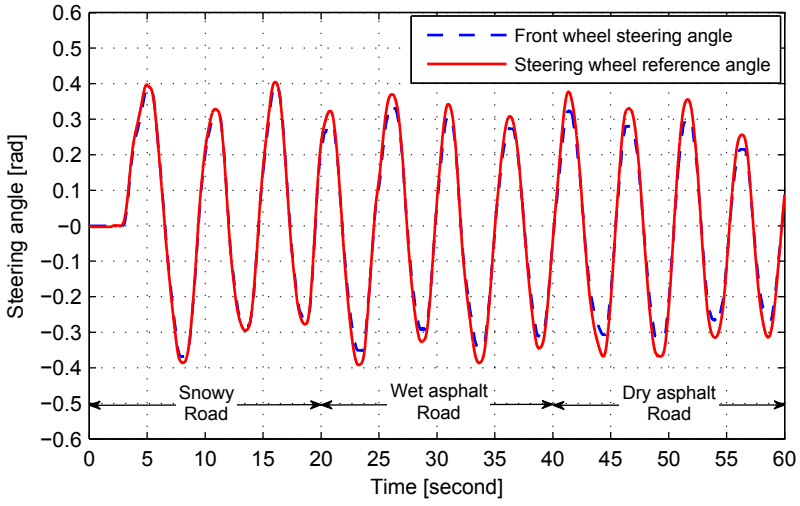

(a) Tracking profiles

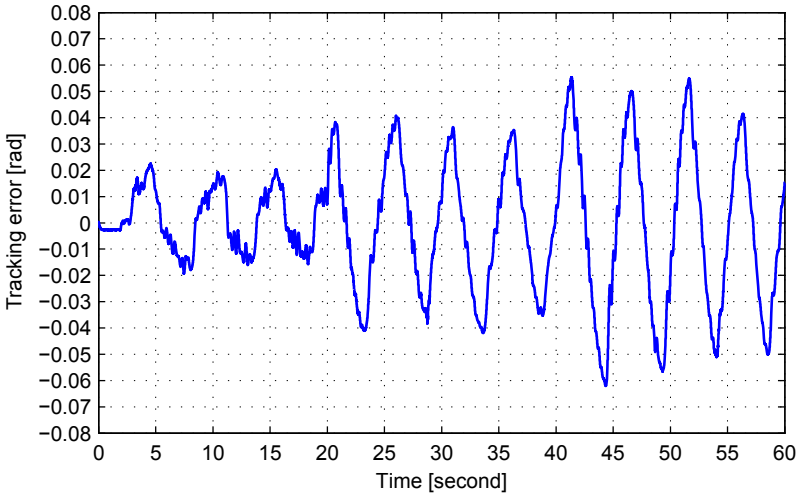

(b) Tracking errors

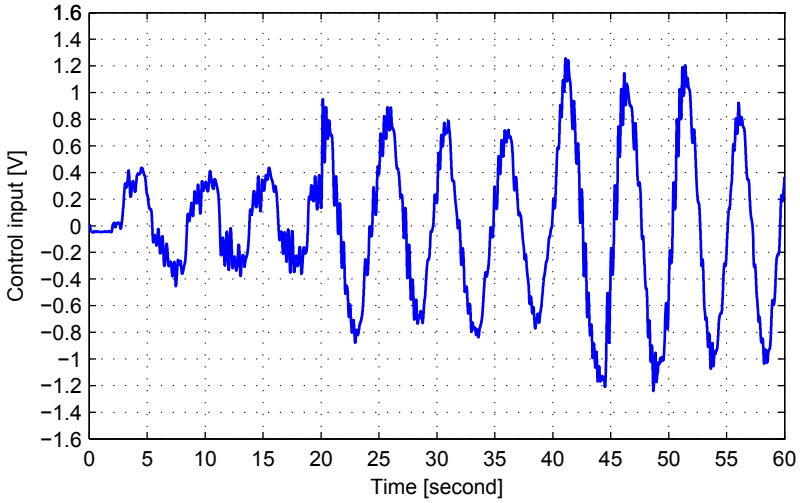

(c) Control inputs

Figure 3.11: Experimental control performance of the conventional sliding mode controller in Case 1.

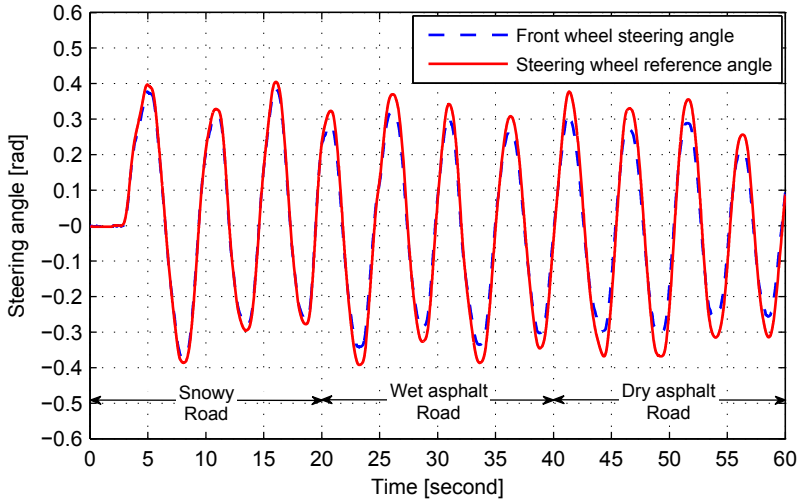

(a) Tracking profiles

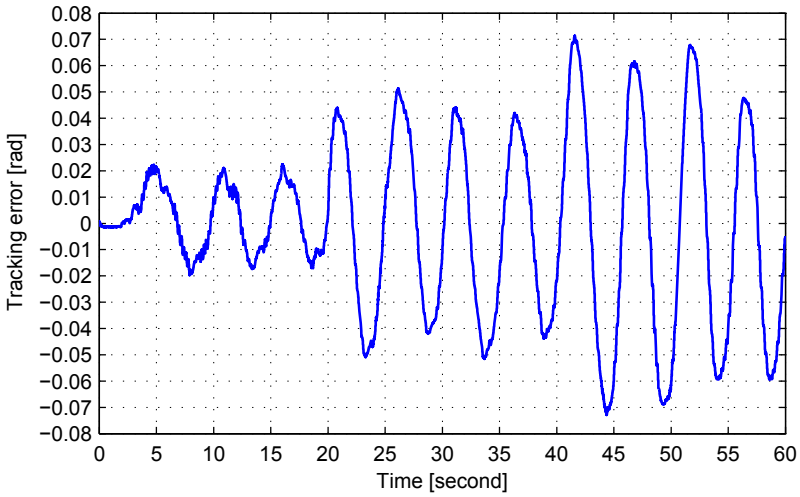

(b) Tracking errors

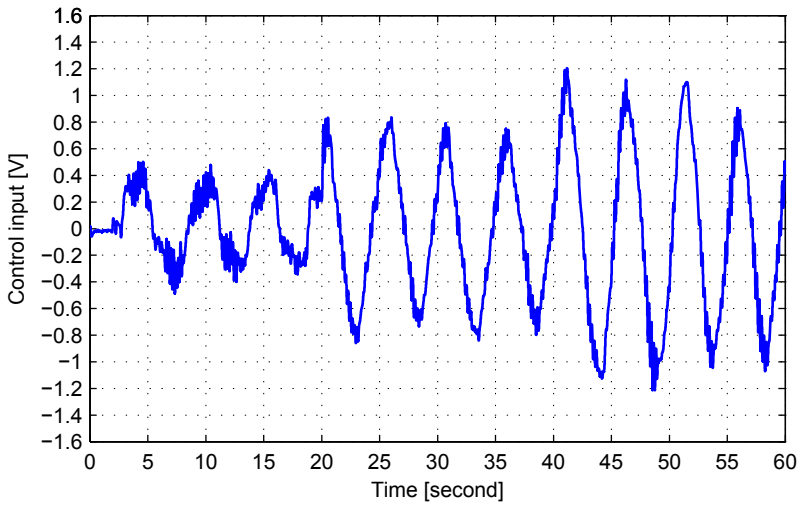

(c) Control inputs

Figure 3.12: Experimental control performance of the H_∞ controller in Case 1.

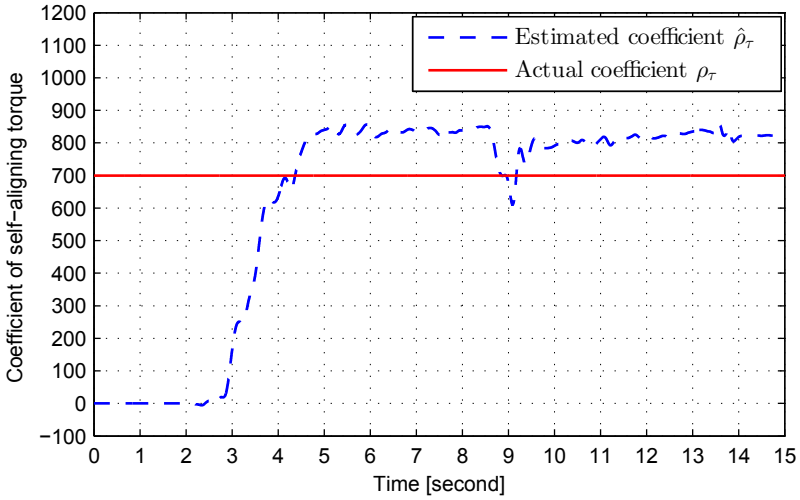

Figure 3.13: Experimental estimation of the coefficient of the self-aligning torque $\hat{\xi}$ in Case 2.

Figure 3.13 shows the estimation of the coefficient of the self-aligning torque under the ASM controller in Case 2. Compared with the simulation result as shown in Figure 3.5, the estimated $\hat{\xi}$ deviates a bit from the actual ξ at the steady state, which may be primarily due to the adaptation perturbation d_a in (3.28) being a constant in this case. At the moment of the 9th second, the estimation curve contains a notched response which stems from the change of the steering angle into a reverse direction.

The tracking profiles of the controllers are shown in Figures 3.14–3.16, which are close to the simulation results shown in Figures 3.6–3.8. It can be seen that the ASM controller is still superior to the conventional sliding mode controller and the H_∞ controller in this case. The peak tracking error under the ASM controller is 0.055 rad, which is less than both the conventional sliding mode controller (0.059 rad) and the H_∞ controller (0.07 rad).

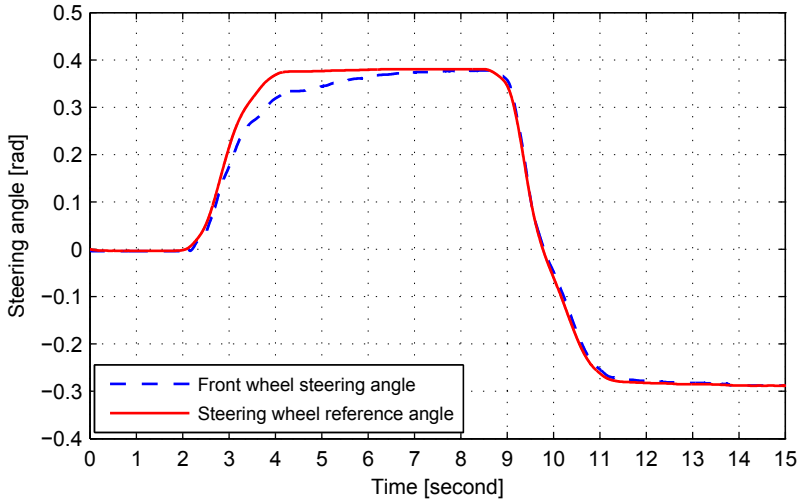

(a) Tracking profiles

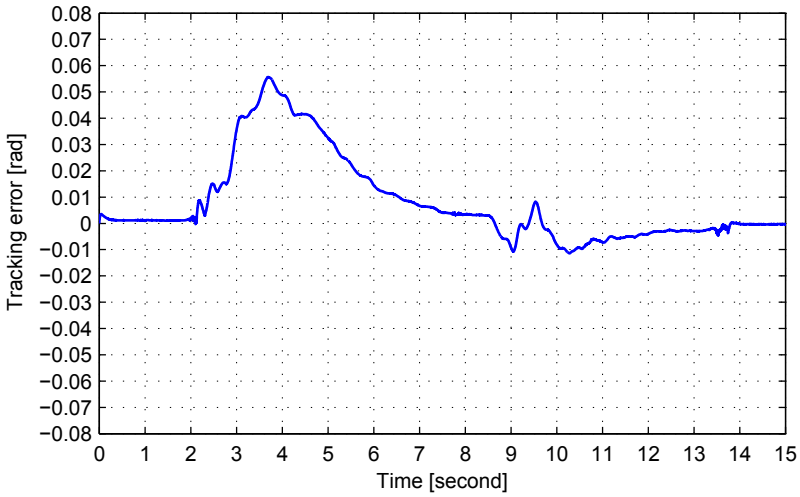

(b) Tracking errors

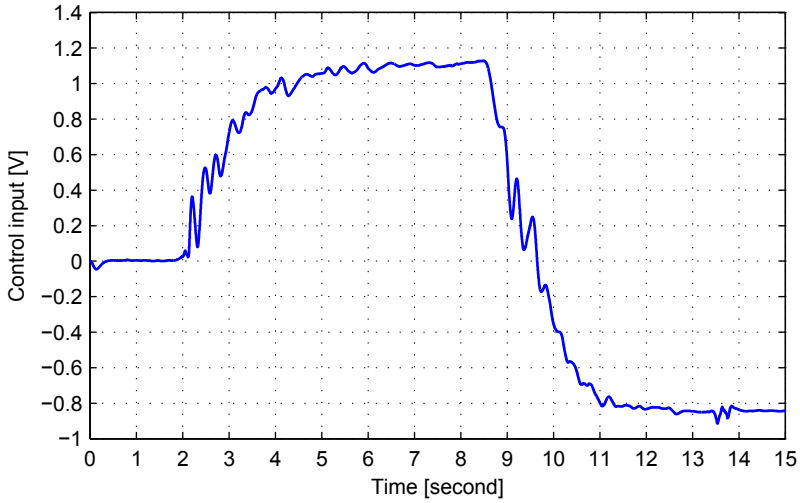

(c) Control inputs

Figure 3.14: Experimental control performance of the ASM controller in Case 2.

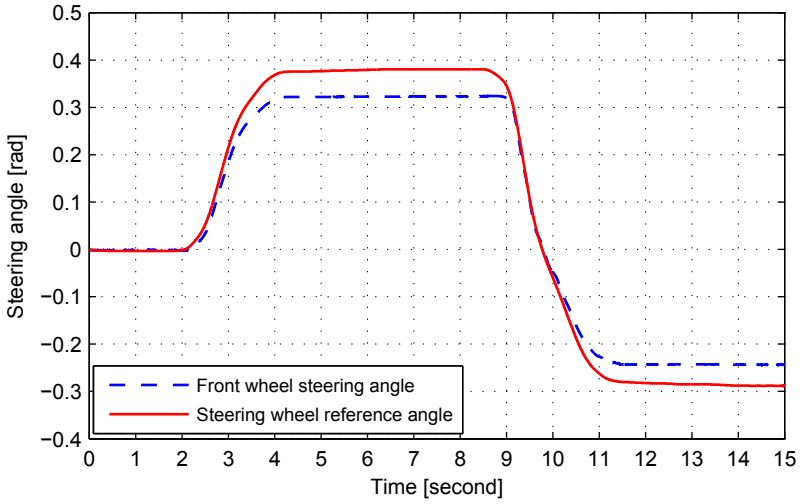

(a) Tracking profiles

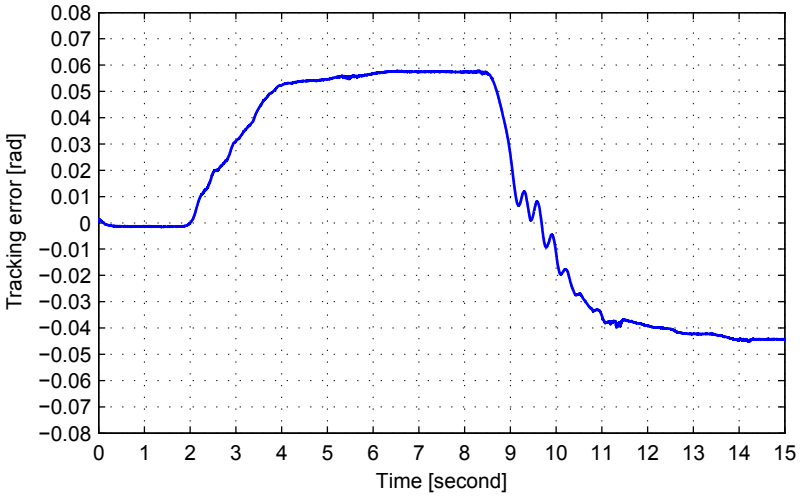

(b) Tracking errors

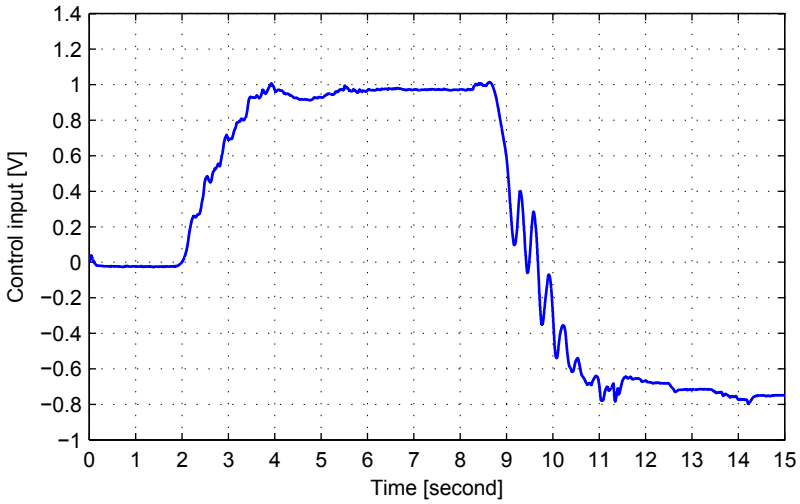

(c) Control inputs

Figure 3.15: Experimental control performance of the conventional sliding mode controller in Case 2.

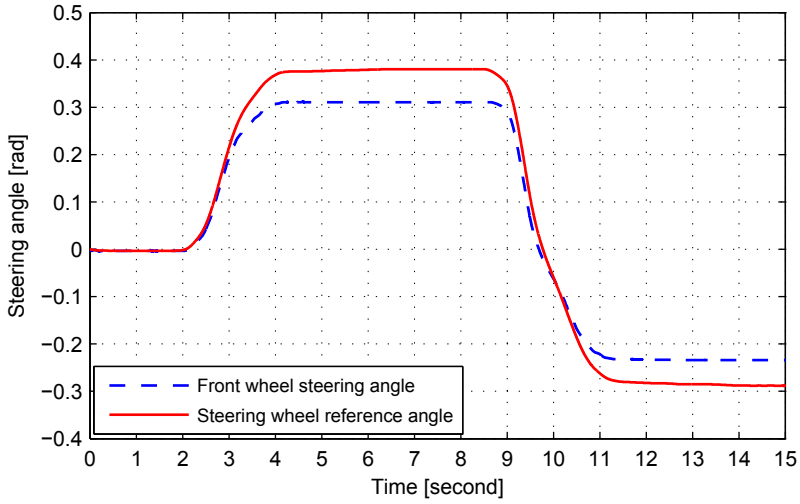

(a) Tracking profiles

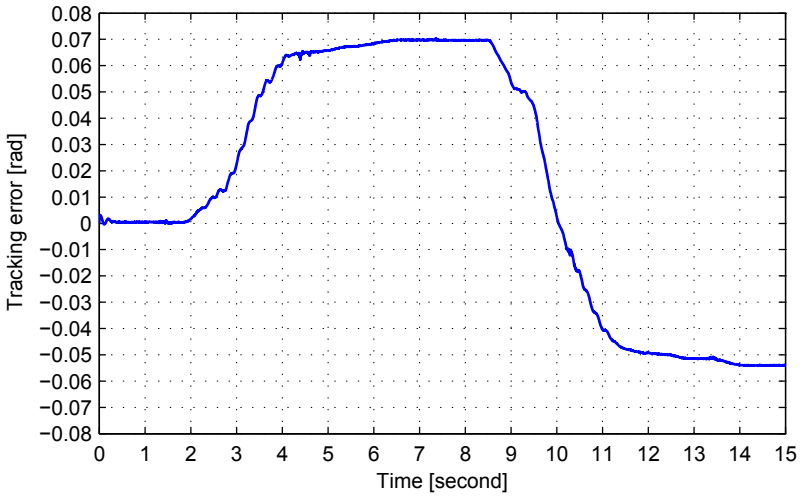

(b) Tracking errors

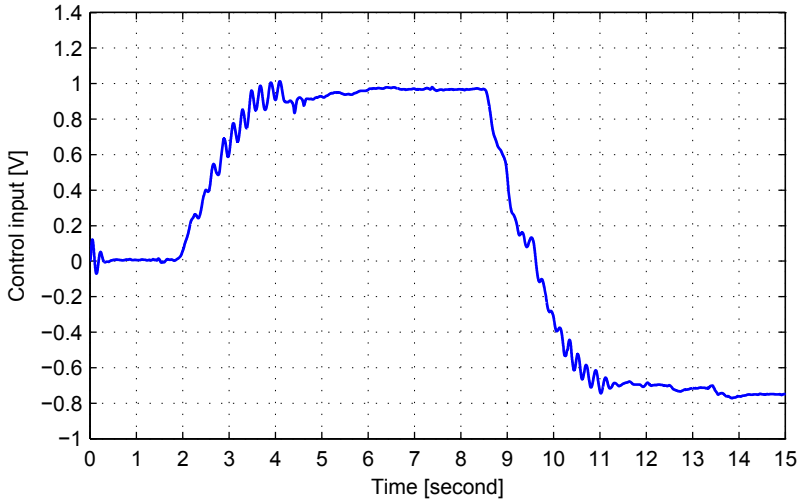

(c) Control inputs

Figure 3.16: Experimental control performance of the H_∞ controller in Case 2.

More importantly, with online estimations of the coefficient of the self-aligning torque ξ, the tracking accuracy of the ASM controller is improved to a large extent with the tracking error almost converging to zeros eventually. Comparatively, the tracking errors under the conventional sliding mode controller and the H_∞ controller both contain significant steady state errors which are due to the insufficient capability to compensate for the self-aligning torque.

3.6 Summary

In this chapter, we combine an adaptive estimation law with sliding mode control and design an ASM controller for SbW systems of road vehicles. The presented ASM control can utilize the adaptive estimation scheme to estimate the self-aligning torque. Thus, a feedforward control input can be formed to specifically compensate for the effect of the self-aligning torque disturbance to improve the tracking precision. The proposed ASM controller can also utilize the sliding mode control component to handle the parametric uncertainties existing in the plant model and unmodeled dynamics to enhance the controller's robustness. Experimental results demonstrate the superiority of the ASM controller. However, the convergence rate of tracking errors of the ASM control is not fast enough. Hence, in the next chapter, we will try to combine the adaptive estimation law with a fast non-singular terminal sliding mode control component to obtain a faster convergence rate on the basis of keeping the intrinsic merits of the ASM control.

Chapter 4

Adaptive Fast Non-Singular Terminal Sliding Mode Control

In Chapter 3 we propose an adaptive sliding mode control for road vehicle SbW systems. The adaptive sliding mode controller can use the adaptive estimation law to estimate the self-aligning torque disturbance to achieve high tracking accuracy, and the sliding mode control component to cope with the parametric uncertainties to enhance the performance robustness. However, the convergence rate of tracking errors of the adaptive sliding mode controller is not yet fast. Thus, in this chapter, we will combine the adaptive estimation law with fast non-singular terminal sliding mode control methodology and design an adaptive fast non-singular terminal sliding mode controller for SbW systems of road vehicles.

4.1 Introduction

As a newly proposed control methodology, fast non-singular terminal sliding mode (FNTSM) control not only has no switching elements in the control input implying less control chattering, but also can guarantee the exponential stability of the control system, which leads to a faster convergence rate of the tracking error in comparison with traditional sliding mode based control methodologies. In [147], based on the bounded information of parametric uncertainties, a fast non-singular terminal sliding mode controller is designed for piezoelectric actuators such that a zero error convergence can be guaranteed in finite time in the presence of disturbance and system uncertainties.

However, the combination of fast non-singular terminal sliding mode control with adaptive control is still rare in industrial applications. In this chapter, we will combine the adaptive estimation scheme for self-aligning torque with the FNTSM control which leads to an adaptive fast non-singular terminal sliding mode (AFNTSM) controller for the SbW system. The adaptive estimation law in the AFNTSM controller is utilized to estimate the self-aligning torque acting on front wheels. The estimated self-aligning torque can not only be provided to the steering wheel feedback motor to generate corresponding 'road feels' for the driver, but also be contributed to a feedforward control input to compensate for the effect of the self-aligning torque disturbance. The FNTSM control law in the AFNTSM controller is used to guarantee a fast convergence rate of the tracking errors especially in the case of shock disturbance rejection, and the performance robustness in dealing with system uncertainties, unmodeled dynamics and other external dis-

turbances.

4.2 Control design

In this section, an AFNTSM control law is proposed, and the stability of the control system is verified in the sense of Lyapunov. The guidelines of the selection of control parameters are elaborated in detail.

4.2.1 Adaptive fast non-singular terminal sliding mode control law

Consider the SbW plant model as shown in (2.13), we first define ψ as

$$\psi = (c - c_0)\dot{x} + (\rho - \rho_0)\text{sign}(\dot{x}). \tag{4.1}$$

Then, we have

$$|\psi| \leq \bar{\psi} = \bar{\Delta}_c|\dot{x}| + \bar{\Delta}_\rho \tag{4.2}$$

where $\bar{\Delta}_c$ and $\bar{\Delta}_\rho$ are the upper bounds of the parametric uncertainties Δ_c and $\Delta\rho$ as defined in (2.24), and $\bar{\psi}$ is the upper bound of ψ, which will be used later.

Define the tracking error e as

$$e = x - x_r \tag{4.3}$$

where x_r is the reference command for the front wheel steering angle to track, which is usually twice differentiable due to the curve of roads. In addition, a sliding variable s is defined as

$$s = e + \lambda|\dot{e}|^r\text{sign}(\dot{e}) \tag{4.4}$$

where $\lambda > 0,\ 1 < r < 2$ are to be designed [148]. It is noted that the expression of $|x|^n \text{sign}(x)$ for $n > 0\ \forall x \in R$ is always smooth and monotonically increasing. Moreover, it was reported in [149] that the terminal sliding mode function defined by

$$s = e + \lambda |\dot{e}|^r \text{sign}(\dot{e}) = 0 \tag{4.5}$$

with the initial conditions of $e(0)$ and $\dot{e}(0)$ is able to converge to zero in a finite time t_f given by

$$t_f = \frac{\lambda^{-\frac{1}{r}}}{1 - \frac{1}{r}} \big| e(0) \big|^{1 - \frac{1}{r}}. \tag{4.6}$$

Subsequently, an equivalent control input [138] shall be presented, which is the solution to the equation given by

$$\dot{s} = \dot{e} + Q(\ddot{x} - \ddot{x}_r) = 0 \tag{4.7}$$

where

$$Q = \lambda r |\dot{e}|^{r-1} \tag{4.8}$$

regardless of all the uncertainties existing in the plant model. Specifically, we set the model parameters as their nominal values and suppose $d = 0$. Consequently, solving (4.7) by utilizing the nominal plant model yields

$$u_0 = \frac{1}{b} \Big[J_0 \ddot{x}_r + \rho_0 \text{sign}(\dot{x}) + c_0 \dot{x} - \frac{J_0}{\lambda r} |\dot{e}|^{2-r} \text{sign}(\dot{e}) \Big]. \tag{4.9}$$

Afterwards, a reaching control input u_1 [115] is introduced:

$$u_1 = -\frac{J_0}{b} \Big[g_1 s + g_2 |s|^{\delta} \text{sign}(s) \Big] \tag{4.10}$$

with $g_1, g_2 > 0, 0 < \delta < 1$ to be designed, and the sliding variable s defined in (4.4).

Lastly, we propose a control input u_2 to specifically compensate for the effect exerted by the self-aligning torque as follows:

$$u_2 = \frac{1}{b}\hat{\xi}\tanh(x) \tag{4.11}$$

with $\hat{\xi}$ the estimation of the actual coefficient ξ which is obtained through the following adaptation law

$$\begin{aligned} \dot{\hat{\xi}} &= -Q\eta\kappa\tanh(x)s \\ b &= \begin{cases} 0 & \text{if } |\hat{\xi}| \geq \bar{\hat{\xi}} \\ 1 & \text{otherwise} \end{cases} \end{aligned} \tag{4.12}$$

where $\eta > 0$ is the adaptation gain to be designed, and b is the switching operator [112] which is able to keep the estimation of ξ within a boundary, namely,

$$|\tilde{\xi}| = |\xi - \hat{\xi}| \leq \bar{\tilde{\xi}}. \tag{4.13}$$

Lemma 4.1: Considering the SbW system model as shown in (2.13) with the parametric uncertainties as shown in (2.24) under the AFNTSM controller given by

$$u = u_0 + u_1 + u_2 \tag{4.14}$$

with u_0, u_1 and u_2 defined in (4.9)–(4.11), we can achieve the following tracking performance.

1) The sliding variable s can converge to the region of

$$|s| \leq \Omega = \min(\Omega_1, \Omega_2) \tag{4.15}$$

$$\Omega_1 = \frac{(h-1)\left|\ddot{x}_r - \frac{1}{\lambda r}|\dot{e}|^{2-r}\text{sign}(\dot{e})\right| + \frac{1}{J_0}(\bar{\psi} + \bar{\bar{\xi}})}{g_1} \tag{4.16}$$

$$\Omega_2 = \left[\frac{(h-1)\left|\ddot{x}_r - \frac{1}{\lambda r}|\dot{e}|^{2-r}\text{sign}(\dot{e})\right| + \frac{1}{J_0}(\bar{\psi} + \bar{\bar{\xi}})}{g_2}\right]^{\frac{1}{\delta}} \tag{4.17}$$

in a finite time. Note that $\bar{\psi}$ is given in (4.1).

2) The tracking error e and its velocity $\dot{e}$ can converge to the region given by

$$\begin{aligned} |e| \leq & 2\Omega \\ |\dot{e}| \leq & \left(\frac{\Omega}{\lambda}\right)^{\frac{1}{r}} \end{aligned} \tag{4.18}$$

in a finite time.

Proof: A Lyapunov function is chosen as

$$V = \frac{1}{2}s^2 + \frac{1}{2\eta J}(\xi - \hat{\xi})^2. \tag{4.19}$$

Then the first-order derivative of V along the system trajectories is:

$$\dot{V} = s\dot{s} + \frac{1}{\eta J}(\xi - \hat{\xi})(\dot{\xi} - \dot{\hat{\xi}}). \tag{4.20}$$

For a specific road condition, ξ is a constant. Due to the relatively high speed and short length of vehicles, the switching between different road conditions happens

instantaneously. Thus, it is assumed that $\dot{\xi} = 0$. Then we have

$$\begin{aligned} \dot{V} =& s\dot{s} + \frac{1}{\eta J}(\xi - \hat{\xi})(-\dot{\hat{\xi}}) \\ =& s\dot{s} + \frac{b}{J}(\xi - \hat{\xi})Q\tanh(x)s. \end{aligned} \tag{4.21}$$

According to $s = e + \lambda|\dot{e}|^r \text{sign}(\dot{e})$, we can differentiate s with the help of (4.14):

$$\begin{aligned} \dot{s} =& \dot{e} + \lambda r|\dot{e}|^{r-1}(\ddot{x} - \ddot{x}_r) \\ =& \dot{e} + Q(\ddot{x} - \ddot{x}_r) \\ =& \dot{e} + Q\Big[-\frac{c}{J}\dot{x} - \frac{\rho}{J}\text{sign}(\dot{x}) - \frac{\xi}{J}\tanh(x) \\ & + \frac{b}{J}u\Big] - Q\ddot{x}_r \\ =& \dot{e} - \frac{c}{J}Q\dot{x} - \frac{\rho}{J}Q\text{sign}(\dot{x}) - \frac{\xi}{J}Q\tanh(x) \\ & + \frac{J_0}{J}Q\ddot{x}_r + \frac{\rho_0}{J}Q\text{sign}(\dot{x}) + \frac{c_0}{J}Q\dot{x} \\ & - \frac{J_0}{J\lambda r}Q|\dot{e}|^{2-r}\text{sign}(\dot{e}) - \frac{J_0}{J}Qg_1 s \\ & - \frac{J_0}{J}Qg_2|s|^\delta \text{sign}(s) + \frac{\hat{\xi}}{J}Q\tanh(x) - Q\ddot{x}_r \\ =& \big(\frac{J_0}{J} - 1\big)(Q\ddot{x}_r - \dot{e}) - \frac{Q}{J}\psi - \frac{\xi}{J}Q\tanh(x) \\ & + \frac{\hat{\xi}}{J}Q\tanh(x) - \frac{J_0}{J}Qg_1 s - \frac{J_0}{J}Qg_2|s|^\delta \text{sign}(s) \end{aligned} \tag{4.22}$$

where $\psi = (c - c_0)\dot{x} + (\rho - \rho_0)\text{sign}(\dot{x})$ is defined in (4.1), and Q is defined in (4.8). Then, substituting (4.22) into (4.21) yields

$$\begin{aligned} \dot{V} =& s\Big[\big(\frac{J_0}{J} - 1\big)(Q\ddot{x}_r - \dot{e}) - \frac{Q}{J}\psi - \frac{\xi}{J}Q\tanh(x) \\ & + \frac{\hat{\xi}}{J}Q\tanh(x) - \frac{J_0}{J}Qg_1 s \\ & - \frac{J_0}{J}Qg_2|s|^\delta \text{sign}(s)\Big] + \frac{\kappa}{J}(\xi - \hat{\xi})Q\tanh(x)s \\ =& [\Upsilon + (\kappa - 1)\Gamma]s - \Lambda_1 s^2 - \Lambda_2|s|^{\delta+1} \end{aligned} \tag{4.23}$$

where

$$\begin{aligned}\Gamma =&\frac{1}{J}(\xi-\hat{\xi})Q\tanh(x)\\ \Upsilon =&\big(\frac{J_0}{J}-1\big)(Q\ddot{x}_r-\dot{e})-\frac{1}{J}Q\psi\\ \Lambda_1 =&\frac{J_0}{J}Qg_1\\ \Lambda_2 =&\frac{J_0}{J}Qg_2.\end{aligned} \tag{4.24}$$

It is seen from (4.24) that the last two terms in (4.23) are non-positive. This means that there exists a bounded region of s, within which the condition of $\dot{V}<0$ can be satisfied. This indicates that the sliding variable s and the estimation error $\tilde{\xi}$ can asymptotically converge to a bounded region.

For the purpose of finding the condition to achieve the finite-time stability [150] of s, another Lyapunov function is defined as

$$V_1=\frac{1}{2}s^2 \tag{4.25}$$

Using (4.22) yields

$$\dot{V}_1=(\Upsilon-\Gamma)s-\Lambda_1 s^2-\Lambda_2|s|^{\delta+1}. \tag{4.26}$$

Next, two cases are considered here.

Case 1) Rewrite (4.26) as follows:

$$\dot{V}_1=-\big(\Lambda_1-\frac{\Upsilon-\Gamma}{s}\big)s^2-\Lambda_2|s|^{\delta+1}. \tag{4.27}$$

Thus, if $\dot{e}\neq 0$ and $\Lambda_1-\frac{\Upsilon-\Gamma}{s}>0$, there exist $\sigma_1,\sigma_2>0$ which satisfy

$$\begin{aligned}\dot{V}_1\leq&-\sigma_1 s^2-\sigma_2|s|^{\delta+1}\\ =&-2\sigma_1 V_1-2^{\frac{\delta+1}{2}}\sigma_2 V_1{}^{\frac{\delta+1}{2}}.\end{aligned} \tag{4.28}$$

The condition of (4.28) can yield the finite-time convergence of s to a region, and the convergence time can be obtained as [134]

$$t_c \leq \frac{1}{(1-\delta)\sigma_1}\ln\left[1+\frac{\sigma_1}{\sigma_2}(2V_{10})^{\frac{1-\delta}{2}}\right] \tag{4.29}$$

with $V_{10} = V_1(s(0))$ the initial condition of the Lyapunov function V_1.

Based on the aforementioned analysis, the way to achieve finite-time convergence is to find the region of s which satisfies $\Lambda_1 - \frac{\Upsilon-\Gamma}{s} > 0$. Furthermore, the expression of $\Lambda_1 - \frac{\Upsilon-\Gamma}{s} > 0$ can be deduced from

$$\begin{aligned} |s| > & \frac{|\Upsilon-\Gamma|}{\Lambda_1} = \\ & \frac{\left|(1-\frac{J}{J_0})\left[\ddot{x}_r - \frac{1}{\lambda r}|\dot{e}|^{2-r}\mathrm{sign}(\dot{e})\right] - \frac{1}{J_0}\psi - \frac{1}{J_0}\tilde{\xi}\tanh(x)\right|}{g_1}. \end{aligned} \tag{4.30}$$

By using the bounds of the system uncertainties, we have

$$\frac{|\Upsilon-\Gamma|}{\Lambda_1} \leq \frac{(h-1)\left|\ddot{x}_r - \frac{1}{\lambda r}|\dot{e}|^{2-r}\mathrm{sign}(\dot{e})\right| + \frac{1}{J_0}(\bar{\psi}+\bar{\tilde{\xi}})}{g_1} = \Omega_1 \tag{4.31}$$

Consequently, the condition of $\Lambda_1 - \frac{\Upsilon-\Gamma}{s} > 0$ can be satisfied when

$$|s| > \Omega_1. \tag{4.32}$$

Thus, the region

$$|s| \leq \Omega_1 \tag{4.33}$$

can be reached in a finite time under the designed AFNTSM controller.

Case 2) Rewrite (4.26) in the form as

$$\dot{V}_1 = -\Lambda_1 s^2 - \left[\Lambda_2 - \frac{\Upsilon - \Gamma}{|s|^{\delta}\text{sign}(s)}\right]|s|^{\delta+1} \tag{4.34}$$

Similarly, the condition of $\Lambda_2 - \frac{\Upsilon-\Gamma}{|s|^{\delta}\text{sign}(s)} > 0$ with $\dot{e} \neq 0$ is able to achieve the finite-time convergence of V_1 to a region. Hence, under the similar analysis as that in *Case 1)*, the region of $|s|$ given by

$$|s| \leq \Omega_2 = \left[\frac{(h-1)\left|\ddot{x}_r - \frac{1}{\lambda r}|\dot{e}|^{2-r}\text{sign}(\dot{e})\right| + \frac{1}{J_0}(\bar{\psi} + \bar{\bar{\xi}})}{g_2}\right]^{\frac{1}{\delta}} \tag{4.35}$$

can also be achieved under the presented AFNTSM controller in a finite time.

Finally, it shall be analyzed that the condition of $\dot{e} = 0$ for the aforementioned two cases is not an interference factor in the finite-time convergence of V_1 to a region. By substituting (4.14) into $J\ddot{x} + c\dot{x} = bu - \rho\text{sign}(\dot{x}) - \tau$ with the condition of $\dot{e} = 0$, we have

$$\ddot{e} = \left(\frac{J_0}{J} - 1\right)\ddot{x}_r - \frac{\psi}{J} - \frac{\tilde{\xi}\tanh(x)}{J} - \frac{J_0}{J}[g_1 s + g_2|s|^{\delta}\text{sign}(s)]. \tag{4.36}$$

Therefore, for $\dot{e} = 0$, we have

$$\ddot{e} = \begin{cases} -\frac{J_0}{J}\left[g_1 - \frac{(1-\frac{J}{J_0})\ddot{x}_r - \frac{1}{J_0}\psi - \frac{\tilde{\xi}\tanh(x)}{J_0}}{s}\right]s - \frac{J_0}{J}g_2|s|^{\delta}\text{sign}(s) \\ \qquad\qquad \neq 0, \quad \text{for } |s| > \Omega_1 \\ -\frac{J_0}{J}g_1 s - \frac{J_0}{J}\left[g_2 - \frac{(1-\frac{J}{J_0})\ddot{x}_r - \frac{1}{J_0}\psi - \frac{\tilde{\xi}\tanh(x)}{J_0}}{|s|^{\delta}\text{sign}(s)}\right]|s|^{\delta}\text{sign}(s) \\ \qquad\qquad \neq 0, \quad \text{for } |s| > \Omega_2 \end{cases} \tag{4.37}$$

from which it is seen that $\dot{e} = 0$ is not an interference factor for $|s| > \Omega_1$ or $|s| > \Omega_2$. In consequence, the finite-time convergence of s can still be achieved in the condition of $\dot{e} = 0$,

Thus, by combining (4.33) and (4.35), it can be concluded that the sliding variable s can converge to the region of $|s| \leq \Omega = \min(\Omega_1, \Omega_2)$ in a finite time by the presented AFNTSM controller.

In order to obtain (4.18), we rewrite (4.4) as

$$e + \left[\lambda - \frac{s}{|\dot{e}|^r \text{sign}(\dot{e})}\right] |\dot{e}|^r \text{sign}(\dot{e}) = 0 \tag{4.38}$$

from which we can clearly see that if $|\dot{e}| > (\frac{\Omega}{\lambda})^{\frac{1}{r}}$, then $\lambda - \frac{s}{|\dot{e}|^r \text{sign}(\dot{e})} > 0$ since $|s| \leq \Omega$. Thus, the function (4.38) keeps the same form leading to the same convergence property as (4.5), which reversely proves that the velocity of the tracking error $\dot{e}$ can converge to the region of

$$|\dot{e}| \leq \left(\frac{\Omega}{\lambda}\right)^{\frac{1}{r}} \tag{4.39}$$

in a finite time. As a consequence, according to (4.38), we can conclude that the tracking error e can converge to the region of

$$|e| \leq \lambda |\dot{e}|^{\frac{1}{r}} + |s| \leq 2\Omega. \tag{4.40}$$

in a finite time equal to $(t_f + t_c)$. The proof is thus completed.

Remark 1: In the AFNTSM controller, the adaptation law is employed to estimate the coefficient of the self-aligning torque ξ without any prior information of ξ. This is the pivotal benefit of adaptive estimation law because the road conditions are usually uncertain in reality. However, the nominal values and bounds of pa-

rameters J, c and ρ can get identified accurately offline. Hence, the effect of these uncertainties on the control performance can be compensated by the FNTSM in the AFNTSM controller fast and effectively.

Remark 2: The tracking errors under conventional sliding mode controllers can also converge to zero theoretically. However, the convergence rate cannot be guaranteed and may be very slow. Based on the theoretical analysis, we can see that the designed AFNTSM controller has a faster convergence rate owing to its implied exponential stability. This indicates that the tracking error under the AFNTSM control can be settled down significantly faster than the ASM control using conventional sliding mode, especially in the case of external shock disturbance rejection as will be detailedly described in the next section.

4.2.2 Selection of control parameters

The AFNTSM controller has been presented with the adaptive estimation law for estimating the self-aligning torque. It is clear that the stability of the overall control system can be guaranteed in the sense of Lyapunov. Besides, the proposed AFNTSM controller possesses a satisfactory tracking accuracy and a faster convergence rate compared with the ASM controller. Nevertheless, all the control parameters of the AFNTSM controller still need to be selected carefully in practical implementation due to the existing of sensors' measuring noises, parametric uncertainties and unmodeled system dynamics in the system.

Selection of λ

It is manifest from (4.5) that the parameter λ crucially determines the tracking bandwidth of the sliding mode function and the decay rate of tracking errors on the sliding surface [115], [112]. Specifically, a smaller λ leads to a larger bandwidth implying a faster response rate and higher tracking accuracy. On the other hand, a larger bandwidth will also amplify the high-frequency measurement noises to the system. In practical implementation, the measurement noises and the time delay related to the experimental setup dominate the minimum applicable λ [115]. Considering these factors, we choose $\lambda = 0.065$ in our case.

Selection of r

From the last term of (4.9) we can see that only the range of $1 < r < 2$ can avoid the singularity problem commonly existing in terminal sliding mode related control [115]. According to the theoretical analysis, increasing the value of r can reduce the convergence time shown in (4.6) but at the cost of bringing extra sensor measuring noises, which may result in excessive chattering in the control input consequently. In order to compromise the convergence rate with the control smoothness, we set $r = 1.2$.

Selection of δ

The parameter δ is utilized to alleviate the control chattering normally existing in the standard non-singular terminal sliding mode control, and its range is usually set as $0 < \delta < 1$ [115]. It is apparently indicated from (4.10) that a larger δ leads to less chattering in the control input u_1 but at the cost of weaker

robustness against parametric uncertainties and unmodeled dynamics. From the actual implementation, $\delta = 0.9$ is found to be acceptable in our case.

Selection of η

The parameter η is the adaptation gain [112] in the proposed adaptation law as shown in (4.12). We can clearly see from the form of Lyapunov function V in (4.19) that the larger η is, the faster V converges to zero, namely, the faster $\hat{\xi}$ converges to ξ. This means that the value of η can critically determine the adaptation bandwidth. A larger η leads to a faster adaptation response implying a high tracking accuracy, but at the cost of more measurement noises added to the system. We find that $\eta = 2.4 \times 10^6$ can work appropriately in the actual implementation.

Selection of g_1 and g_2

The values of g_1 and g_2 should be positive. Besides, there is no restriction on whether they should be constants or time varying. In order to predict the bound of the tracking error, we set g_1 and g_2 as [115]:

$$\begin{aligned} g_1 =& 25\big[(h-1)\big|\ddot{\theta}_r - \frac{1}{\lambda r}|\dot{e}|^{2-r}\text{sign}(\dot{e})\big| + \frac{1}{J_0}\bar{\psi}\big] \\ g_2 =& 15\big[(h-1)\big|\ddot{\theta}_r - \frac{1}{\lambda r}|\dot{e}|^{2-r}\text{sign}(\dot{e})\big| + \frac{1}{J_0}\bar{\psi}\big] \end{aligned} \tag{4.41}$$

implied by (4.15)–(4.18).

4.3 Controllers for comparison

To demonstrate the great advantages of the proposed AFNTSM controller, a conventional fast non-singular terminal sliding mode (FNTSM) controller and an adaptive sliding mode (ASM) controller are also designed according to the methods employed in [115], [151], respectively. The conventional FNTSM controller is compared to illustrate the higher tracking accuracy of the AFNTSM controller owing to the accurate estimation for self-aligning torques, and the ASM controller is compared to verify the faster convergence rate of the AFNTSM controller. Here, the design results are straightly given for simplicity.

4.3.1 Fast non-singular terminal sliding mode control

The control input of the FNTSM controller without adaptation [115] is given by

$$u_{FNTSM} = u_0 + u_1 \tag{4.42}$$

where u_0 and u_1 are defined in (4.9) and (4.10), respectively. Note that in the conventional FNTSM control, the self-aligning torque cannot be adaptively estimated and compensated effectively. Thus, we regard the self-aligning torque as an external disturbance in the FNTSM control system, and define ψ_{FNTSM} which corresponds to the parameter ψ in (4.1) as

$$\psi_{FNTSM} = (c - c_0)\dot{x} + (\rho - \rho_0)\text{sign}(\dot{x}) + \tau. \tag{4.43}$$

Then, the upper bound of ψ_{FNTSM} is given by

$$\bar{\psi}_{FNTSM} = \bar{\Delta}_c|\dot{x}| + \bar{\Delta}_\rho + \bar{\tau} \tag{4.44}$$

where $\bar{\Delta}_c$ and $\bar{\Delta}_\rho$ are defined in (2.24), and $\bar{\tau}$ represents the upper bound of the self-aligning torque τ, whose value is set as

$$\bar{\tau} = 270 \text{ Nm}. \tag{4.45}$$

4.3.2 Adaptive sliding mode control

The ASM controller [151] is designed as:

$$\begin{aligned} u_{ASM} =& \frac{1}{b}\Big\{ J_0\varpi\dot{e}_{ASM} + J_0\ddot{x}_r + c_0\dot{x} + \rho_0\text{sign}(\dot{x}) \\ &+ \epsilon s_{ASM} + \big[\bar{\Delta}_J\varpi|\dot{e}_{ASM}| + \bar{\Delta}_J|\ddot{x}_r| + \bar{\Delta}_c|\dot{x}| \\ &+ \bar{\Delta}_\rho\big]\text{sign}(s_{ASM}) + \tilde{\xi}\tanh(x)\Big\} \end{aligned} \tag{4.46}$$

where $\epsilon > 0$, and $e_{ASM} = x_r - x$ represents the tracking error under the ASM control. In (4.46), $\tilde{\xi}$ denotes the estimation of the coefficient ξ under the ASM control, whose adaptation law is given by

$$\frac{d(\tilde{\xi})}{dt} = \frac{\mu_2\epsilon}{J_0}\tanh(x)s_{ASM} + \mu_2\tanh(x)\dot{s}_{ASM} \tag{4.47}$$

with $\mu_2 > 0$, and s_{ASM} the sliding variable under the ASM control defined as

$$s_{ASM} = \dot{e}_{ASM} + \varpi e_{ASM} \tag{4.48}$$

where $\varpi > 0$.

Accounting for our plant model as given in (2.13), the values of these control parameters under the ASM control are selected as

$$\varpi = 15, \quad \epsilon = 45, \quad \mu_2 = 2640. \tag{4.49}$$

4.4 Simulation results

Before the experimental implementation of the designed AFNTSM controller, we study the simulation results for evaluating the controller performance. In this section, simulation of the AFNTSM controller, the FNTSM controller and the ASM controller is carried out by MATLAB Simulink, simulation results are compared and analyzed. In order to demonstrate the superiority of the proposed AFNTSM controller in terms of high tracking precision, strong robustness against varying road conditions and fast convergence rate, two cases with the variations of road conditions are considered.

4.4.1 Case 1: slalom path following in various road conditions

We maneuver the steering wheel shown in Figure 2.1(b) to generate a reference command that is approximate to a sinusoidal waveform as a simulation of a slalom path for the vehicle to track. The angle signal collected by the sensor installed on the steering wheel is the steering angle of the steering wheel. Multiplying this sensor signal by a scale factor accounting for the angle transmission from the steering wheel to the front wheels, we can get the reference angle for the controllers that are under test. To demonstrate the AFNTSM controllers' robustness against various road conditions, a time-varying coefficient of the self-aligning torque ξ is

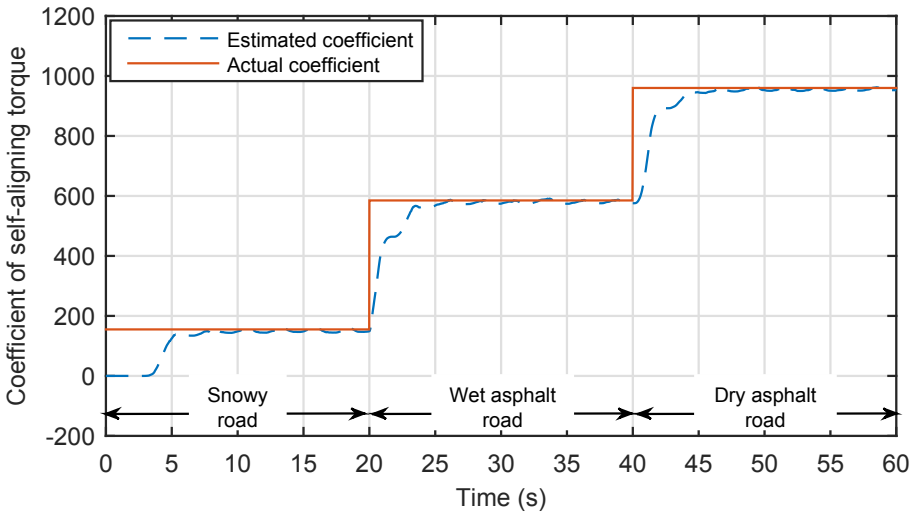

Figure 4.1: Simulated estimated coefficient of the self-aligning torque under the AFNTSM controller in Case 1.

given by

$$\xi = \begin{cases} 158, & 0 < t \leq 20\,\text{s}, \quad \text{Snowy road} \\ 590, & 20 < t \leq 40\,\text{s}, \quad \text{Wet asphalt road} \\ 966, & 40 < t \leq 60\,\text{s}, \quad \text{Dry asphalt road} \end{cases} \tag{4.50}$$

to represent three different road surfaces on which the front wheels will be exerted by different self-aligning torques. The simulation results in this case are shown in Figures 4.1–4.3.

From Figure 4.1 we can see that the adaptive estimation law in the developed AFNTSM controller can estimate the coefficient of self-aligning torque precisely. There exists some very slight chattering in the line of the 'Estimated coefficient', which is mainly caused by the sensor measurement noises existing in the reference signal. As shown in Figure 4.2, the peak tracking errors of the AFNTSM controller is about -0.008 rad, which occur at the beginning of the changes of road conditions due to the adaptive learning procedure of the adaptive estimation law. Once the estimation of the self-aligning torque disturbance is finished, the tracking error can

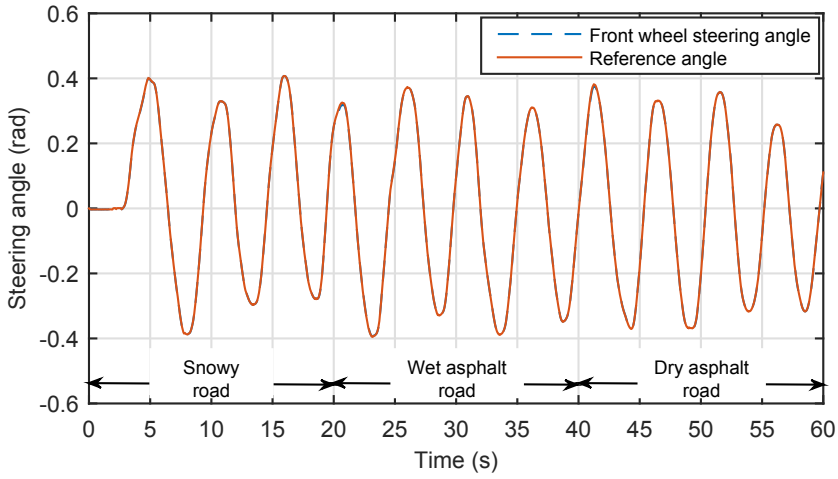

(a)

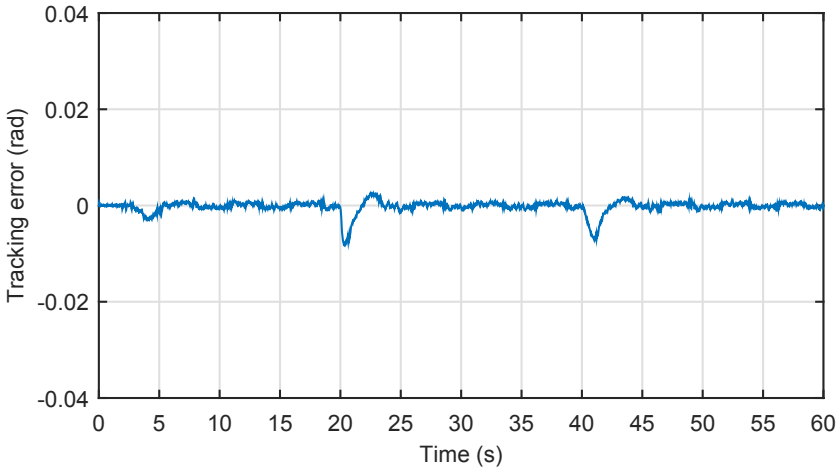

(b)

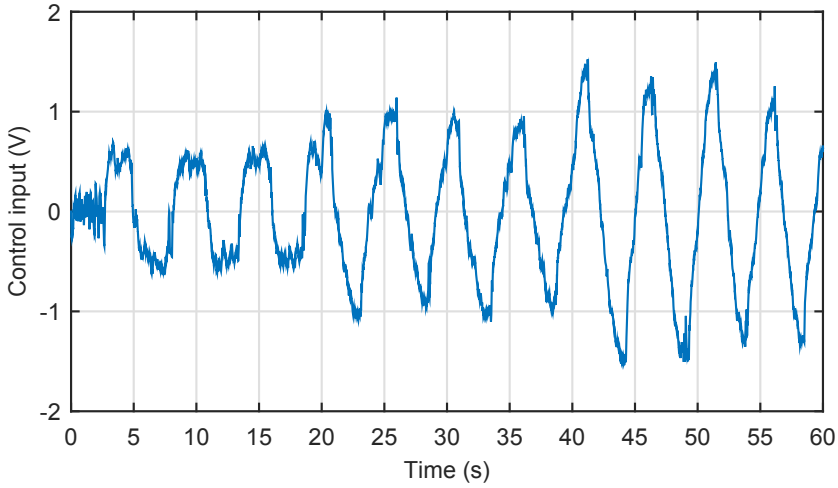

(c)

Figure 4.2: Simulated control performance of the AFNTSM controller in Case 1. (a) Tracking profile. (b) Tracking error. (c) Control input.

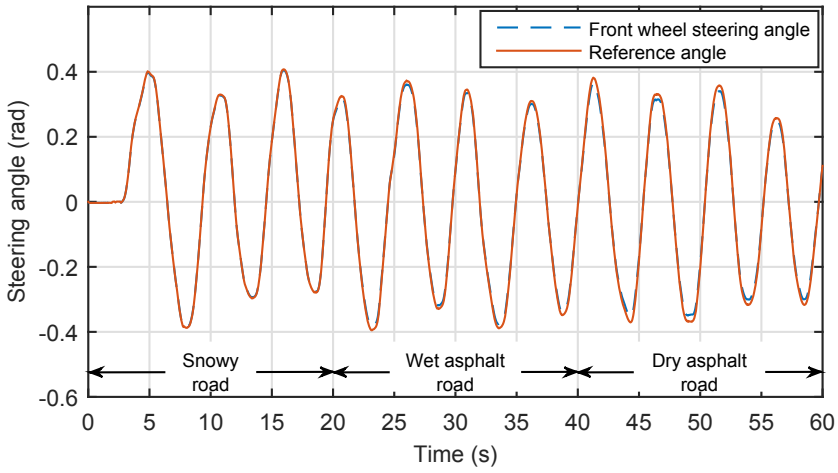

(a)

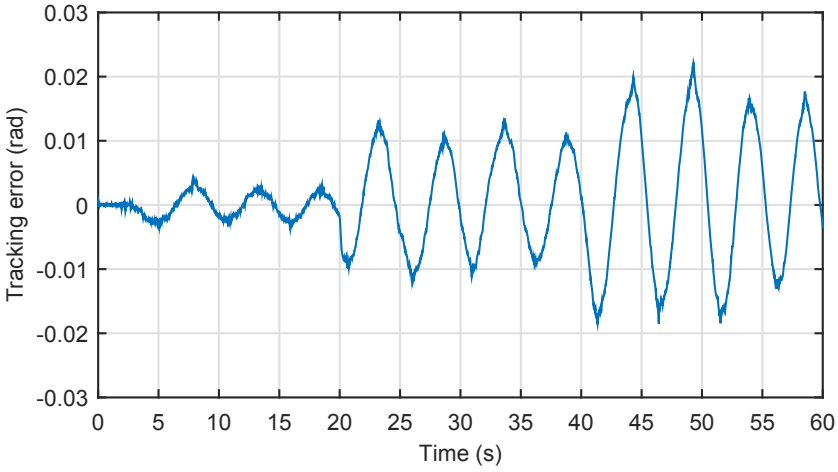

(b)

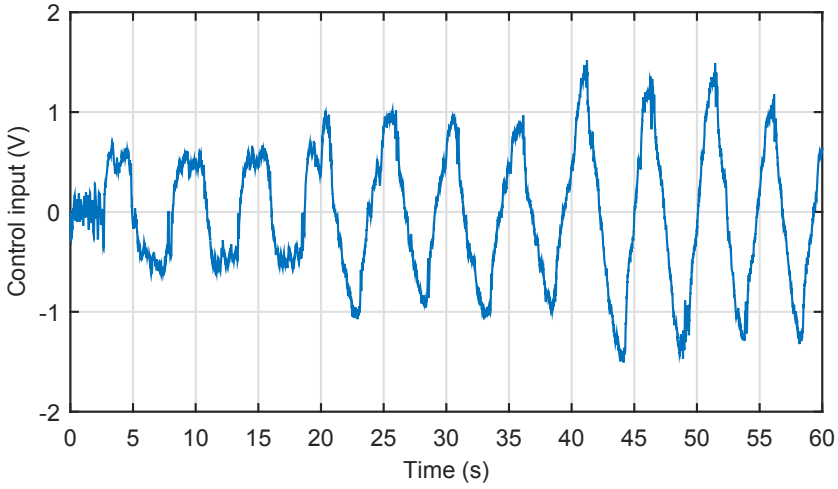

(c)

Figure 4.3: Simulated control performance of the conventional FNTSM controller in Case 1. (a) Tracking profile. (b) Tracking error. (c) Control input.

converge to a very small region (close to zero). However, in the simulation performance of the FNTSM controller as shown in Figure 4.3, the peak tracking errors in the three periods are 0.005 rad, 0.014 rad and 0.02 rad, respectively. Besides, the steady state errors of the FNTSM controller get increased with the increasing of self-aligning torques due to the lack of effective estimation and compensation of the self-aligning disturbance. Hence, the superiority of the AFNTSM controller in the aspect of high tracking accuracy has been indicated compared with the FNTSM controller.

4.4.2 Case 2: external shock disturbance rejection

In reality, it is very common for a vehicle to come across external shock disturbances such as small bumps on road or road edges which are higher than the road surface. By the effect of these shock disturbance, the steering angles of a running vehicle's front wheels will deviate from the original one in a sudden. Thus, whether the designed controller can force the front wheel steering angle to converge to the original one fast enough is an important factor to evaluate the performance of an SbW system. In this case, simulation of shock disturbance rejection with a duration of 10 s is carried out for the AFNTSM controller and the ASM controller. The reference command for the controllers is set as zero to approximately represent that the vehicle is running in a straight path without any steering. To exclude the impact of the road conditions and focus on the rejection on shock disturbances, the road condition is assumed to be constant, and the coefficient of the self-aligning torque is set as $\xi = 158$.

The simulation results of the AFNTSM controller and the FNTSM controller in

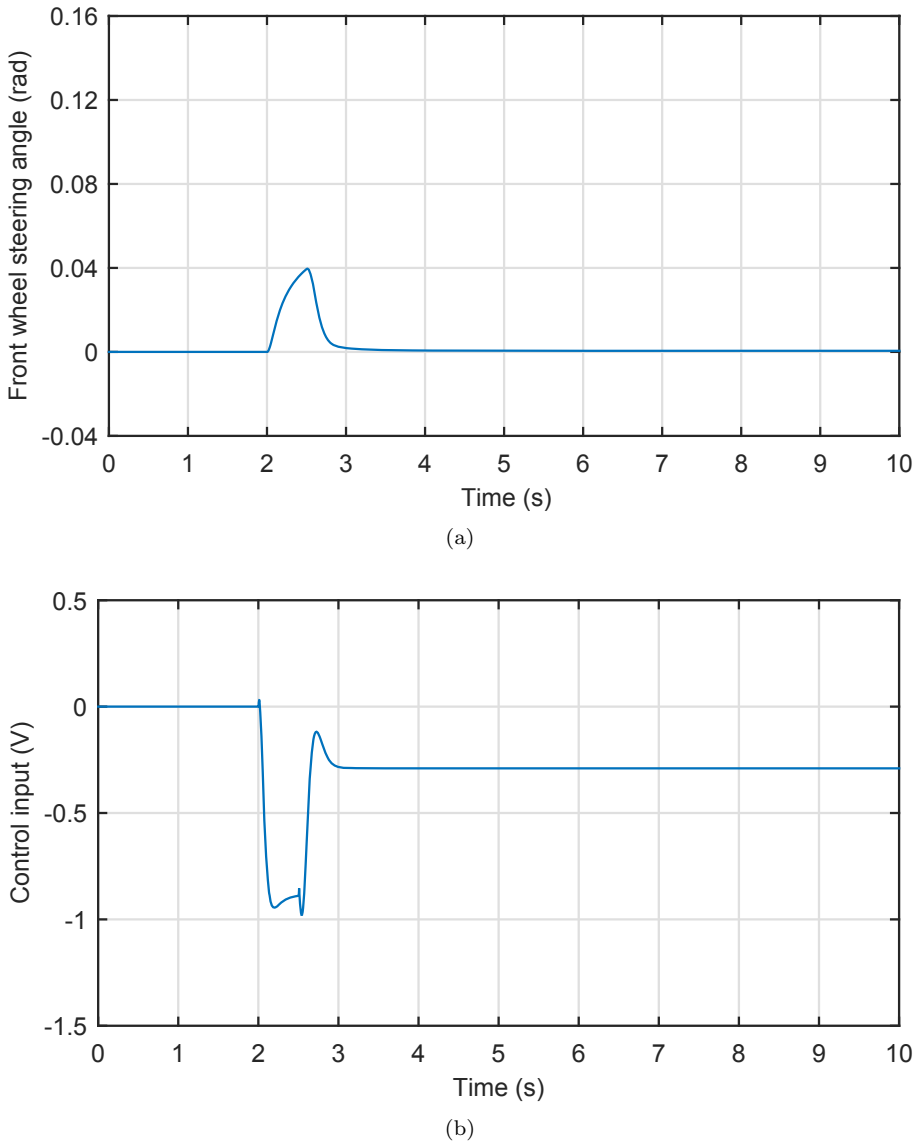

Figure 4.4: Simulated control performance of the AFNTSM controller in Case 2. (a) Tracking profile. (b) Control input.

the case of shock disturbance rejection are shown in Figures 4.4–4.5. From Figure 4.4 we can see that the peak tracking error is 0.04 rad, and it takes about just one second (the 2nd second to the 3rd second) for the tracking error to converge to zero. However, in the simulation result of the ASM controller as shown in Figure 4.5, the peak tracking error is 0.13 rad, and it takes about 4 seconds (2nd second to 6th second) for the tracking error to converge to zero. Thus, the superiority of the designed AFNTSM controller has been indicated in this case compared with

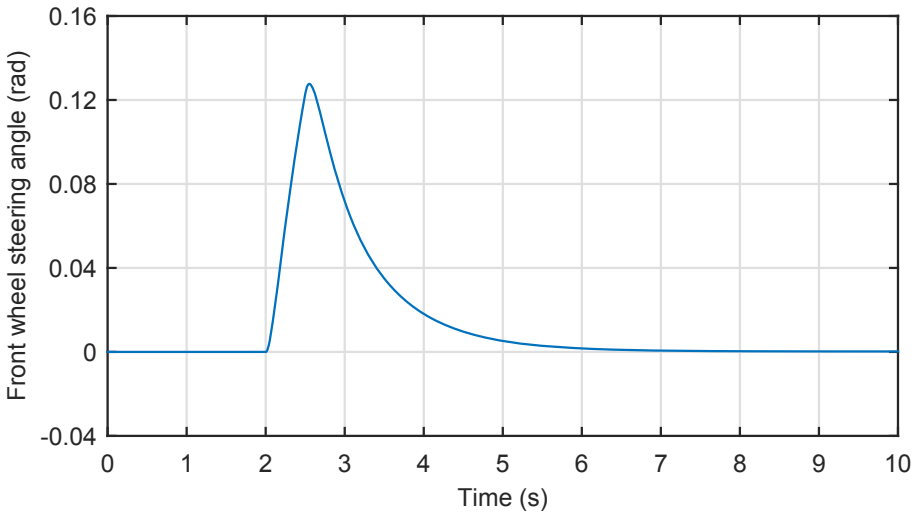

(a)

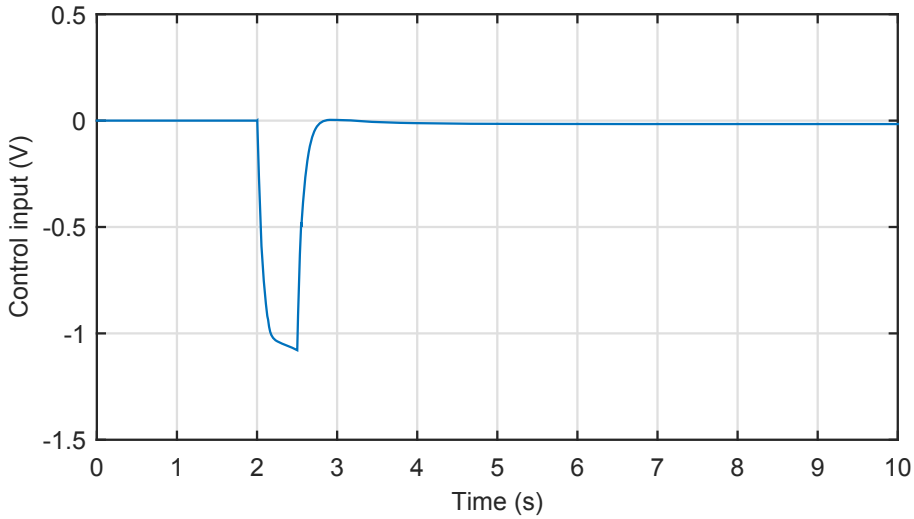

(b)

Figure 4.5: Simulated control performance of the ASM controller in Case 2. (a) Tracking profile. (b) Control input.

the ASM controller in terms of smaller tracking errors and faster convergence rate.

4.5 Experimental results

In this section, we carry out the experiments on the actual SbW experimental setup to verify the designed controllers with a sampling period of 1 ms. In order to show that the designed AFNTSM controller can be effectively implemented on

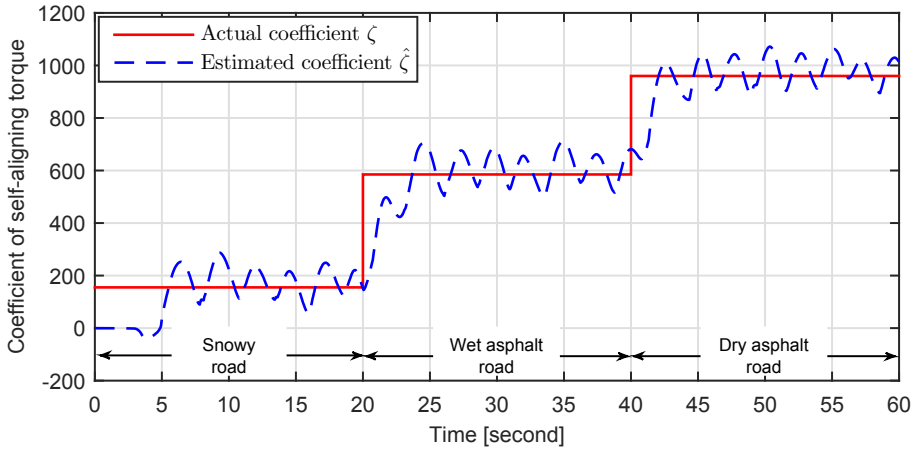

(a)

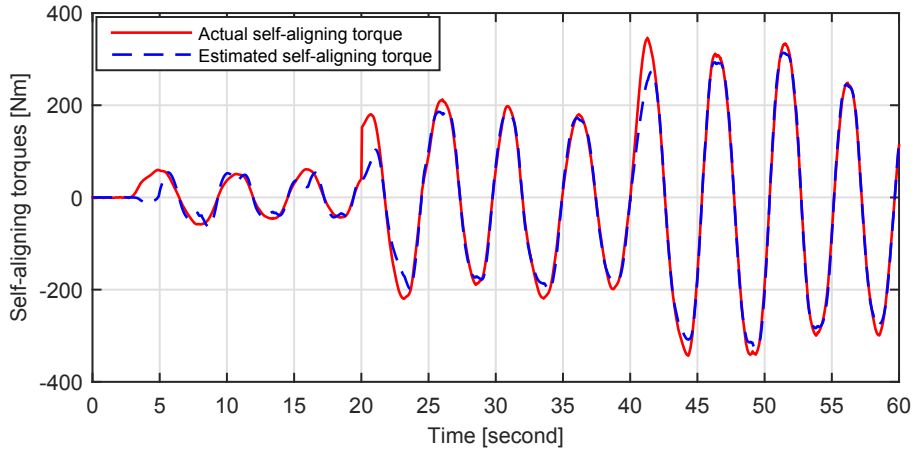

(b)

Figure 4.6: Experimental adaptive estimation results under the AFNTSM control in Case 1. (a) Estimated coefficient of the self-aligning torque $\hat{\xi}$. (b) Estimated self-aligning torque.

the SbW experimental platform and can also possess similar superiority indicated in the simulation results, identical cases with the same reference commands and road conditions as those in the simulation are considered in this section.

It is manifest from Figure 4.6(a) that the designed adaptation law is able to estimate the time-varying coefficient of the self-aligning torque ξ in relation to the variation of road conditions appropriately. We can see that there is more chattering in the line of the estimated coefficient $\hat{\xi}$ compared with the simulation result as shown in Figure 4.1. The main reason for the chattering may be the effect of the

measurement noises introduced by the angle sensors installed on the steering wheel and the pinion-and-rack system. Despite that there is chattering in the estimated coefficient, the estimated self-aligning torque is fairly close to the actual one as shown in Figure 4.6(b).

The superiority of the AFNTSM controller in the aspect of high tracking accuracy to the conventional FNTSM controller without effective estimation of the self-aligning torque is evidently indicated in Figures 4.7–4.8. The experimental results are similar to the simulation results shown in Figures 4.2–4.3, which have more chattering caused by sensor measurement noises. We can see from Figure 4.7 that the peak tracking errors of the AFNTSM controller during the three periods of different road conditions are 0.012 rad, 0.018 rad and 0.016 rad, respectively. The peak tracking errors of the second and the third periods appear at the beginning of the changes of the road conditions, when the new value of ξ starts to appear to be estimated by the adaptation law. No matter how large the self-aligning torque is, the tracking errors can converge into a small region if the estimated coefficient of the self-aligning torque $\hat{\xi}$ is in the region close to the actual one ξ. In addition, due to the fast-convergence characteristic of the AFNTSM controller, the peak tracking errors can converge to the steady ones in a very short time. Thus, there is almost no apparent difference between the values of the peak errors and the steady ones.

As a comparison, the corresponding peak tracking errors under the conventional FNTSM control shown in Figure 4.8 are 0.011 rad, 0.021 rad and 0.03 rad, respectively. Furthermore, we can see that the steady state tracking errors of the conventional FNTSM controller are not as small as the ones under the AFNTSM control stabilizing at 0.01 rad approximately regardless of the change of road con-

ditions, but deteriorate with the increasing of the self-aligning torque. These all illustrate the advantages of the AFNTSM control over the FNTSM control.

It is also noted that the chattering phenomenon existing in the AFNTSM control is less severe than that in the FNTSM control. The main reason for this can be explained by that the control input of the FNTSM controller given by (4.42) has a larger $\bar{\psi}_{FNTSM}$ than the parameter $\bar{\psi}$ in the AFNTSM controller, which is shown in (4.2) and (4.44). Based on the definition of g_1 and g_2 as shown in (4.41), we can see that the FNTSM controller thus has larger g_1 and g_2 than those of the AFNTSM controller. Larger g_1 and g_2 lead to a faster convergence rate of tracking errors but at the cost of more chattering. Therefore, the chattering existing in the FNTSM control is more obvious than that of the AFNTSM control.

As shown in Figure 2.1, our experimental setup cannot be tested on real roads yet to come across a preliminarily placed obstruction. Moreover, the tests will be carried out on both the AFNTSM and ASM controllers. Thus, the external shock disturbances acting on them should be the same for a fair comparison. For these reasons, we artifically generate a pulse signal and add it to the control inputs of both the AFNTSM and ASM controllers. In this way, the pulse signal will behave as shock disturbance. The pulse signal has an amplitude of 1.2 V, a width of 0.5 s and starts at the 2nd second during the experiment.

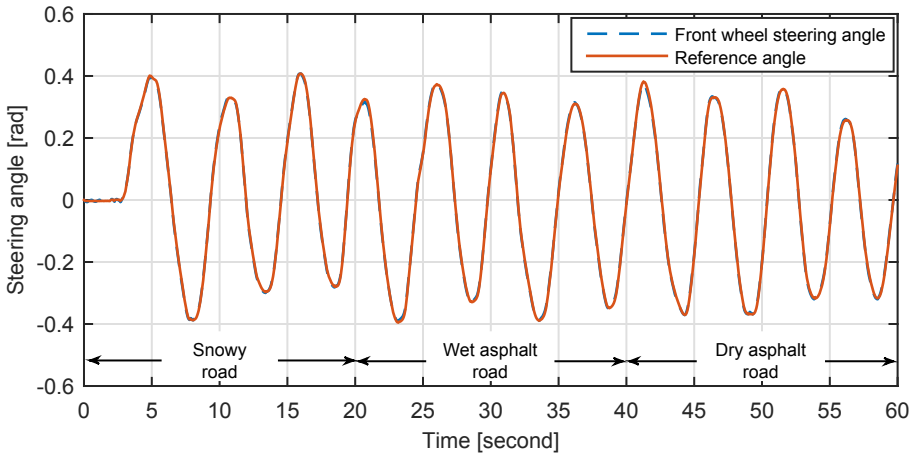

(a)

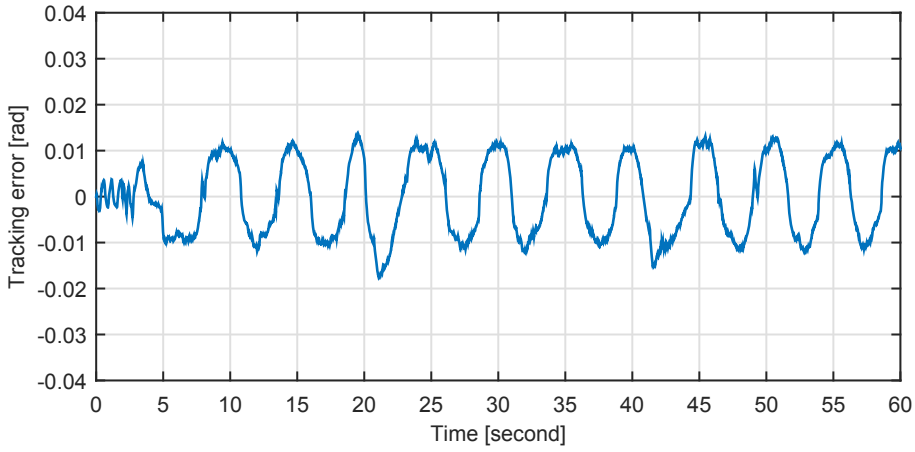

(b)

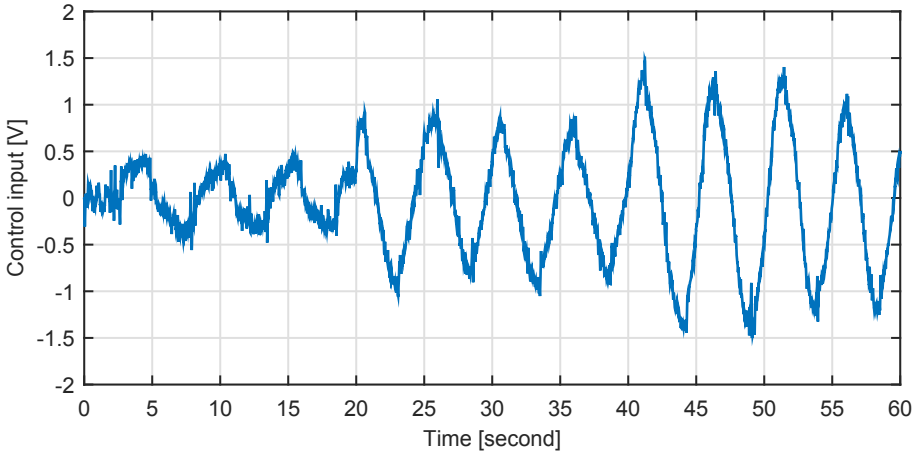

(c)

Figure 4.7: Experimental control performance of the AFNTSM controller in Case 1. (a) Tracking profile. (b) Tracking error. (c) Control input.

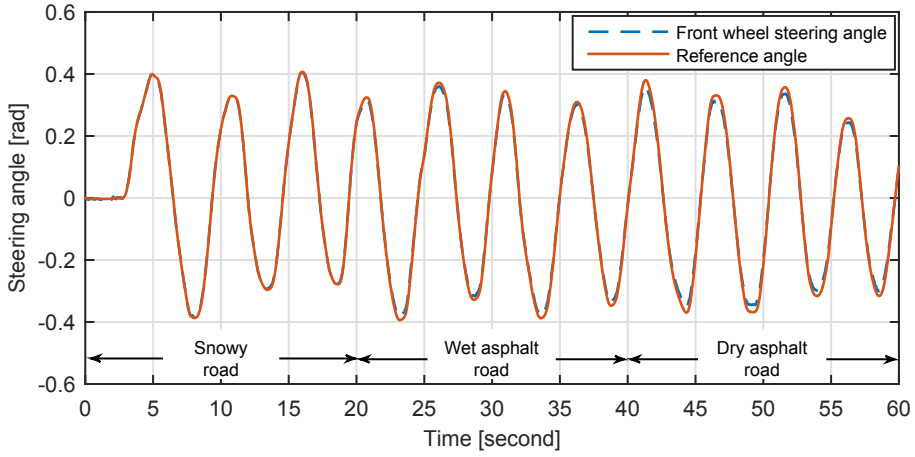

(a)

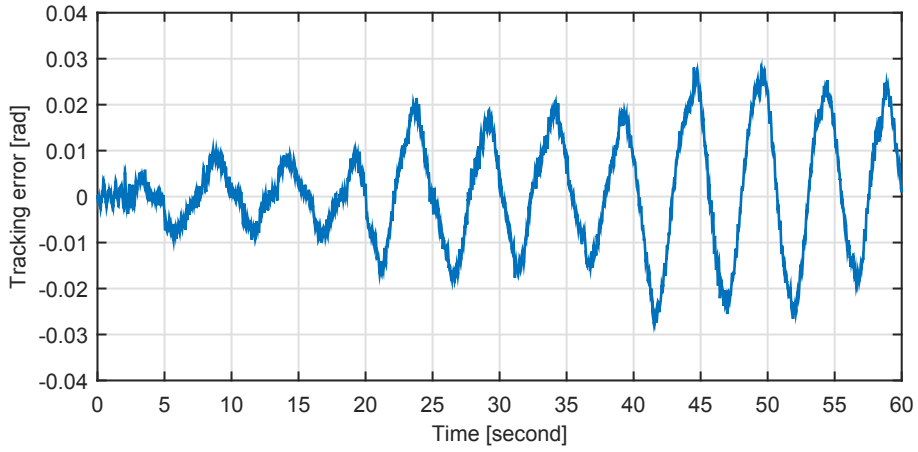

(b)

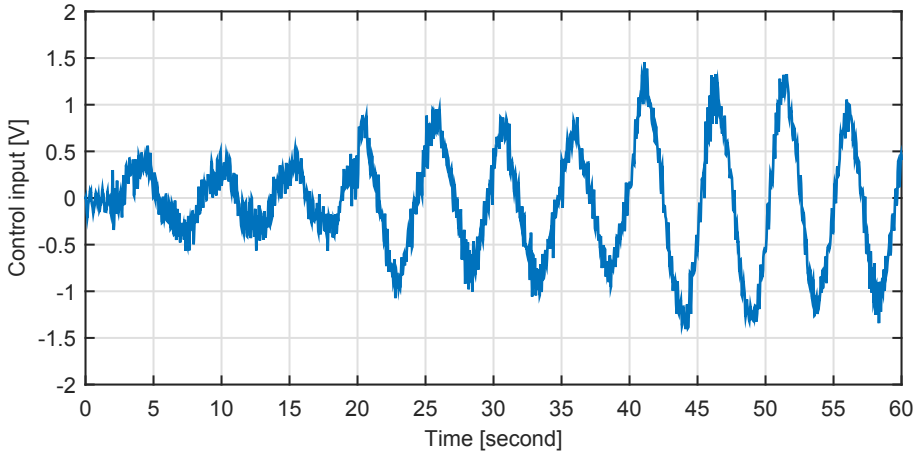

(c)

Figure 4.8: Experimental control performance of the conventional FNTSM controller in Case 1. (a) Tracking profile. (b) Tracking error. (c) Control input.

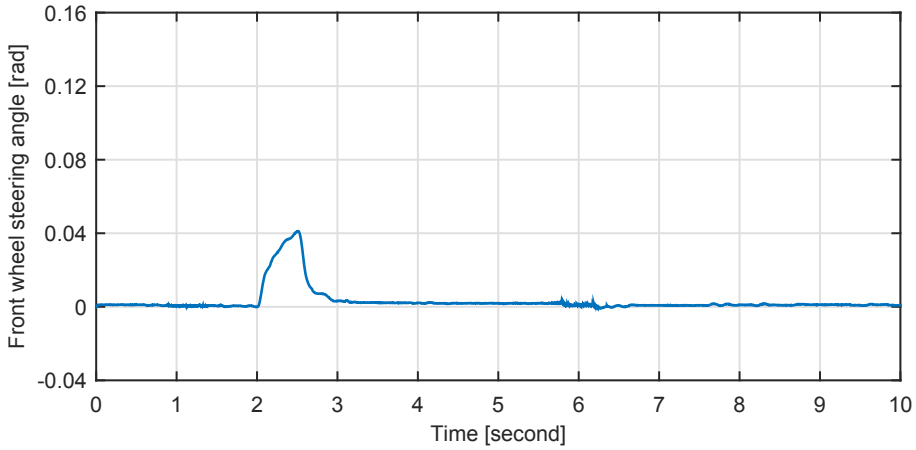

(a)

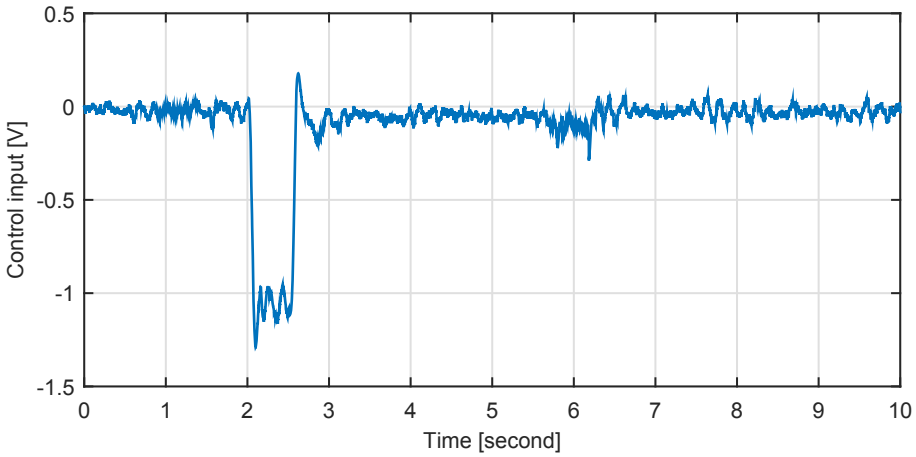

(b)

Figure 4.9: Experimental control performance of the AFNTSM controller in Case 2. (a) Tracking profile. (b) Control input.

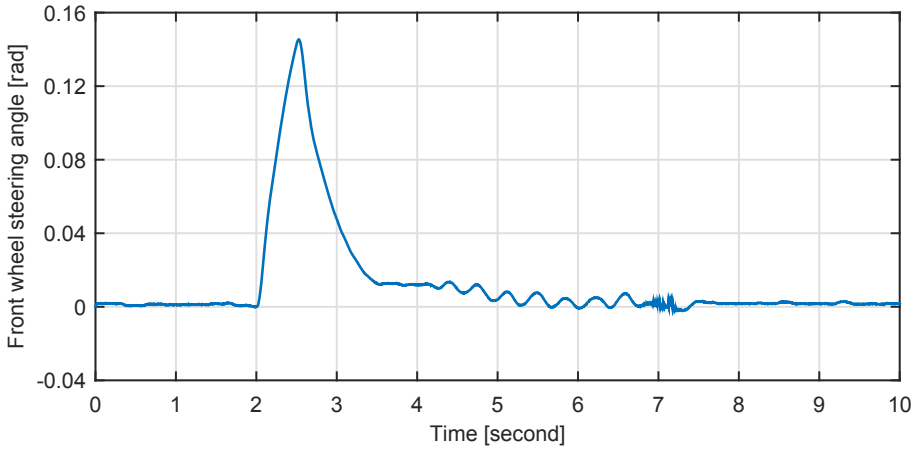

(a)

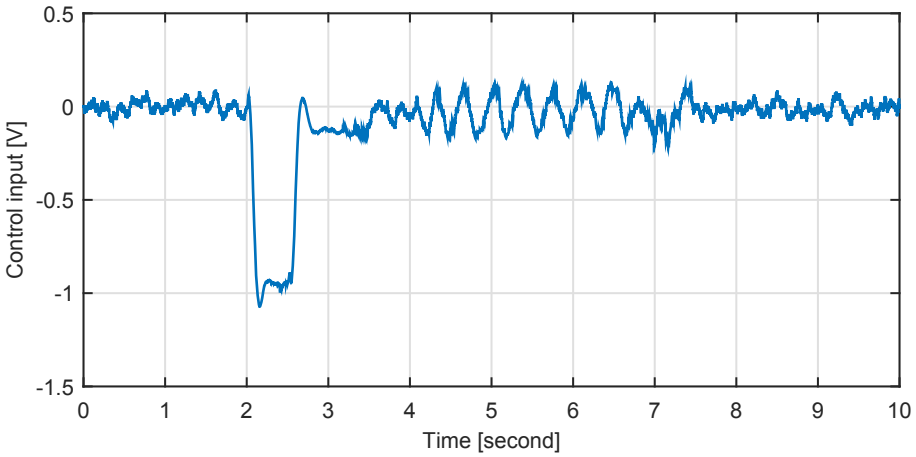

(b)

Figure 4.10: Experimental control performance of the ASM controller in Case 2. (a) Tracking profile. (b) Control input.

The experimental results of the AFNTSM and ASM controllers in rejecting external shock disturbances are shown in Figures 4.9–4.10. The experimental results are close to the simulation results as shown in Figures 4.4–4.5 but with more chattering due to sensor measurement noises. The peak tracking error under the AFNTSM control is about 0.04 rad, which is much less than that of the ASM controller whose value is almost 0.15 rad. More significantly, the convergence rate of the AFNTSM controller is much faster than that of the ASM controller. Within just one second (from the 2nd second to the 3rd second), the AFNTSM controller can force the tracking error to converge to almost zero. However, it takes nearly 5 seconds (from the 2nd second to the 7th second) for the tracking error of the ASM controller to converge to zero. In addition, from the 4th second to the 7th second, there exists non-negligible chattering in the control input of the ASM controller, which consequently results in the oscillations of the front wheels that ought to stay in a steady state. Thus, the superiority of the AFNTSM controller in terms of fast convergence rate and control smoothness has also been verified in comparison with the ASM controller.

4.6 Summary

In this chapter, an AFNTSM control methodology combining the FNTSM control and the adaptive estimation law is developed for the SbW system such that the control system can not only estimate and compensate for the self-aligning torque disturbance effectively, but also force the tracking error to converge fast in external shock disturbance rejection. The stability of the AFNTSM control

system is proved in the sense of Lyapunov. Furthermore, the selection guidelines of the control parameters are elaborated to tradeoff among measurement noises, unmodeled dynamics and expected control performance in practice. Finally, experimental results are shown to demonstrate the superiority of the AFNTSM controller with higher tracking accuracy and faster convergence rate in comparison with the conventional FNTSM controller and the ASM controller. However, the proposed AFNTSM controller requires an accurate plant model of the SbW system, which motivates us to develop a sliding mode-based active disturbance rejection controller that is less dependent on the accuracy of plant models.

Chapter 5

Sliding Mode-based Active Disturbance Rejection Control

In Chapters 3 and 4, an ASM control law and an AFNTSM control law have been proposed to effectively estimate and compensate for the self-aligning torque, and satisfactory performances are obtained. However, the controllers are designed based on a self-aligning torque dynamical model. The self-aligning torque mathematical model we used is a simplified one on the basis of small slip angle assumption. In reality, the self-aligning torque model is much more complicated with respect to many factors such as vehicle speed and yaw rate. Hence, a control methodology that is less dependent on the accurate mathematical models of self-aligning torque and other frictions is necessary in our case, which motivates us to design an active disturbance rejection controller for our SbW system.

5.1 Introduction

As an effective control methodology which has been widely used in numerous aspects in industry, active disturbance rejection control (ADRC) plays a pivotal role in nonlinear control, especially for the plant models with unknown or unmodeled disturbance dynamics. With ADRC, the unknown disturbances can be estimated and compensated actively, which enhances the robustness of the feedback control loop, and makes the controller less dependent on accurate mathematical models of the physical dynamics.

In [152], linear active disturbance-rejection control is investigated. It is shown that linear active disturbance-rejection control structure can be changed to a two-degree-of-freedom internal model control structure, and the widely adopted bandwidth-tuning method for linear active disturbance-rejection control is equivalent to tuning the two time constants of the setpoint filter and the disturbance-rejection filter in internal model control. In [153], a model-independent controller based on the active disturbance rejection control technique, which can estimate and compensate model uncertainties and unknown disturbances in real time, is designed for a bidirectional Buck-Boost converter control in flywheel energy storage system. In [154], a linear active disturbance rejection controller and a hybrid position estimation strategy combining the high-frequency current injection for low-speed region with the electromotive force estimation for high-speed region are integrated into the same control structure which is applied for sensorless control of internal permanent-magnet synchronous motors.

In the SbW control system, the self-aligning torque is the main disturbance

existing in the plant model. And the dynamic model of self-aligning torques is very complicated and usually time-varying. Thus, in order to estimate the self-aligning torque disturbance, we design an active disturbance rejection controller with an extended state observer for road vehicle SbW systems.

5.2 Control design

In this section, the plant model of the SbW system is reformulated in state space, and a nonlinear extended state observer is designed for states observation. A sliding mode-based active disturbance rejection control (SMADRC) law is proposed for the SbW system, and the stability of the control system is proved in the sense of Lyapunov. Based on experimental implementations, the selections of control parameters are also elaborated.

5.2.1 Reformulation of plant model

According to (2.13), the plant model of the SbW system has been given by

$$J\ddot{x} + c\dot{x} + \rho\text{sign}(\dot{x}) + \tau = bu \tag{5.1}$$

In (5.1),

$$\begin{aligned} J &= J_0 + \Delta_J \\ c &= c_0 + \Delta_c \\ \rho &= \rho_0 + \Delta_\rho. \end{aligned} \tag{5.2}$$

where J_0, c_0 and ρ_0 are the nominal values of the parameters J, c and ρ; Δ_J, Δ_c and Δ_ρ are the corresponding parametric uncertainties.

Considering the parametric uncertainties, we rewrite the plant model as

$$J_0\ddot{x} + c_0\dot{x} + \rho_0 \text{sign}(\dot{x}) + \Delta + \tau = bu \tag{5.3}$$

where

$$\Delta = \Delta_J\ddot{x} + \Delta_c\dot{x} + \Delta_\rho \text{sign}(\dot{x}). \tag{5.4}$$

In (5.4), Δ can be regarded as the lumped uncertainties of the plant model; Δ_J, Δ_c and Δ_ρ are the parametric uncertainties of the parameters J, c and ρ as defined in (2.24). Setting $y_1 = x$, $y_2 = \dot{x}$, and rewriting the plant model (5.3) yields

$$\begin{cases} \dot{y}_1 = y_2 \\ \dot{y}_2 = F(y_1, y_2, t) + \kappa u \end{cases} \tag{5.5}$$

where

$$\begin{aligned} F(y_1, y_2, t) = & -\frac{c_0}{J_0}\dot{x} - \frac{\rho_0}{J_0}\text{sign}(\dot{x}) - \frac{\Delta}{J_0} - \frac{\xi}{J_0}\tanh(x) \\ \kappa = & \frac{b}{J_0}. \end{aligned} \tag{5.6}$$

From now on, we will use (5.6) as the plant model for observer and controller design.

5.2.2 Extended state observer design

To deal with the strong nonlinearity of the SbW system and estimate the plant states accurately, a nonlinear extended-state observer is introduced here. We use an extended state y_3 to represent the unknown nonlinear term $F(y_1, y_2, t)$ which is continuously differentiable and bounded, namely, $F(y_1, y_2, t) = y_3$. Then

the plant model of the SbW system can be rewritten as

$$\begin{cases} \dot{y}_1 = y_2 \\ \dot{y}_2 = y_3 + \kappa u \\ \dot{y}_3 = \gamma(t) \end{cases} \tag{5.7}$$

where $\gamma(t)$, i.e., the derivative of y_3, is bounded in practice. The conditions of $(y_1, y_2) = (0, 0)$ and $(\dot{y}_1, \dot{y}_2) = (0, 0)$ yields $\gamma(t) = 0$. Then, by defining $e_1 = v_1 - y_1$, we can express the nonlinear extended state observer in the following form [155]

$$\begin{cases} \dot{v}_1 = v_2 - \alpha_1 e_1 \\ \dot{v}_2 = v_3 - \alpha_2 \text{fal}(e_1, \delta_1, \psi) + \kappa u \\ \dot{v}_3 = -\alpha_3 \text{fal}(e_1, \delta_2, \psi) \end{cases} \tag{5.8}$$

where v_1, v_2 and v_3 are the estimations of y_1, y_2 and y_3; α_1, α_2 and α_3 are observer gains. The expression of the function $\text{fal}(e, \delta, \psi)$ is given by

$$\text{fal}(e, \delta, \psi) = \begin{cases} e/\psi^{1-\delta} & |e| \leq \psi \\ \\ |e|^{\delta}\text{sign}(e) & |e| > \psi \end{cases} \tag{5.9}$$

where the parameters $\psi > 0$ and $0 < \delta < 1$ are control parameters to be selected to affect the observing performance of the designed nonlinear extended state observer.

For simplicity, $\text{fal}(e_1, \delta_1, \psi)$ and $\text{fal}(e_1, \delta_2, \psi)$ are expressed by $f_1(e_1)$ and $f_2(e_1)$, respectively, in the sequel.

Subtracting (5.8) from (5.7) yields the error system

$$\begin{cases} \dot{e}_1 = e_2 - \alpha_1 e_1 \\ \dot{e}_2 = e_3 - \alpha_2 f_1(e_1) \\ \dot{e}_3 = -\gamma(t) - \alpha_3 f_2(e_1) \end{cases} \tag{5.10}$$

where $e_j = v_j - y_j$, and $j = 1, 2, 3$.

Remark 1: The derivative of $f_1(e_1)$ is defined as $f_1{}'(e_1)$, and the derivative of $f_2(e_1)$ is defined as $f_2{}'(e_1)$. Note that $f_1{}'(e_1) > 0$ and $f_2{}'(e_1) > 0$ because the function of fal$(\cdot)$ is a monotonous increasing function.

Definition 5.1: If the region Λ is with the origin as the vertex, and all state trajectories of a system remaining in Λ after a specific time will finally converge to the origin, then the region Λ is called a self-stable region of a system.

Based on the error system as shown in (5.10), the following error functions are obtained:

$$\begin{aligned} n_2(e_1, e_2) &= e_2 - \alpha_1 e_1 + g_1 m_1(e_1)\text{sign}(e_1) \\ n_3(e_1, e_2, e_3) &= e_3 - \alpha_2 f_1(e_1) - \alpha_1(e_2 - \alpha_1 e_1) \\ &\quad + g_2 m_2(e_1, e_2)\text{sat}(n_2(e_1, e_2)/m_1(e_1)) \end{aligned} \tag{5.11}$$

where $m_1(e_1)$ and $m_2(e_1, e_2)$ are continuous and positive-definite, and $m_1(0) = 0$, $m_2(0, 0) = 0$ [155]. Note that the two constants g_1 and g_2 satisfy $g_1 > 1$ and $g_2 > 1$. Make region $\Lambda_3 = \{(e_1, e_2, e_3) : |n_3(e_1, e_2, e_3)| \leq m_2(e_1, e_2)\}$ and region $\Lambda_2 = \{(e_1, e_2, e_3) : |n_2(e_1, e_2)| \leq m_1(e_1)\}$. For simplicity, we denote $m_1(e_1)$ by m_1, $m_1\text{sig}(e_1)$ by $m_1\text{sig}$, $m_2(e_1, e_2)$ by m_2, $n_2(e_1, e_2)$ by n_2, and $n_3(e_1, e_2, e_3)$ by n_3.

Theorem 5.1 [155]: For the error system (5.10), if

$$m_2 > \frac{(g_1+1)^2}{g_2-1}\left|\frac{dm_1}{de_1}\right||n_2| \tag{5.12}$$

and there are proper gains α_1, α_2 and α_3 leading to $\dot{V}_{n_3m_2} < 0$, then the error system (5.10) is convergent. Moreover, the observed states v_1, v_2 and v_3 converge to the actual states y_1, y_2 and y_3.

Proof: We first consider a trajectory $(e_1, e_2, e_3) \in \Lambda_3$. According to the structure of Λ_3, we get

$$\begin{aligned}\alpha_2 f_1(e_1) + \alpha_1(e_2 - \alpha_1 e_1) - m_2(1 + g_2\text{sat}(n_2/m_1)) \leq e_3 \\ \leq \alpha_2 f_1(e_1) + \alpha_1(e_2 - \alpha_1 e_1) + m_2(1 - g_2\text{sat}(n_2/m_1)).\end{aligned} \tag{5.13}$$

Then we define

$$V_{n_2m_1} = \frac{1}{2}({n_2}^2 - {m_1}^2). \tag{5.14}$$

Consider that $V_{n_2m_1} \geq 0$. Differentiating $V_{n_2m_1}$ yields

$$\begin{aligned}\dot{V}_{n_2m_1} =& n_2(n_3 - g_2m_2\text{sat}(n_2/m_1)) \\ & \left(g_1n_2\frac{dm_1\text{sig}}{de_1} - m_1\frac{dm_1}{de_1}\right)(n_2 - g_1m_1\text{sig}).\end{aligned} \tag{5.15}$$

Since there exists $|n_3| \leq m_2$ in region Λ_3, we obtain

$$n_2(n_3 - g_2m_2\text{sat}(n_2/m_1)) \leq -(g_2-1)|n_2|m_2. \tag{5.16}$$

Then, the following inequality establishes:

$$\begin{aligned}\left(n_2 g_1 \frac{dm_1 \text{sig}}{de_1} - m_1 \frac{dm_1}{de_1}\right)(n_2 - g_1 m_1 \text{sig}) \\ \leq (g_1+1)^2 |n_2|^2 \left|\frac{dm_1}{de_1}\right|.\end{aligned} \tag{5.17}$$

Considering (5.16) and (5.17), we get

$$\dot{V}_{n_2 m_1} \leq -(g_2 - 1)|n_2| m_2 + (g_1+1)^2 |n_2|^2 \left|\frac{dm_1}{de_1}\right|. \tag{5.18}$$

According to $V_{n_2 m_1} \geq 0$ with $(e_1, e_2) \neq (0,0)$ and

$$m_2 > \frac{(g_1+1)^2}{g_2 - 1}\left|\frac{dm_1}{de_1}\right|\left|n_2\right| \tag{5.19}$$

there exists $\dot{V}_{n_2 m_1} < 0$. Therefore, trajectory (e_1, e_2) is drawn to region Λ_2. We call $(\tilde{e}_1, \tilde{e}_2)$ a limit point of a trajectory (e_1, e_2) if (e_1, e_2) reaches a point $(\tilde{e}_1, \tilde{e}_2)$ on the boundary of Λ_2 in infinite time, which leads to $\dot{V}_{n_2 m_1}(\tilde{e}_1, \tilde{e}_2) = 0$. We can obtain $(\tilde{e}_1, \tilde{e}_2) = (0,0)$ because that the origin is the only point on the boundary of Λ_2 that makes $\dot{V}_{n_2 m_1} = 0$. The trajectory of (e_1, e_2) will either straightforwardly converge to the origin or reach the boundary in finite time and enter into region Λ_2. Thus, considering that the trajectory (e_1, e_2) has already been in λ_2 after a certain time and the structure of Λ_2, we have the following inequality:

$$\begin{aligned}\alpha_1 e_1 - m_1(1 + g_1 \text{sign}(e_1)) \leq e_2 \\ \leq \alpha_1 e_1 + m_1(1 - g_1 \text{sign}(e_1)).\end{aligned} \tag{5.20}$$

Define

$$V_1 = \frac{1}{2} {e_1}^2 \tag{5.21}$$

Then, the first-order derivative of V_1 is given by

$$\dot{V}_1 = e_1\dot{e}_1 = e_1(e_2 - \alpha_1 e_1) \leq -(g_1 - 1)|e_1|m_1. \tag{5.22}$$

Hence, there exists $e_1 \neq 0$ leading to $\dot{V}_1 < 0$, and $e_1 \to 0$ is satisfied. We also obtain $e_2 \to 0$ according to the structure of Λ_2. Moreover, $e_3 \to 0$ can be obtained from (5.13). Region Λ_3 is the self-stable region of system (5.10) according to the definition, and the trajectories in Λ_3 will eventually converge to the origin.

Lastly, we consider the situation that the trajectory of (e_1, e_2, e_3) is outside Λ_3, namely, $V_{n_3m_2} \geq 0$. Supposing $|\gamma(t)| < \Gamma$ in (5.10), we define

$$V_{n_3m_2} = \frac{1}{2}({n_3}^2 - {m_2}^2). \tag{5.23}$$

Then the first-order derivative of $V_{n_3m_2}$ is given by

$$\begin{aligned}\dot{V}_{n_3m_2} =& n_3\left(\frac{\partial n_3}{\partial e_3}\dot{e}_3 + \frac{\partial n_3}{\partial e_2}\dot{e}_2 + \frac{\partial n_3}{\partial e_1}\dot{e}_1\right) \\ &- m_2\left(\frac{\partial m_2}{\partial e_2}\dot{e}_2 + \frac{\partial m_2}{\partial e_1}\dot{e}_1\right).\end{aligned} \tag{5.24}$$

We define

$$m_2 = \begin{cases} g_3|n_2|, & |n_2| \geq m_1 \\ \\ g_3 m_1, & |n_2| < m_1 \end{cases} \tag{5.25}$$

where g_3 is a constant. Based on (5.19) and (5.25), we obtain the following inequality:

$$g_3 > \frac{(g_1 + 1)^2}{g_2 - 1}\left|\frac{dm_1}{de_1}\right|. \tag{5.26}$$

Then we have

$$m_2 \mathrm{sat}(n_2/m_1) = g_3 n_2. \tag{5.27}$$

Furthermore, the first-order derivative of $V_{n_3 m_2}$ is given by

$$\begin{aligned}
\dot{V}_{n_3 m_2} =& {n_3}^2(-\alpha_1 + g_2 g_3) \\
&+ n_2 n_3 \bigg(\alpha_1 g_2 g_3 - {g_2}^2 {g_3}^2 - \alpha_2 {f_1}'(e_1) \\
&+ g_1 g_2 g_3 \frac{dm_1 \mathrm{sig}}{de_1} \bigg) - m_1 \mathrm{sig} n_3 \bigg(\alpha_3 \frac{|f_3(e_1)|}{m_1} \\
&- \alpha_2 g_1 {f_1}'(e_1) + {g_1}^2 g_2 g_3 \frac{dm_1 \mathrm{sig}}{de_1} \bigg) \\
&+ n_3 \gamma(t) - m_2 n_3 \frac{\partial m_2}{\partial e_2} - m_2 n_2 \bigg(\alpha_1 \frac{\partial m_2}{\partial e_2} \\
&- g_2 g_3 \frac{\partial m_2}{\partial e_2} + \frac{\partial m_2}{\partial e_1} \bigg) \\
&+ g_1 m_2 m_1 \mathrm{sig} \bigg(\alpha_1 \frac{\partial m_2}{\partial e_2} + \frac{\partial m_2}{\partial e_1} \bigg).
\end{aligned} \tag{5.28}$$

Note that $V_{n_3 m_2} \geq 0$ is equal to $|n_3| \geq m_2$ and $\gamma(t) < \Gamma$. The following inequality is obtained

$$\begin{aligned}
\dot{V}_{n_3 m_2} \leq& {n_3}^2(-\alpha_1 + g_2 g_3) + {n_3}^2 \Big| \alpha_1 g_2 - {g_2}^2 g_3 \\
&- \frac{\alpha_2}{g_3} {f_2}'(e_1) \Big| + {n_3}^2 g_1 g_2 \left| \frac{dm_1 \mathrm{sig}}{de_1} \right| \\
&+ \frac{{n_3}^2}{g_3} \left| - \alpha_3 \frac{|f_3(e_1)|}{m_1} + \alpha_2 g_1 {f_2}'(e_1) \right| \\
&+ |n_3| \Gamma + {n_3}^2 {g_1}^2 g_2 \left| \frac{dm_1 \mathrm{sig}}{de_1} \right| + {n_3}^2 \left| \frac{\partial m_2}{\partial e_2} \right| \\
&+ \frac{{n_3}^2}{g_3} \left| \frac{\partial m_2}{\partial e_1} + \alpha_1 \frac{\partial m_2}{\partial e_2} - g_2 g_3 \frac{\partial m_2}{\partial e_2} \right| \\
&+ \frac{g_1 {n_3}^2}{g_3} \left| \frac{\partial m_2}{\partial e_1} + \alpha_1 \frac{\partial m_2}{\partial e_2} \right|
\end{aligned} \tag{5.29}$$

By adjusting α_2 and α_3, we have

$$\begin{aligned} {n_3}^2\left|\alpha_1 g_2 - {g_2}^2 g_3 - \frac{\alpha_2}{g_3} {f_2}'(e_1)\right| &= 0 \\ \frac{{n_3}^2}{g_3}\left| - \alpha_3 \frac{|f_3(e_1)|}{m_1} + \alpha_2 g_1 {f_2}'(e_1)\right| &= 0. \end{aligned} \tag{5.30}$$

Moreover, we get

$$\begin{aligned} \dot{V}_{n_3 m_2} \leq & {n_3}^2(-\alpha_1 + g_2 g_3) \\ & + {n_3}^2\left|\frac{dm_1 \mathrm{sig}(e_1)}{de_1}\right| g_1 g_2 (1 + g_1) + |n_3|\Gamma \\ & + {n_3}^2\left|\frac{\partial m_2}{\partial e_2}\right| + \frac{{n_3}^2}{g_3}\left|\frac{\partial m_2}{\partial e_1} + \alpha_1 \frac{\partial m_2}{\partial e_2}\right. \\ & \left. - g_2 g_3 \frac{\partial m_2}{\partial e_2}\right| + \frac{g_1 {n_3}^2}{g_3}\left|\frac{\partial m_2}{\partial e_1} + \alpha_1 \frac{\partial m_2}{\partial e_2}\right|. \end{aligned} \tag{5.31}$$

When $(e_1, e_2, e_3) \neq (0, 0, 0)$, there exists α_1 leading to $\dot{V}_{n_3 m_2} < 0$. Therefore, trajectory (e_1, e_2, e_3) is to be drawn into region Λ_3. Suppose a trajectory (e_1, e_2, e_3) reaching a point $(\tilde{e}_1, \tilde{e}_2, \tilde{e}_3)$ on the boundary of Λ_3 with unlimited time, then $(\tilde{e}_1, \tilde{e}_2, \tilde{e}_3)$ is regarded as a limit point of (e_1, e_2, e_3), and $\dot{V}_{n_3 m_2}(\tilde{e}_1, \tilde{e}_2, \tilde{e}_3) = 0$. Since the origin is the only point on the boundary of Λ_3 that makes $\dot{V}_{n_3 m_2} = 0$, we obtain $(\tilde{e}_1, \tilde{e}_2, \tilde{e}_3) = 0$. The trajectory (e_1, e_2, e_3) will immediately converge to the origin or reach the boundary in a finite time and enter into the region Λ_3. Hence, if appropriate parameters α_1, α_2 and α_3 are selected, the observed states v_1, v_2 and v_3 will converge to x_1, x_2 and x_3.

5.2.3 Sliding mode-based active disturbance rejection control law

It has been proved that the system state observing error can converge to a bounded region under the designed nonlinear state observer, namely,

$$\begin{aligned} |e_3| =& |y_3 - v_3| \\ =& |F - \hat{F}| \leq \bar{\Delta}_F \end{aligned} \tag{5.32}$$

where $\hat{F}$ is the estimation of state F and $\bar{\Delta}_F$ is the upper bound of e_3.

The tracking error e of the SbW system is defined as

$$e = x_r - x \tag{5.33}$$

where x_r is the reference command which is usually twice differentiable due to road curves, and x is the system output. Then, we define the sliding variable s as

$$s = \dot{e} + \lambda e \tag{5.34}$$

where $\lambda > 0$ is to be designed. Therefore, the design of the SMADRC input is given as

$$\begin{aligned} u =& \frac{-\hat{F} + u_0}{\kappa} \\ u_0 =& \big(|\ddot{x}_r| + \bar{\Delta}_F + \lambda|\dot{e}|\big)\text{sign}(s). \end{aligned} \tag{5.35}$$

Lemma 5.1: Considering the SbW system model as shown in (2.13) with the parametric uncertainties described in (2.24) and under the SMADRC law of (5.35), the tracking error of the SbW system can asymptotically converge to zero for a given reference command.

proof: Define the Lyapunov function V as

$$V = \frac{1}{2}s^2. \tag{5.36}$$

Then, differentiating V with the help of (5.3) and (5.35) yields

$$\begin{aligned}
\dot{V} =& s\dot{s} \\
=& s(\ddot{e} + \lambda\dot{e}) \\
=& s(\ddot{x}_r - \ddot{x} + \lambda\dot{e}) \\
=& s\big[\ddot{x}_r + (\hat{F} - F) + \lambda\dot{e} - u_0\big] \\
=& s\big[\ddot{x}_r + (\hat{F} - F) + \lambda\dot{e} - (|\ddot{x}_r| + \bar{\Delta}_F \\
& + \lambda|\dot{e}|)\text{sign}(s)\big] \\
=& \ddot{x}_r s + (\hat{F} - F)s + \lambda\dot{e}s - |\ddot{x}_r||s| - \bar{\Delta}_F|s| \\
& - \lambda|\dot{e}||s| \\
=& (\ddot{x}_r s - |\ddot{x}_r||s|) + \big[(\hat{F} - F)s - \bar{\Delta}_F|s|\big] \\
& + (\lambda\dot{e}s - \lambda|\dot{e}||s|).
\end{aligned} \tag{5.37}$$

Since the following inequations establishes

$$\begin{aligned}
\ddot{x}_r s \leq& |\ddot{x}_r||s| \\
(\hat{F} - F)s \leq& \bar{\Delta}_F|s| \\
\lambda\dot{e}s \leq& \lambda|\dot{e}||s|
\end{aligned} \tag{5.38}$$

we can easily conclude that

$$\begin{aligned}\dot{V} &= (\ddot{x}_r s - |\ddot{x}_r||s|) + \left[(\hat{F} - F)s - \bar{\Delta}_F|s|\right] \\ &\quad + (\lambda \dot{e} s - \lambda|\dot{e}||s|) \\ &\leq 0.\end{aligned} \tag{5.39}$$

Thus, the proof is completed.

Remark 1: To alleviate undesired possible chattering phenomenon caused by the discontinuous term $\big(|\ddot{x}_r| + \bar{\Delta}_F + \lambda|\dot{e}|\big)\text{sign}(s)$ existing in the control input u of the SMADRC as given in (5.35), we adopt the boundary layer technique, i.e., using the following saturation function to replace the standard signum function:

$$\text{sat}(q) = \begin{cases} q/h, & \text{if } |q| < h \\ \\ \text{sign}(q), & \text{if } |q| \geq h \end{cases} \tag{5.40}$$

where h is the boundary layer thickness to be designed. A larger h leads to less chattering but at the cost of the regression of tracking precision. In this SMADRC design for the SbW system, $h = 0.9$ is found to be satisfactory to compromise between tracking accuracy and control smoothness.

Remark 2: The selection of parameters α_i $(i = 1, 2, 3)$ crucially impacts the estimation performance of the nonlinear extended state observer in the SMADRC. In order to simplify the process of control parameters tuning and reduce the difficulty of control implementation, we adopt the parameterization method proposed by [156]:

$$\alpha_1 = 3\omega; \quad \alpha_2 = 3\omega^2; \quad \alpha_3 = \omega^3 \tag{5.41}$$

where ω is the observer bandwidth which is the only tuning parameter of the observer. Increasing the observer bandwidth ω will augment the estimation rate and accuracy at the cost of introducing extra sensor measurement noises. Considering this tradeoff, we set $\omega = 25$. Similarly, as a parameter significantly determining the tracking bandwidth of the sliding mode function (5.34), a larger λ accelerates the decay of the tracking error on the sliding surface, but also results in more sensor measurement noises. We find that $\lambda = 6$ is an acceptable value in real-time implementation. To achieve accurate states estimation by the nonlinear extended states observer, we set the values of the parameters shown in (5.8) as $\delta_1 = \delta_2 = 0.05$, $\psi = 0.85$.

5.3 Controllers for comparison

To demonstrate the advantages and superiority of the proposed SMADRC, a PD-based active disturbance rejection controller (PDADRC) and a conventional sliding mode controller (CSMC) are also designed. The design results of these two controllers are given directly for simplicity.

5.3.1 PD-based active disturbance rejection control

For a fair comparison, the nonlinear extended state observer of the PDADRC is designed identical to the one of the SMADRC with the same observer gains as given by (5.41). However, in the feedback control loop, we utilize PD control component to replace the sliding mode control component existing in the SMADRC.

The control input u_{PD} of the PDADRC is given by

$$\begin{aligned} u_{PD} &= \frac{-\hat{F} + u_1}{\kappa} \\ u_1 &= K_P e + K_D \dot{e} \end{aligned} \tag{5.42}$$

with $\hat{F}$ the estimation of state F defined in (5.6); e the tracking error defined in (5.33); K_P and K_D the proportional gain and the derivative gain to be designed, respectively. In our case, we set K_P and K_D as

$$K_P = 50, \quad K_D = 15. \tag{5.43}$$

5.3.2 Conventional sliding mode control

According to [144], the CSMC is designed as

$$u_{csm} = \frac{1}{b}(\bar{J}\lambda_{csm}|\dot{e}| + \bar{J}|\ddot{x}_r| + \bar{c}|\dot{x}| + \bar{\rho} + \bar{\tau})\text{sat}(s_{csm}) \tag{5.44}$$

where $s_{csm} = \dot{e} + \lambda_{csm} e$ is the sliding variable under the CSMC with $\lambda_{csm} = 16$; $\text{sat}(\cdot)$ is the same saturation function defined in (5.40) with the same boundary layer thickness; $\bar{J}$, $\bar{c}$ and $\bar{\rho}$ represent the upper bounds of the parameters J, c and ρ, respectively; and $\bar{\tau}$ is the upper bound of the self-aligning torque acting on the front wheels. For a fair comparison, the upper bounds of the parameters J, c and ρ of the CSMC are

$$\begin{aligned} \bar{J} &= J_0 + \bar{\Delta}_J \\ \bar{c} &= c_0 + \bar{\Delta}_c \\ \bar{\rho} &= \rho_0 + \bar{\Delta}_\rho \end{aligned} \tag{5.45}$$

where the values of these parameters are given in (2.24).

5.4 Simulation results

Before the experimental implementation of the designed sliding mode-based active disturbance rejection controller, we study the simulation results to evaluate its performance. In this section, simulation of the SMADRC, the PDADRC and the CSMC is carried out, and the simulation results are compared and analyzed. In order to demonstrate the superiority of the proposed SMADRC in terms of high tracking accuracy, strong robustness against varying road conditions and fast convergence rate, three cases are considered in this section.

5.4.1 Case 1: slalom path following

To mimic a slalom path for a vehicle to follow in our experimental setup, we maneuver the steering wheel shown in Figure 2.1(b) to generate an approximate sinusoidal signal. Then, the steering wheel angle sensor collects the corresponding steering angle. By multiplying this angle sensor signal by the corresponding scaling factor from the steering wheel to the front wheels, a steering wheel reference angle is obtained and input to the controllers under test. In order to test the controllers' robustness against the variation of road conditions, we also set the values of the coefficient of the self-aligning torque ξ as

$$\xi = \begin{cases} 150, & 0 < t \leq 20\,\text{s}, \quad \text{Snowy road} \\ 580, & 20 < t \leq 40\,\text{s}, \quad \text{Wet asphalt road} \\ 950, & 40 < t \leq 60\,\text{s}, \quad \text{Dry asphalt road} \end{cases} \tag{5.46}$$

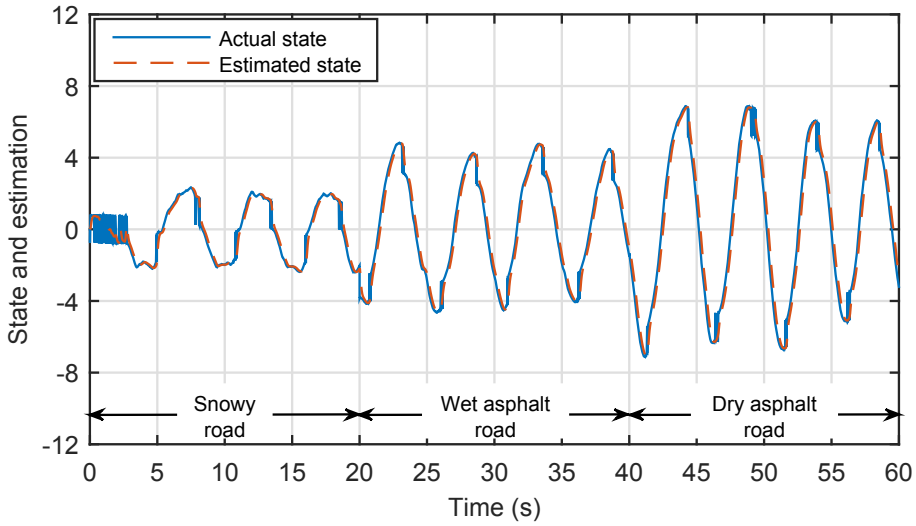

Figure 5.1: Simulated state estimation result of the SMADRC in Case 1.

to represent the change of the road conditions during the experiments. The simulation results for this case are shown in Figures 5.1–5.4.

From Figure 5.1 we can see that the estimation performance of the nonlinear extended state observer in the designed SMADRC is satisfactory. The estimated state $\hat{F}$ can follow the actual state F fast and accurately. Due to the existing of the term of standard signum function, in the line of the 'Actual state', there exists high-frequency chattering. The nonlinear extended state observer cannot estimate such high-frequency chattering due to the observer bandwidth limitation. However, the baseband signal of the actual state can be estimated accurately leading to high tracking accuracy of the proposed SMADRC.

It can be clearly seen from Figure 5.2 that the tracking error of the sliding mode-based active disturbance rejection controller is bounded in the region of -0.005 rad to 0.005 rad regardless of the increasing of the self-aligning torque disturbance. However, in the simulation results of the PD-based active disturbance rejection controller and the conventional sliding mode controller as shown in Figures 5.3–

5.4, the peak tracking errors of the PDADRC are 0.018 rad, 0.024 rad and 0.026 rad, and the peak tracking errors of the CSMC are 0.021 rad, 0.035 rad and 0.06 rad in the three periods. We can see that compared with the PD-based active disturbance rejection controller and the conventional sliding mode controller, the designed sliding mode-based active disturbance rejection controller possesses higher tracking precision and stronger robustness against varying road conditions.

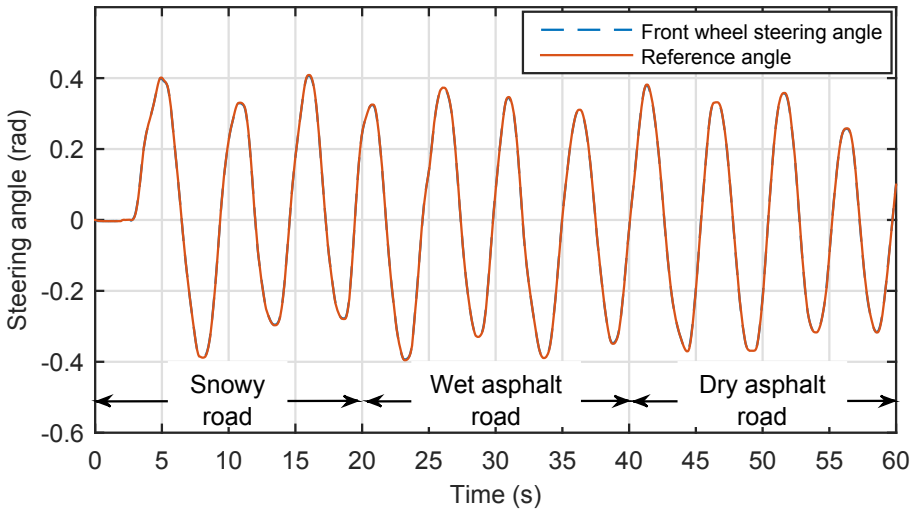

(a) Tracking profile

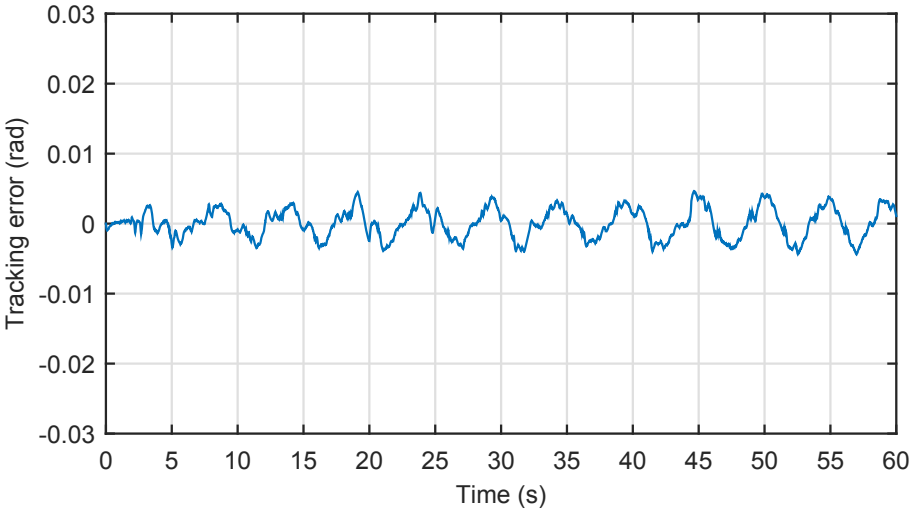

(b) Tracking error

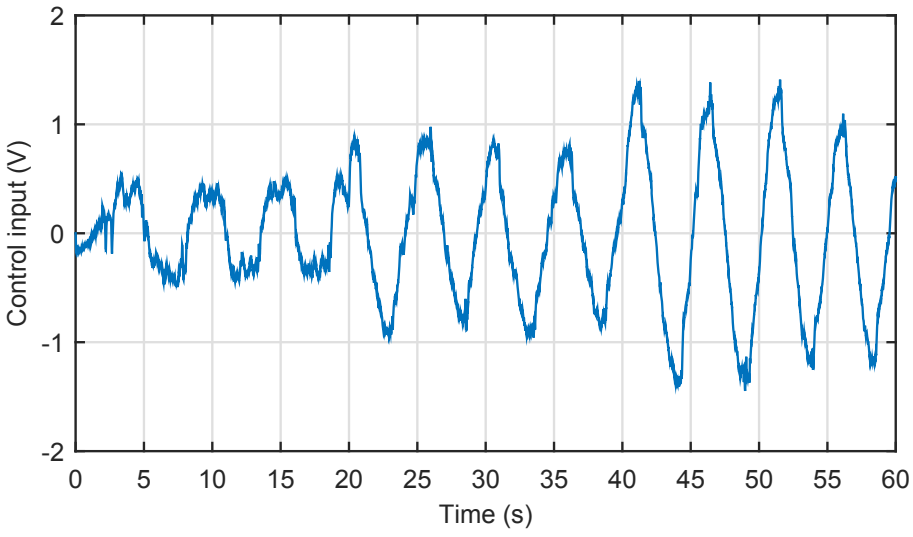

(c) Control input

Figure 5.2: Simulated control performance of the SMADRC in Case 1.

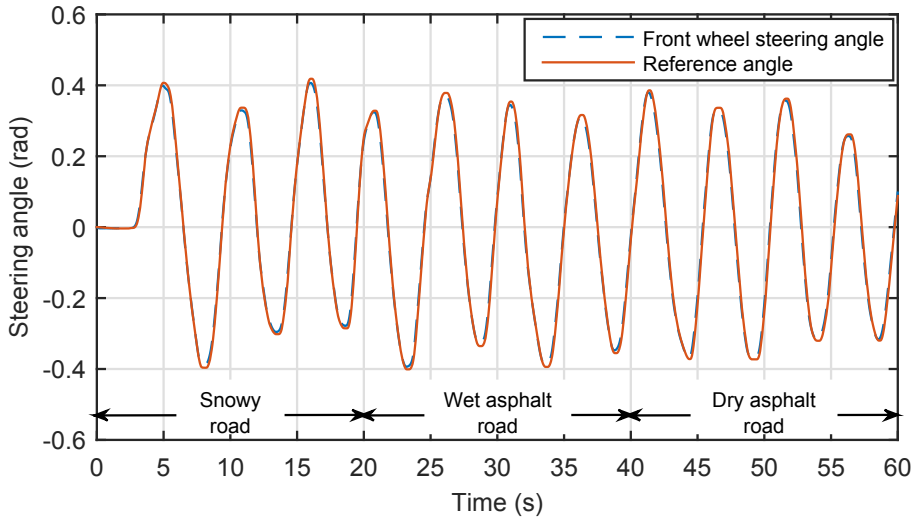

(a) Tracking profile

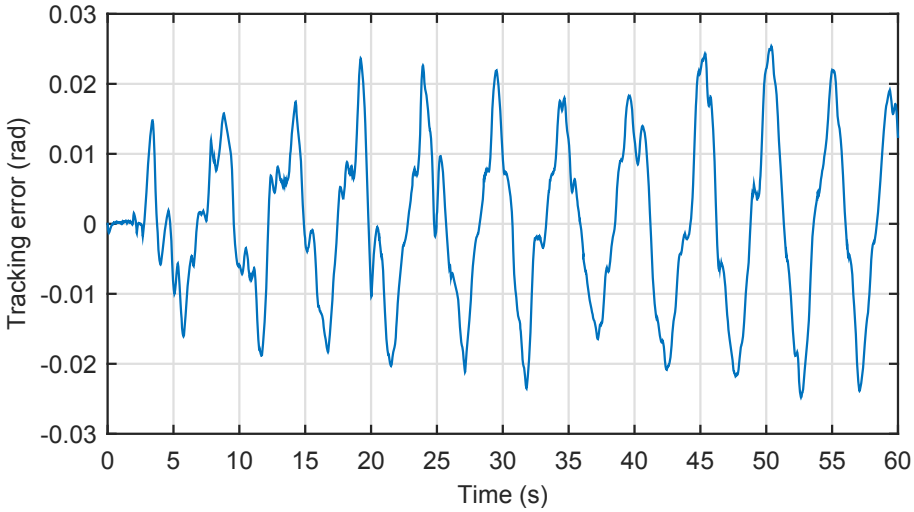

(b) Tracking error

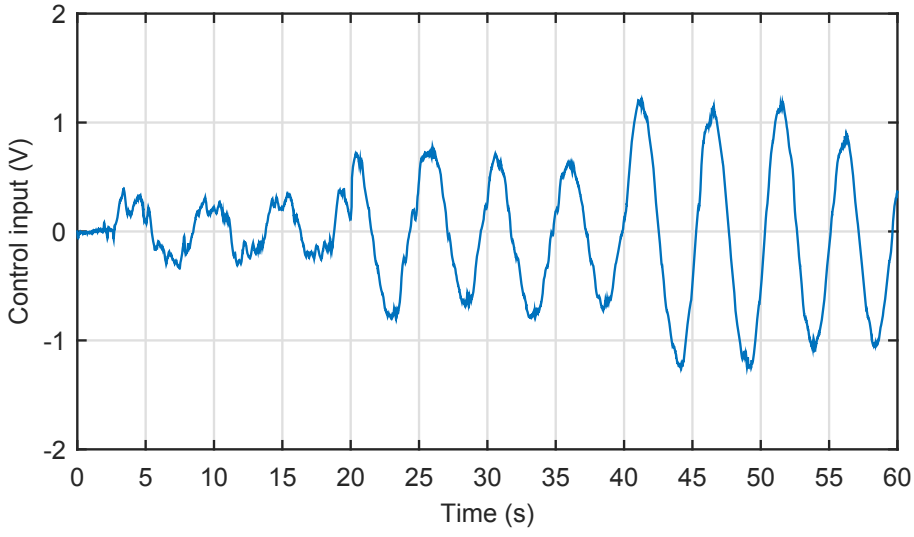

(c) Control input

Figure 5.3: Simulated control performance of the PDADRC in Case 1.

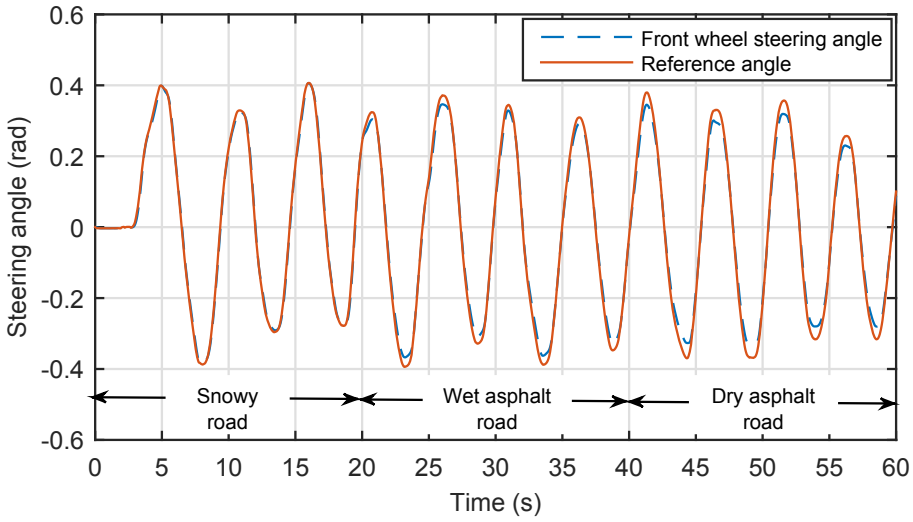

(a) Tracking profile

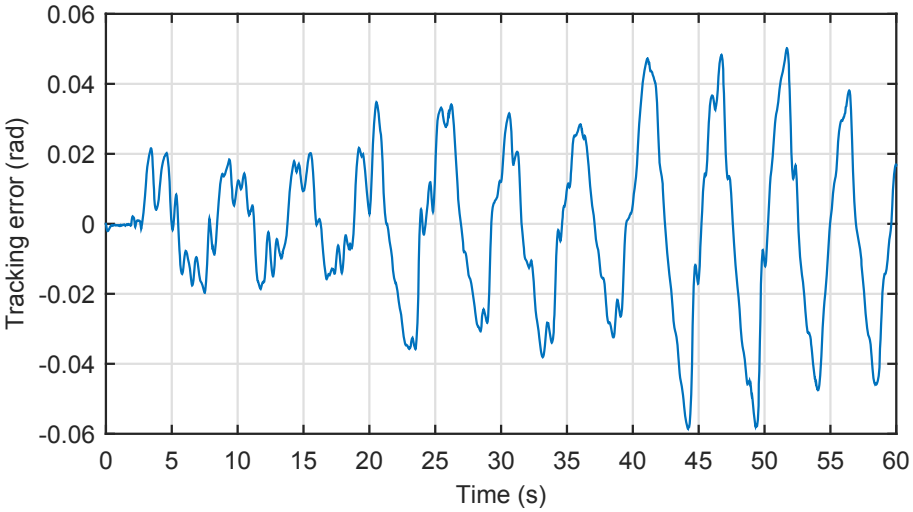

(b) Tracking error

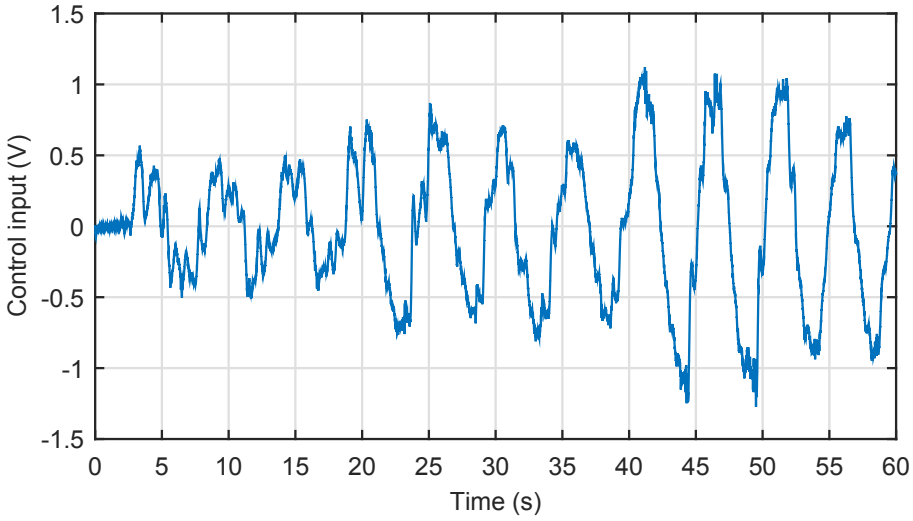

(c) Control input

Figure 5.4: Simulated control performance of the CSMC in Case 1.

5.4.2 Case 2: circular path following

In order to test the controllers' performances when the SbW equipped vehicle has a sharp and long turning in reality, we consider a road path being straight at first and then followed by circular curves. We maneuver the steering wheel and generate the reference command as shown in Figure 5.5(a). The simulation of quick steering under the three controllers is carried out with a duration of 15 seconds and a sampling period of 1 ms. The road condition in this case is set as dry asphalt road, namely, the value of the coefficient of the self-aligning torque is set as $\xi = 950$.

The simulation results of the three controllers in this case are shown in Figures 5.5–5.7. In Figure 5.5, we can see that the peak tracking error of the SMADRC are under 0.01 rad, and the steady state tracking error is almost close to zero. However, for the PDADRC, the peak tracking errors as shown in Figure 5.6 are approximately 0.02 rad. It is indicated in Figure 5.7 that the peak tracking error of the CSMC is about 0.055 rad, and the steady state error has no tendency to converge to zero or a small region close to zero. Thus, the superiority of the sliding mode-based active disturbance rejection controller in the case of circular path following has been demonstrated by simulation.

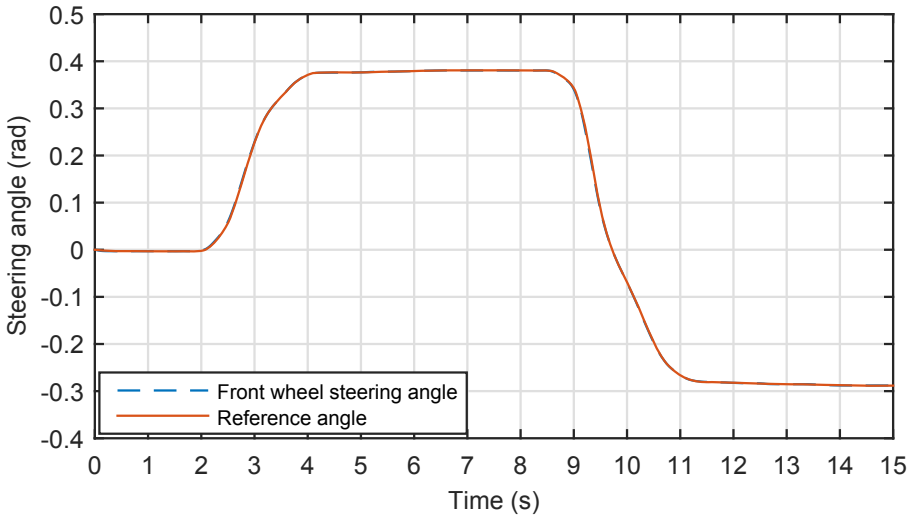

(a) Tracking profile

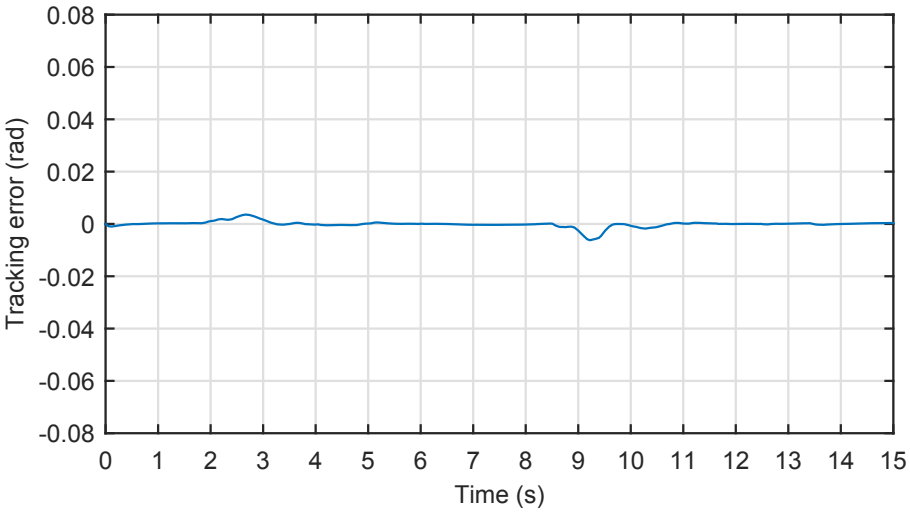

(b) Tracking error

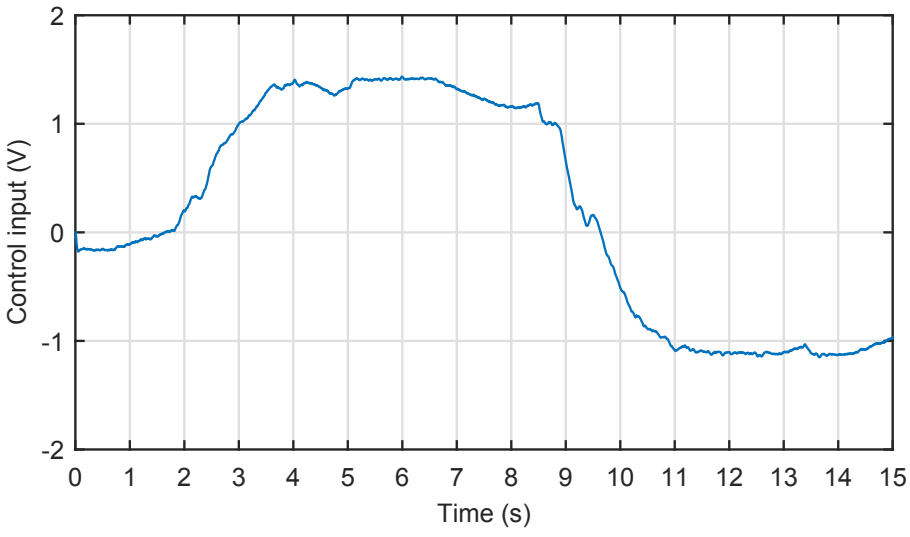

(c) Control input

Figure 5.5: Simulated control performance of the SMADRC in Case 2.

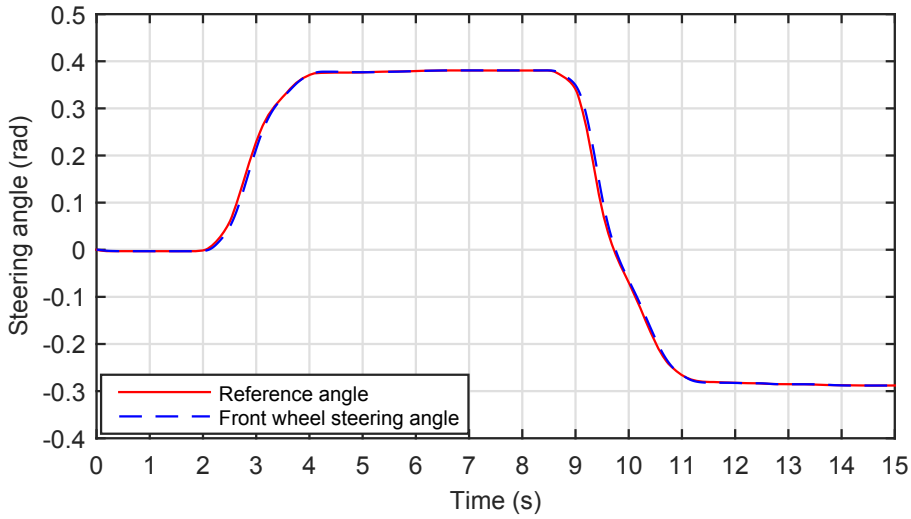

(a) Tracking profile

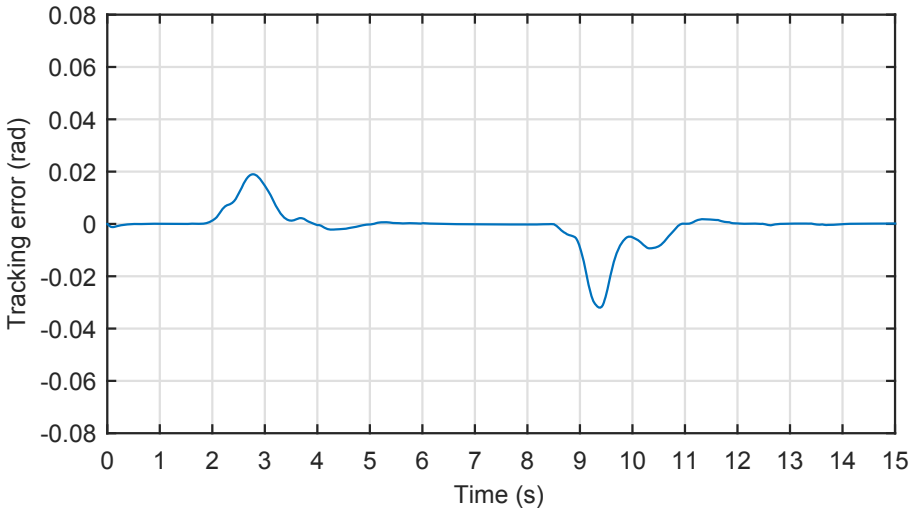

(b) Tracking error

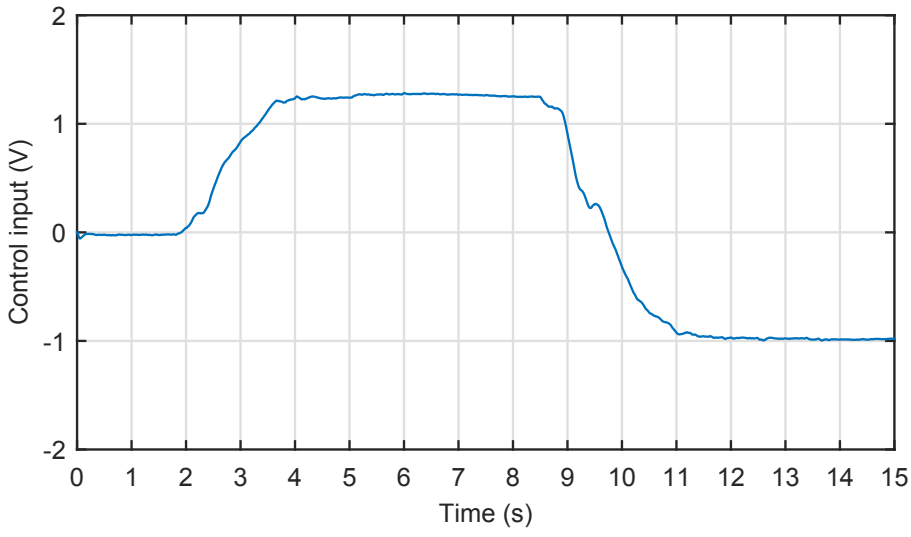

(c) Control input

Figure 5.6: Simulated control performance of the PDADRC in Case 2.

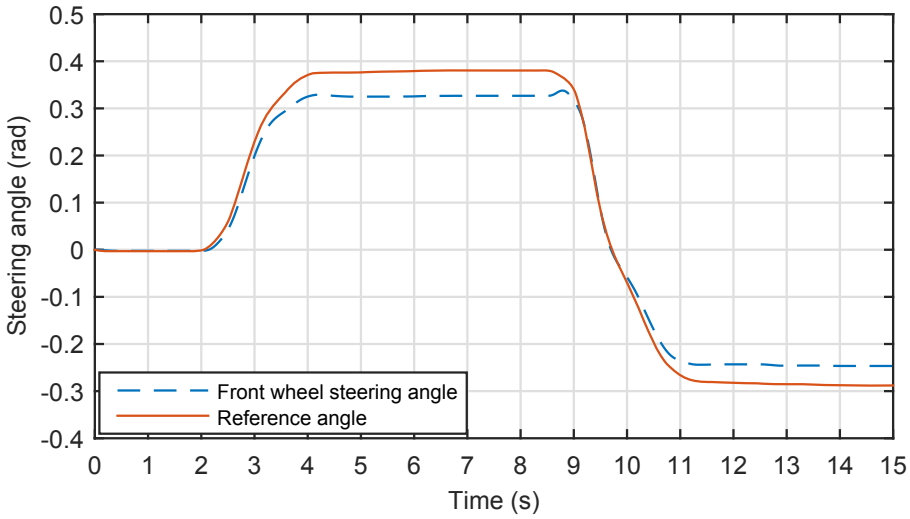

(a) Tracking profile

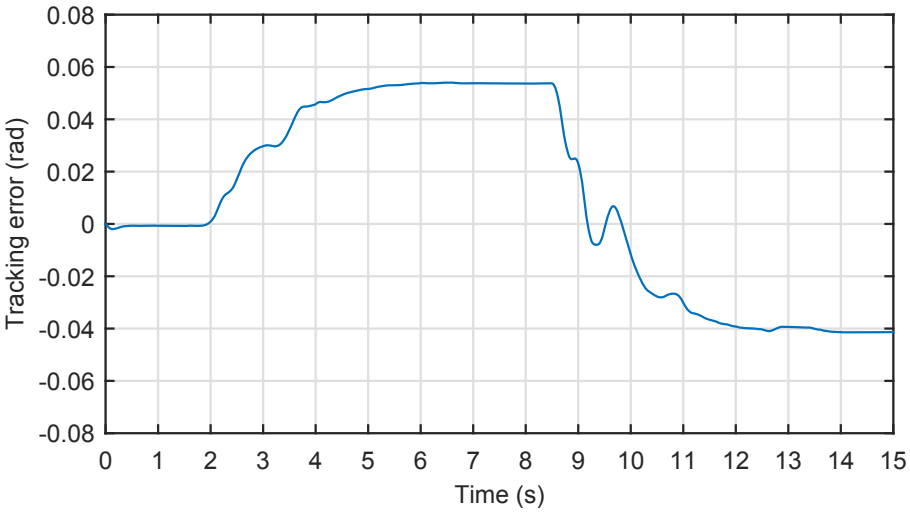

(b) Tracking error

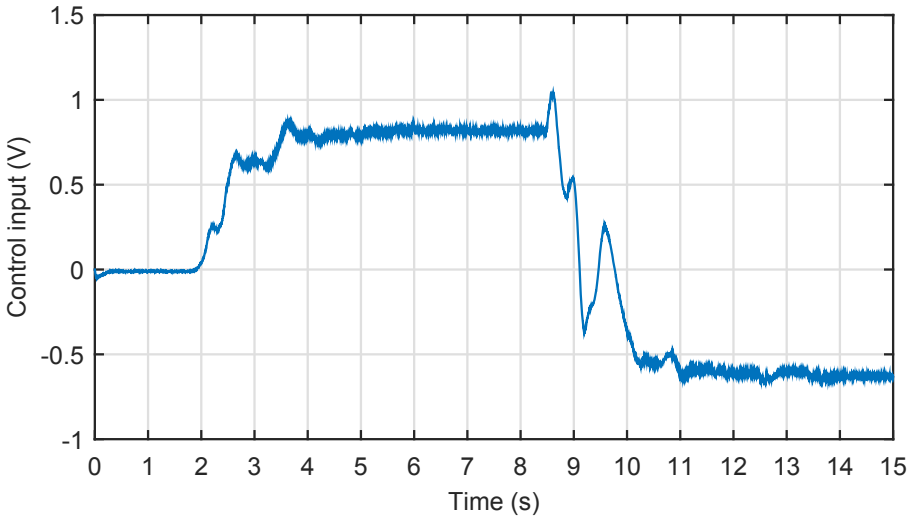

(c) Control input

Figure 5.7: Simulated control performance of the CSMC in Case 2.

5.4.3 Case 3: shock disturbance rejection

In reality, there exists another common situation, in which a vehicle running along a straight path comes across a sudden shock disturbance such as a bump or a brick on road. Thus, it is significant for a controller designed for SbW systems to force front wheels back to their original position fast and actively. In other words, the controller should be designed to own a fast convergence rate of tracking errors. In this case, we carry out the simulation of shock disturbance rejection with a duration of 10 seconds. In order to mimic a straight path for the vehicle to follow, the reference command for the control system is set as zero. The road surface is set as an consistent snowy road with the coefficient of the self-aligning torque $\xi = 150$ to exclude the interference of road conditions. For a fair comparison, a pulse signal with an amplitude of 1.2 V, a width of 0.5 s is generated and added to the control inputs of the SMADRC, the PDADRC and the CSMC at the 2nd second during the simulation to mimic the same shock disturbance.

The simulation results of the three controllers in this case are shown in Figures 5.8–5.10. We can clearly see that the peak tracking error of the SMADRC is about 0.008 rad, which is less than those of the PDADRC (0.025 rad) and the CSMC (0.059 rad). And the convergence time of the SMADRC is about 1 second, which is also less than those of the PDADRC (2 seconds) and the CSMC (2 seconds). Thus, it is demonstrated that the designed sliding mode-based active disturbance rejection controller can possess not only higher tracking accuracy but also faster convergence rate compared with the PD-based active disturbance rejection controller and the conventional sliding mode controller in the case of external disturbance rejection by simulation.

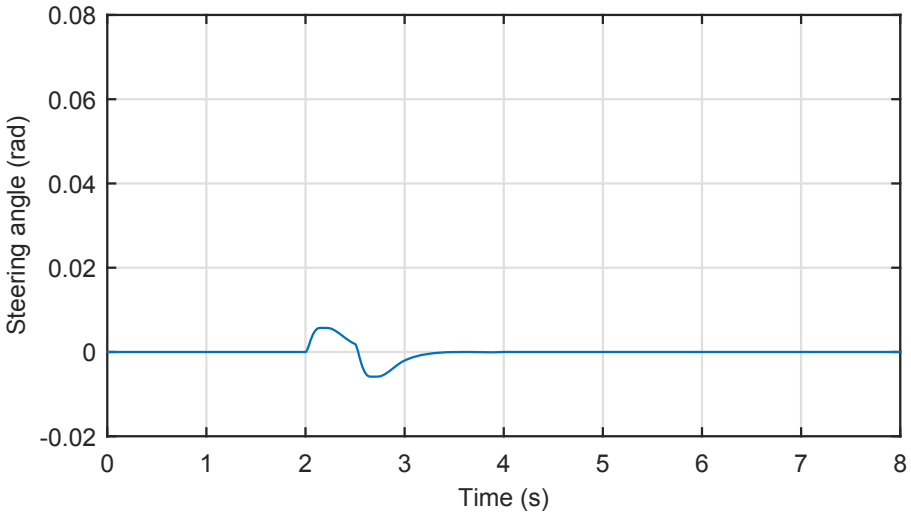

(a) Tracking profile

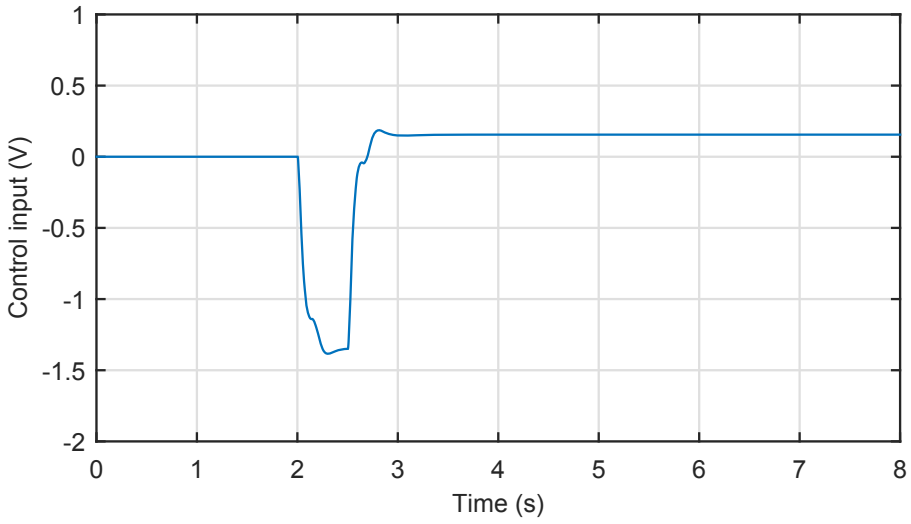

(b) Control input

Figure 5.8: Simulated control performance of the SMADRC in Case 3.

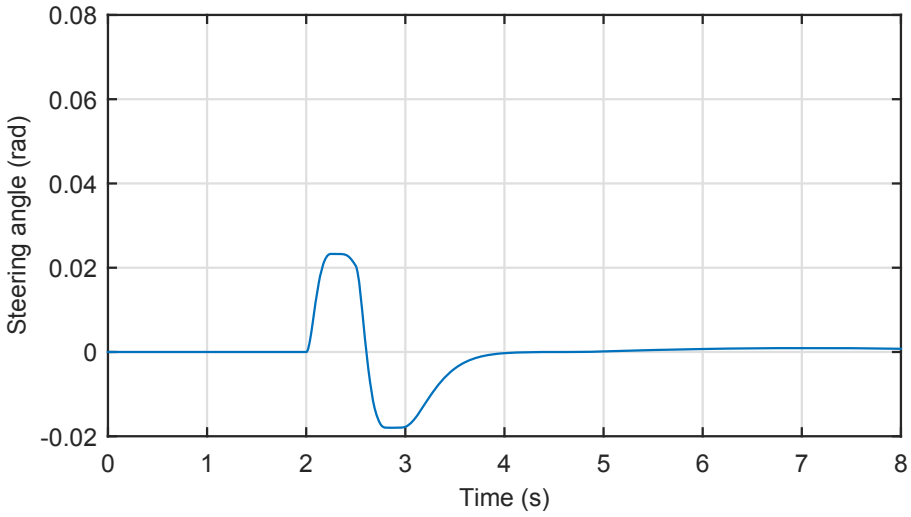

(a) Tracking profile

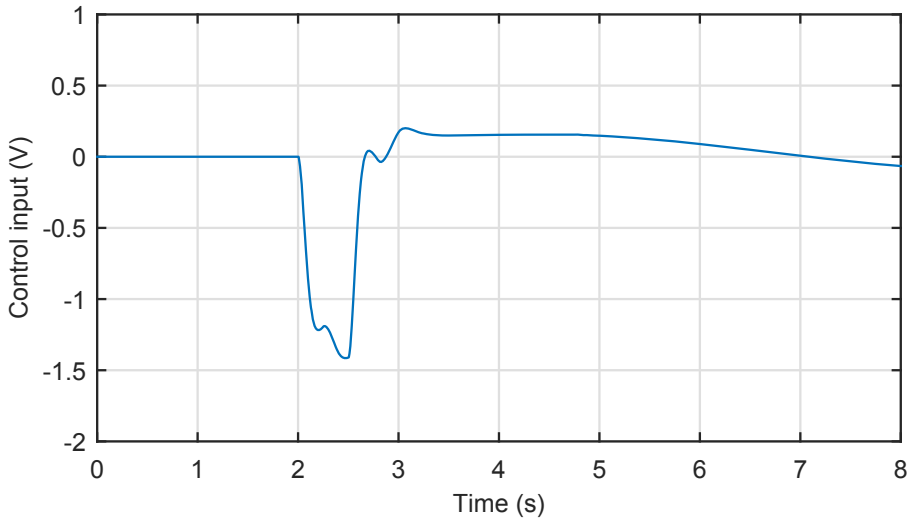

(b) Control input

Figure 5.9: Simulated control performance of the PDADRC in Case 3.

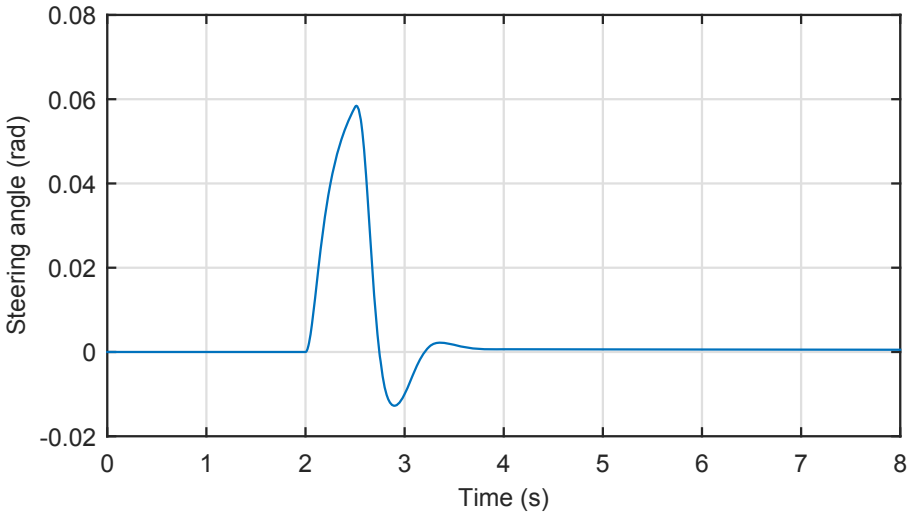

(a) Tracking profile

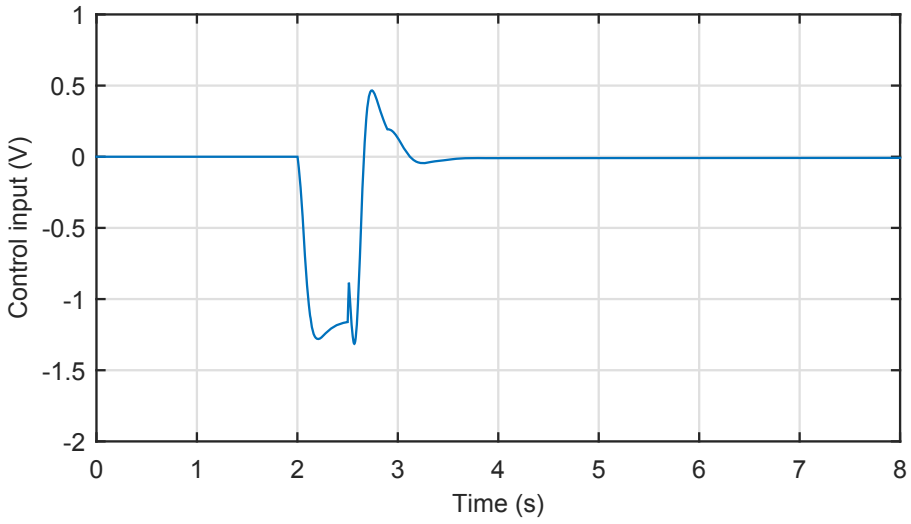

(b) Control input

Figure 5.10: Simulated control performance of the CSMC in Case 3.

5.5 Experimental results

In this section, the experiments are carried out on the actual SbW experimental setup to verify the designed controllers with a sampling period of 1 ms. For the purpose of indicating that the designed AFNTSM controller can be effectively implemented on the SbW experimental platform and can also possess similar superiority indicated in the simulation results, identical cases with the same reference commands and road conditions as those in the simulation are considered in this section.

From Figure 5.11 we can see that the estimation state $\hat{F}$ can track the actual one F effectively. The chattering existing in the curve of the actual state F, which is larger compared with that in the simulation result shown in Figure 5.1, is believed to be caused by sensor measurement noises and the effect of the discontinuous term $-\frac{\rho_0}{J_0}\text{sign}(\dot{y})$ in state F as given in (5.6). And from Figure 5.11(b) we can see that the estimation error ε_3 is within a bounded region of around 2.5.

Figures 5.12–5.14 indicate the control performances of the three controllers in slalom path following under the variation of road conditions. Similar to the simulation results as shown in Figures 5.2–5.4, it is manifest that the tracking performance of the SMADRC is superior to those of the PDADRC and the CSMC. With the estimation of the extended state F by the nonlinear extended state observer and the sliding mode control component, the SMADRC can force the tracking errors to remain in the range of -0.006 rad to 0.006 rad regardless of the evident increase of the self-aligning torque disturbance. However, under the PDADRC, the peak tracking errors during the three different periods of different road conditions are

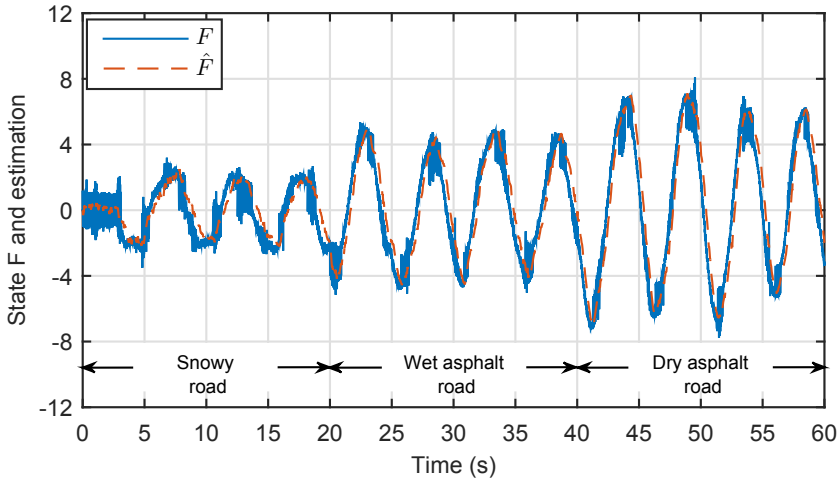

(a) Estimation of state F

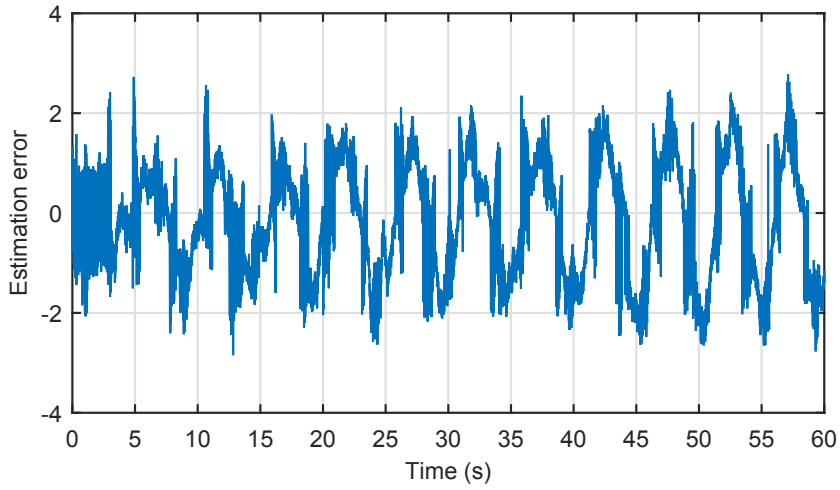

(b) Estimation error $\varepsilon_3 = \hat{F} - F$

Figure 5.11: Experimental state estimation result of the SMADRC in Case 1.

approximately 0.018 rad, 0.024 rad and 0.028 rad, respectively. It is because that the PD control component in the PDADRC is not as robust as the sliding mode one in the SMADRC against system uncertainties and varying road conditions. Due to the lack of effective estimation of the nonlinear states in the plant model, the CSMC cannot effectively compensate for the effect of the friction-related forces and the self-aligning torque. Hence, the tracking accuracy of the CSMC is pretty sensitive to the change of road conditions, which results in the peak errors of about 0.018 rad, 0.035 rad and 0.055 rad during the three periods.

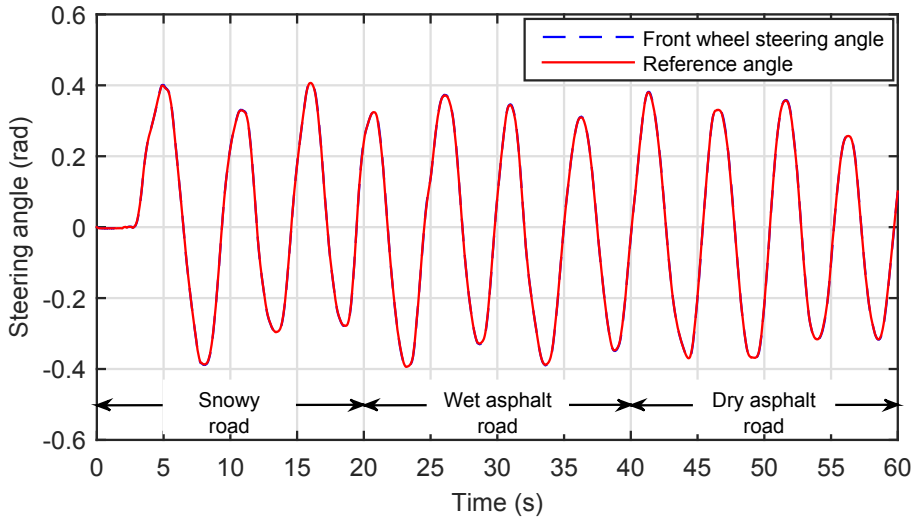

(a) Tracking profile

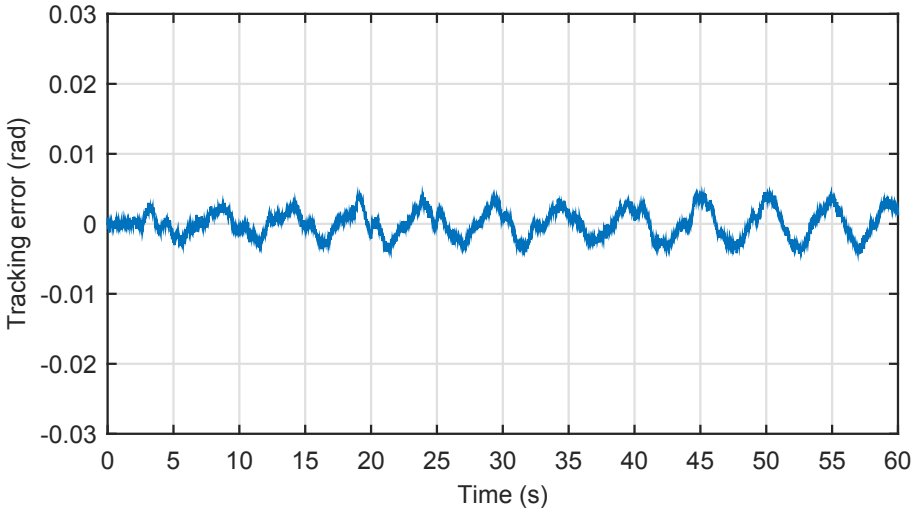

(b) Tracking error

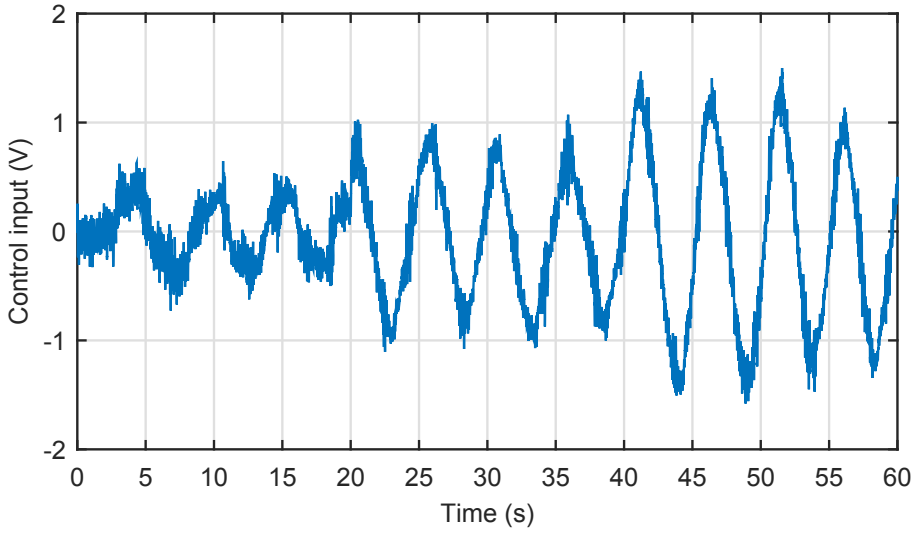

(c) Control input

Figure 5.12: Experimental control performance of the SMADRC in Case 1.

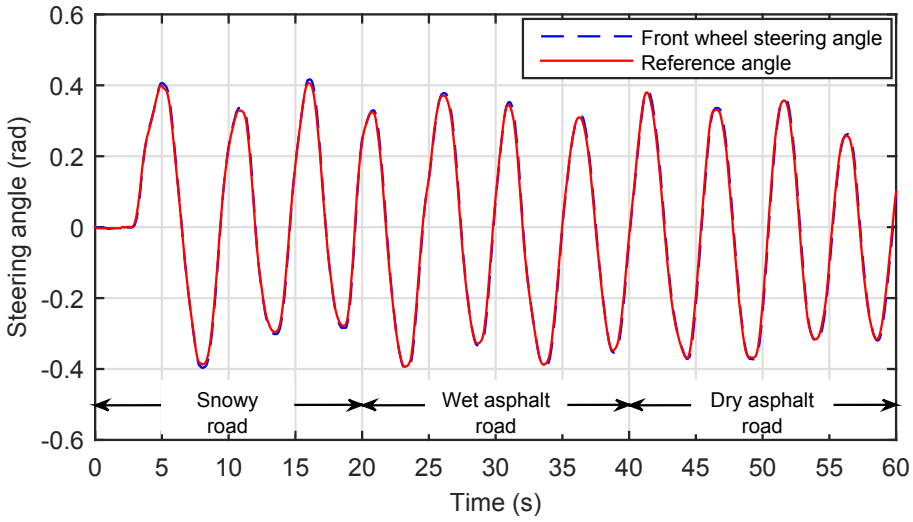

(a) Tracking profile

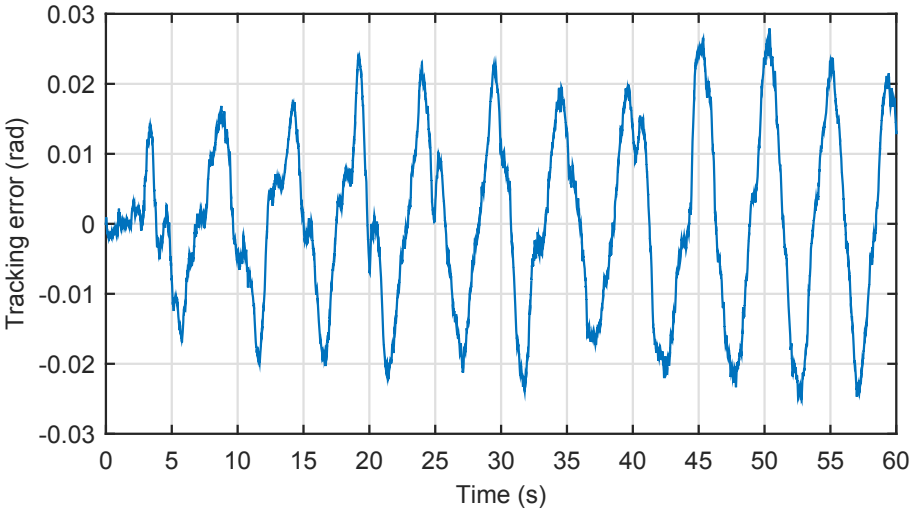

(b) Tracking error

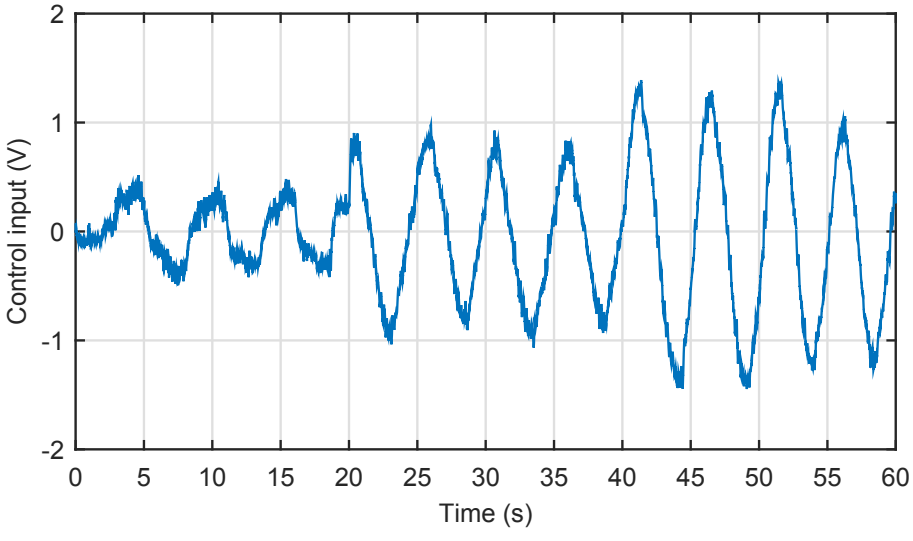

(c) Control input

Figure 5.13: Experimental control performance of the PDADRC in Case 1.

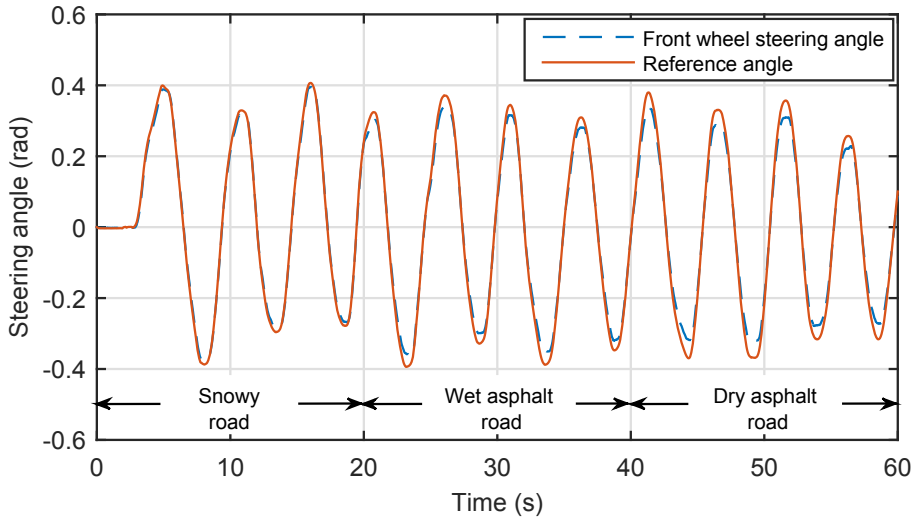

(a) Tracking profile

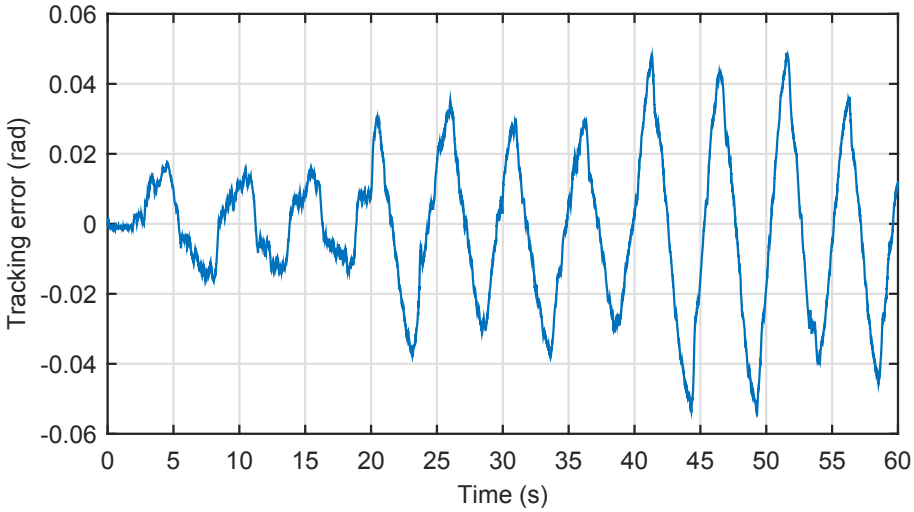

(b) Tracking error

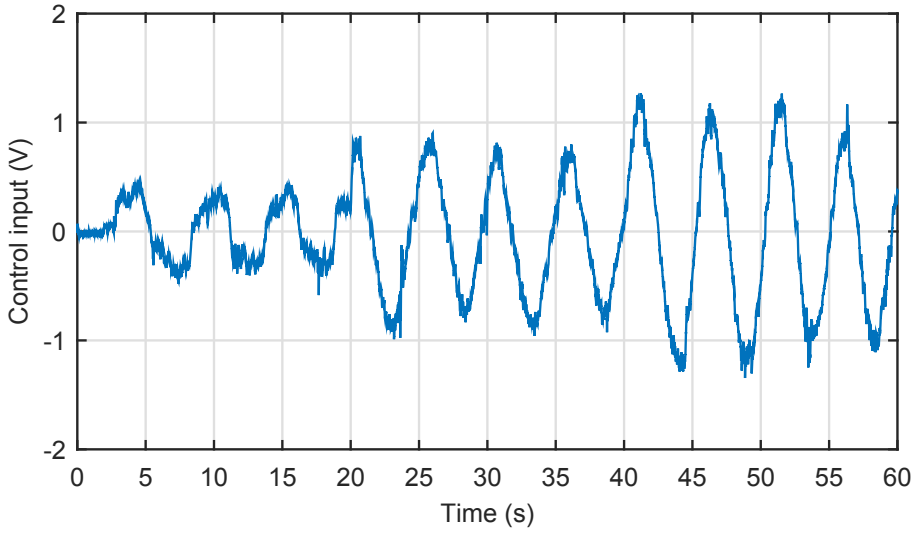

(c) Control input

Figure 5.14: Experimental control performance of the CSMC in Case 1.

Compared with the simulation results as shown in Figures 5.5–5.7, the experimental results of quick steering shown in Figures 5.15–5.17 are pretty similar but contain more chattering due to the effect of sensor measurement noises. We can clearly see from the experimental results that the tracking accuracy of the SMADRC is extremely high in this case compared with the PDADRC and the CSMC. The tracking error under the SMADRC is almost zero only except the moments when the front wheels start to steer. However, the peak tracking errors under the SMADRC are still small enough (under 0.01 rad). For the PDADRC, the steady state tracking error is also close to zero but with more vibrations, but the peak tracking errors (0.02 rad and -0.035 rad) are apparently larger than those of the SMADRC. The experimental results shown in Figure 7.7 indicates that the tracking error under the CSMC cannot converge to zero or a region close to zero in this case. The peak tracking errors of the CSMC are 0.04 rad and -0.035 rad, respectively, which are the largest in the three controllers. Moreover, the steady state tracking error under the CSMC is also much larger in comparison with those of the SMADRC and the PDADRC.

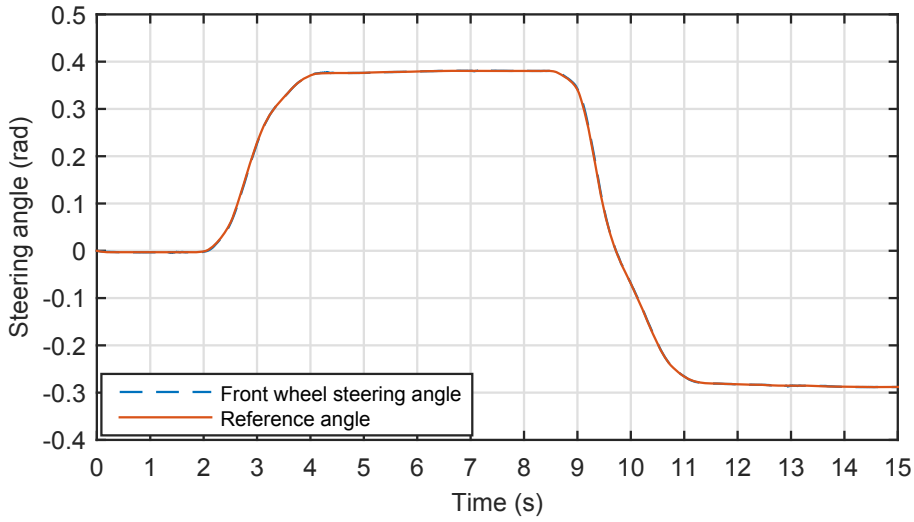

(a) Tracking profile

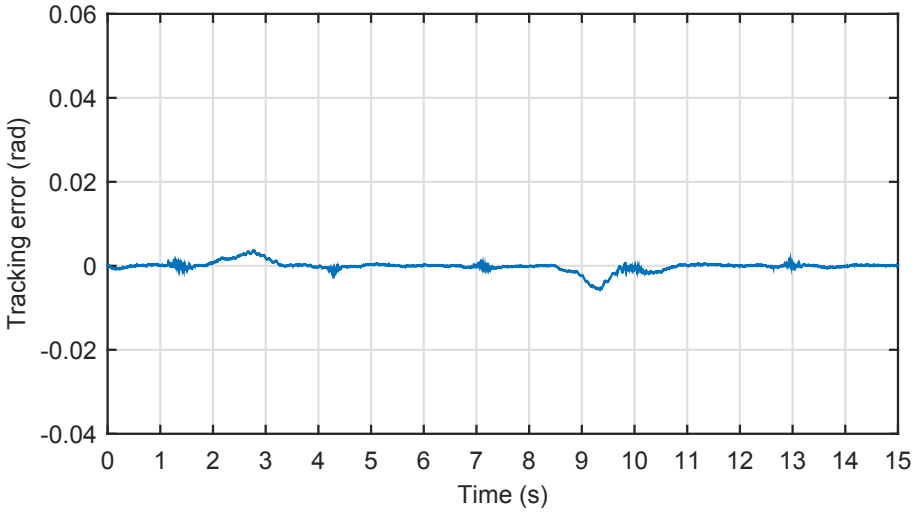

(b) Tracking error

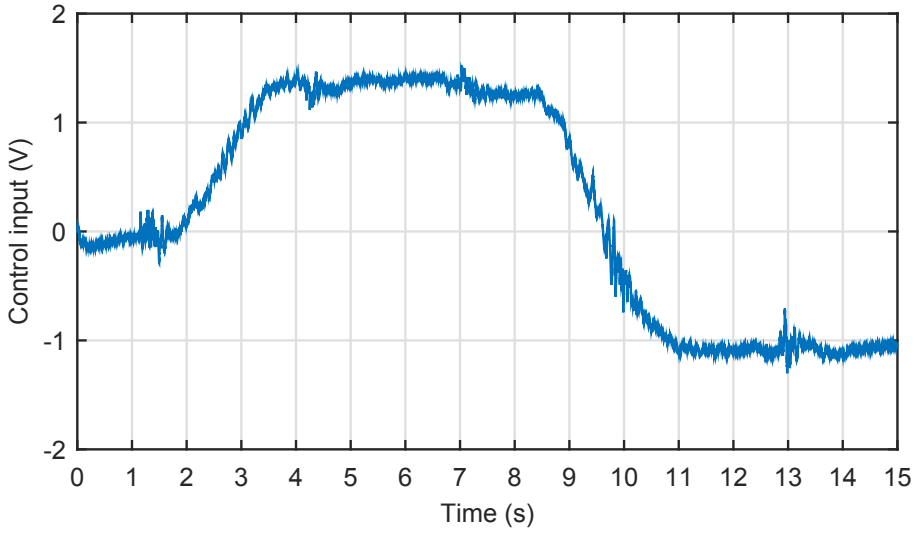

(c) Control input

Figure 5.15: Experimental control performance of the SMADRC in Case 2.

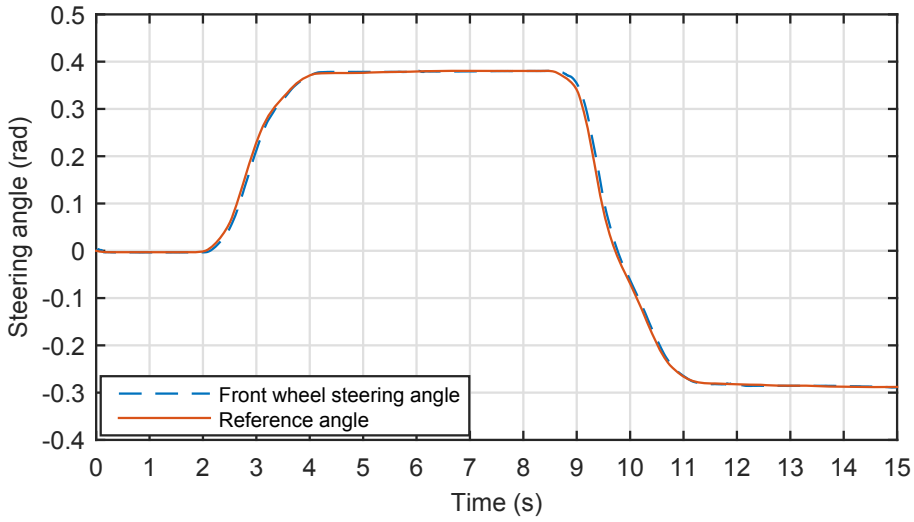

(a) Tracking profile

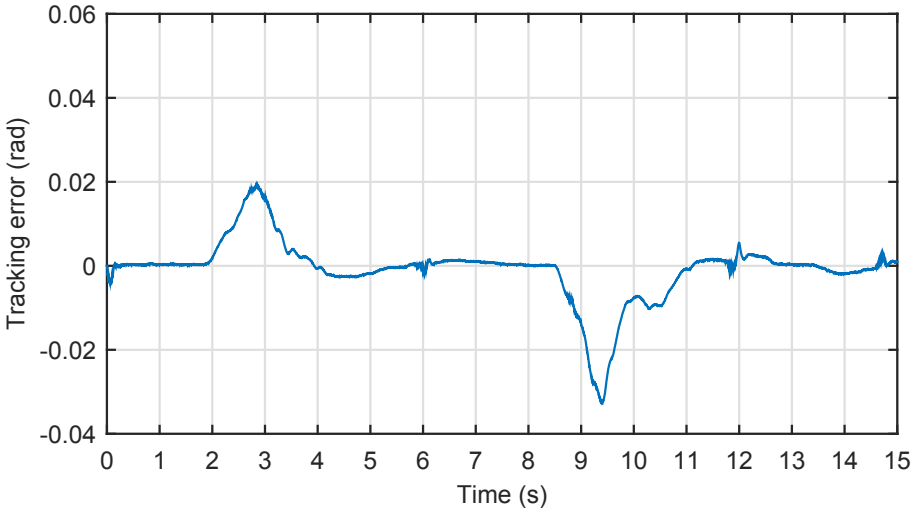

(b) Tracking error

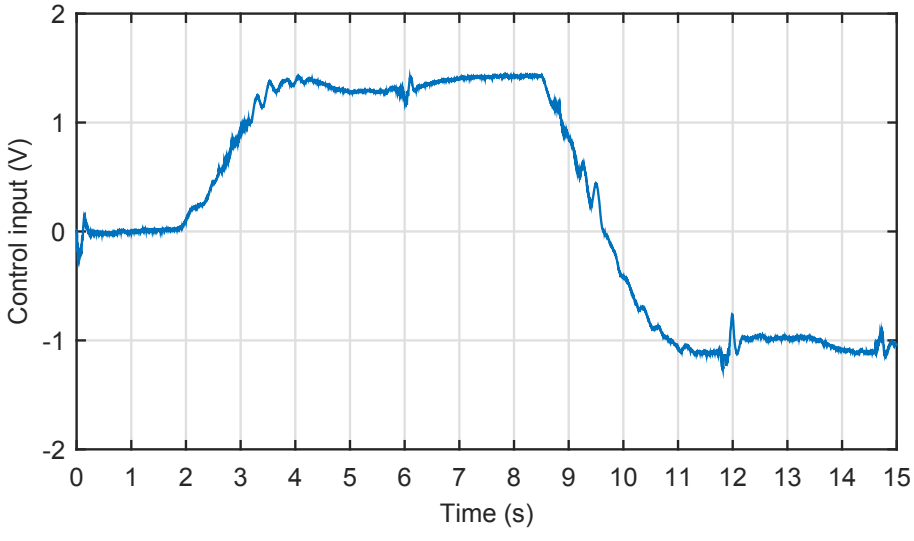

(c) Control input

Figure 5.16: Experimental control performance of the PDADRC in Case 2.

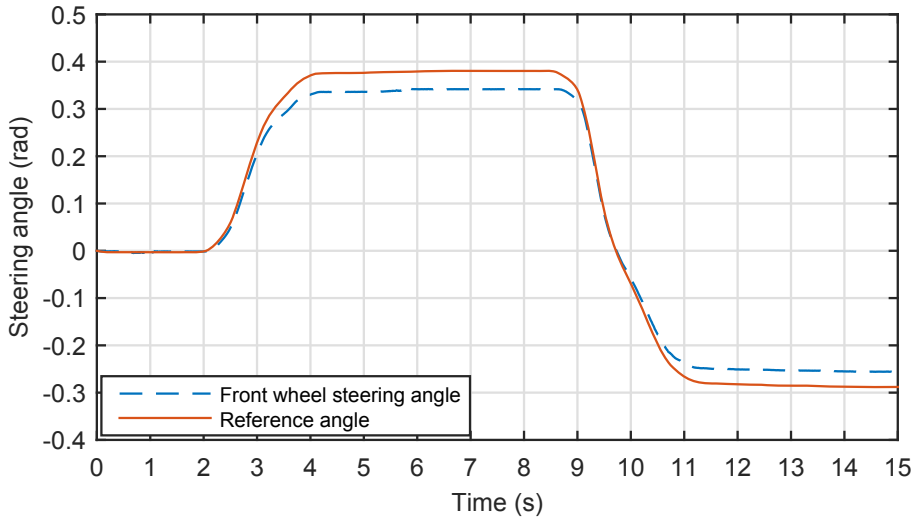

(a) Tracking profile

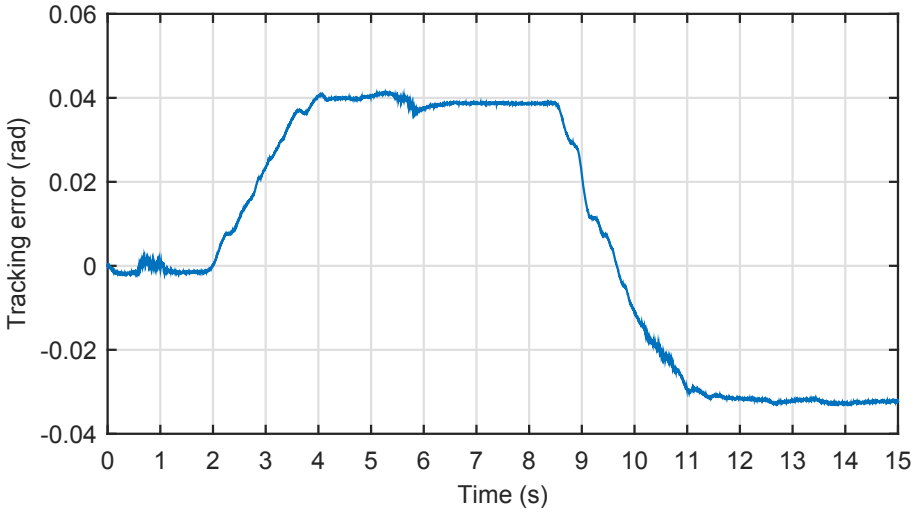

(b) Tracking error

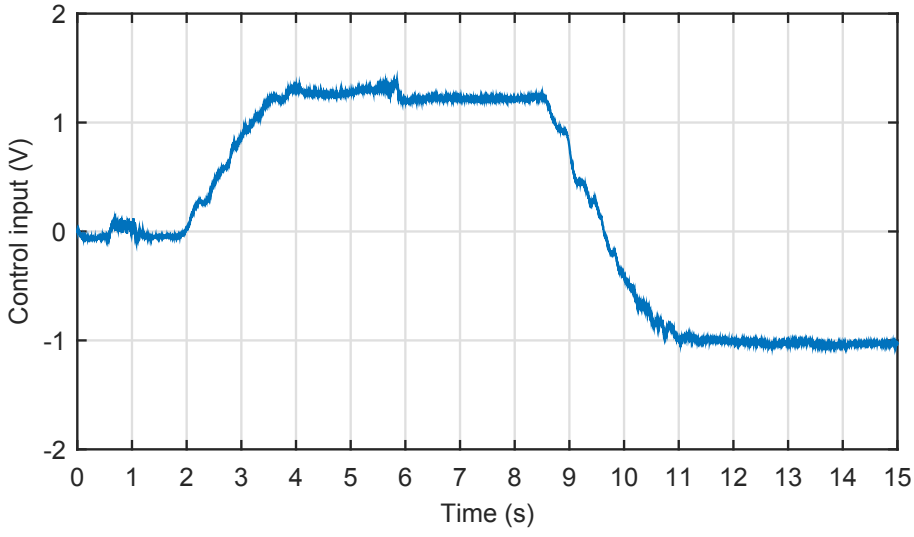

(c) Control input

Figure 5.17: Experimental control performance of the CSMC in Case 2.

The experimental results of external disturbance rejection are shown in Figures 5.18–5.20, which are close to the simulation results as shown in Figures 5.8–5.10 to a large extent. We can see clearly that the peak tracking error under the SMADRC is approximately 0.008 rad, which is much less than those of the PDADRC (0.025 rad) and the CSMC (0.085 rad). More importantly, the SMADRC can force the tracking error to converge to zero approximately within 1 second (from the 2nd second to the 3rd second). However, for the PDADRC, it takes about 2 seconds (the 2nd second to the 4th second) for the tracking error to converge to zero. The performance of the CSMC is the worst in this case, not only because the peak tracking error under the CSMC is the largest (nearly 0.085 rad), but also because it takes nearly 5 seconds (the 2nd second to the 7th second) for the tracking error to converge to zero. Thus, the excellent control performance of the SMADRC in terms of fast converge rate and shock disturbance rejection has been thoroughly demonstrated in comparison with the PDADRC and the CSMC.

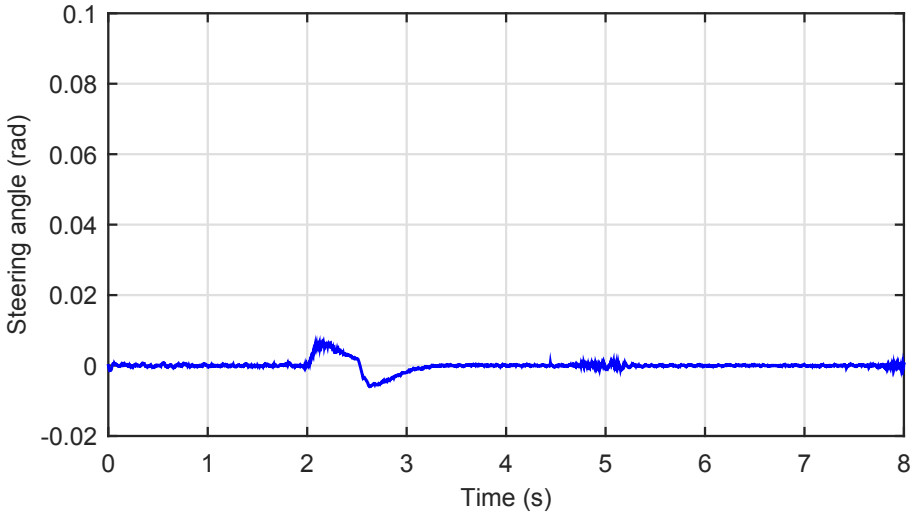

(a) Tracking profile

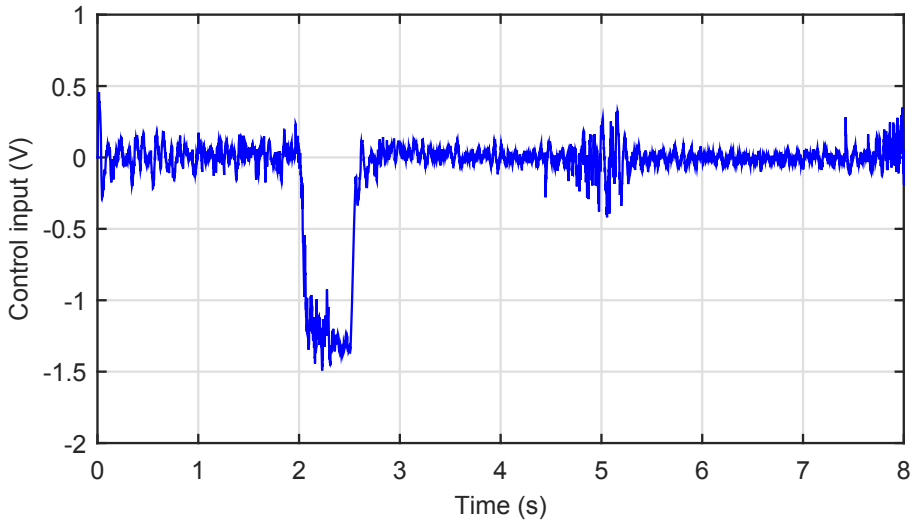

(b) Control input

Figure 5.18: Experimental control performance of the SMADRC in Case 3.

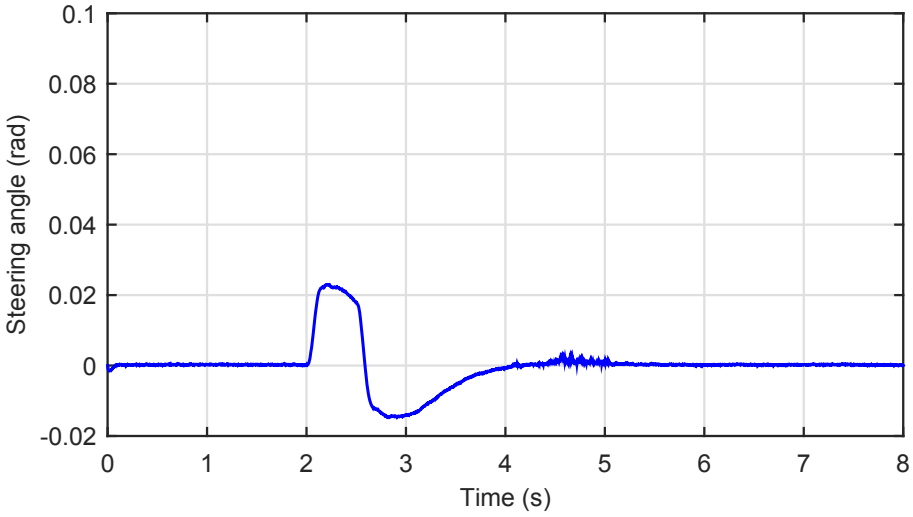

(a) Tracking profile

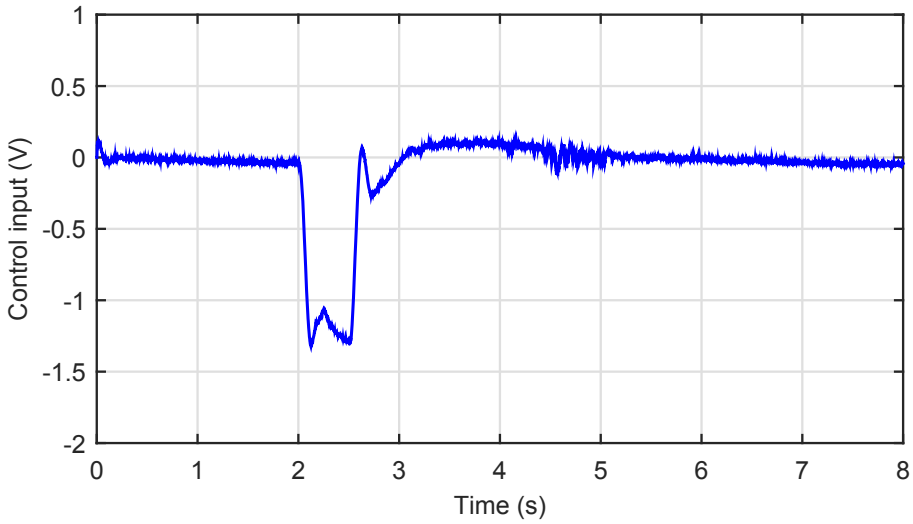

(b) Control input

Figure 5.19: Experimental control performance of the PDADRC in Case 3.

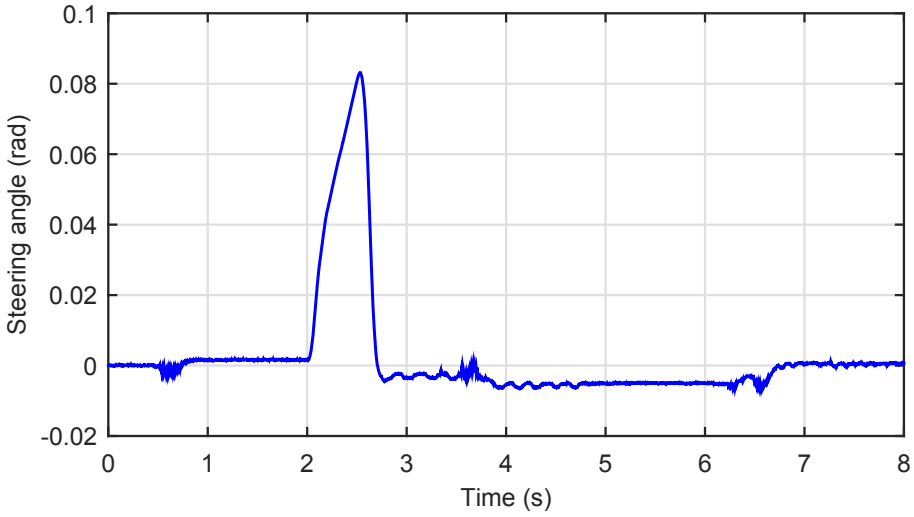

(a) Tracking profile

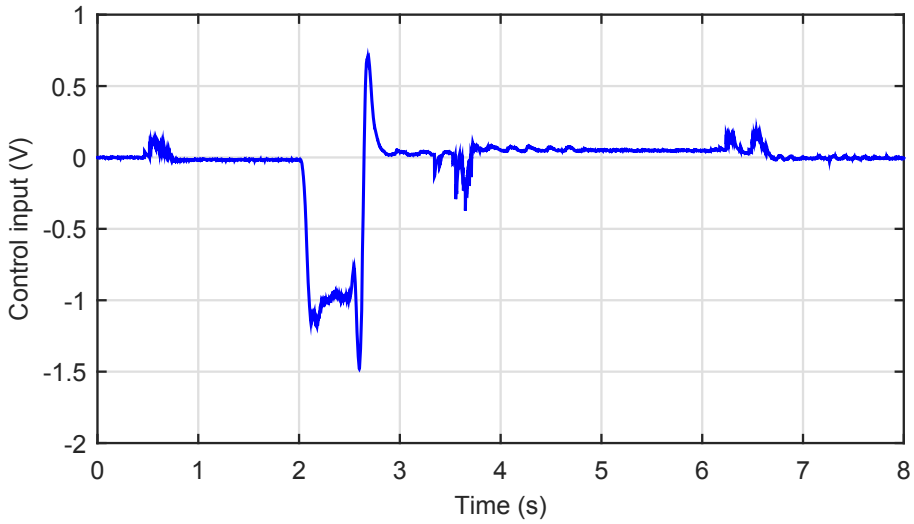

(b) Control input

Figure 5.20: Experimental control performance of the CSMC in Case 3.

5.6 Summary

In this chapter an SMADRC scheme with a nonlinear extended state observer and a sliding mode control component is proposed for the SbW system of a road vehicle, which can estimate the nonlinear extended state of the plant model accurately and guarantee the control robustness against system uncertainties and varying road conditions effectively. The stability of the SMADRC system is proved in the sense of Lyapunov. The experimental results in slalom path following, quick steering and shock disturbance rejection are shown to manifest the superiority of the designed SMADRC in terms of high tracking accuracy, strong robustness to handle system uncertainties and the change of road conditions, and fast convergence rate of tracking errors in comparison with a PDADRC and a CSMC.

Chapter 6

Iterative Learning Control

We have proposed an adaptive sliding mode controller, an adaptive fast nonsingular terminal sliding mode controller and a sliding mode-based active disturbance rejection controller, experimentally implemented these controllers to the SbW system, and achieved satisfactory experimental results. However, in the aspect of high tracking accuracy, there is still room for improvement. The iterative learning control is a control methodology known as its high tracking accuracy due to its iterative learning property. In this chapter, we will investigate an iterative learning controller as the performance benchmark for the SbW system under periodic steering commands.

6.1 Introduction

Iterative learning control (ILC) was originally introduced by Arimoto [130]. As a relatively effective control method for systems performing repetitive tasks and relating to nonlinear dynamics, ILC is essentially a feedforward control scheme which is able to overcome the drawbacks of feedback control algorithms by changing

the control input iteratively from trial to trial. The objective of ILC is to utilize the repetitive nature of the process and the past control information to alter the shape of demand profile such that the high-precision motion tracking can be achieved.

In [157], a combination of model-based and iterative learning control is proposed for direct-drive robots in repetitive motion tasks, in which the model-based part is used to compensate much of the nonlinear and coupled robot dynamics, and the iterative learning control part is used to improve the quantitative prediction of performance. A novel combination of iterative learning control and model predictive control is proposed in [158] for glycemic control in type-1 diabetes mellitus, which can learn from an individual's lifestyle allowing the control performance to be improved from day to day. In [159], M.-B. Radac *et al.* propose a model-free trajectory tracking of multiple-input and multiple-output systems by optimizing the reference input primitives in a model-free iterative learning control framework without using knowledge of the controlled process.

Motivated by the merits of ILC, in this chapter, we will design an iterative learning controller based on the ILC design methodology and apply the controller to our SbW system. The convergence property will be analyzed and the simulation results will be illustrated.

6.2 Control design

As described in Chapter 2, the plant model of the SbW system is

$$J\ddot{x} + c\dot{x} + \rho\text{sign}(\dot{x}) + \xi\tanh(x) = bu \tag{6.1}$$

where $J = J_0 + \Delta_J$, $c = c_0 + \Delta_c$. Thus, we can rewrite (6.2) into following form:

$$J_0\ddot{x} + c_0\dot{x} + [\Delta_J\ddot{x} + \Delta_c\dot{x} + \rho\text{sign}(\dot{x}) + \xi\tanh(x)] = bu \tag{6.2}$$

By treating the impact of the system uncertainties $\Delta_J\ddot{x} + \Delta_c\dot{x}$, the self-aligning torque τ and the Coulomb friction τ_{cf} as external disturbances to the steering system and ignoring them temporarily, we have a simplified linear second-order differential equation:

$$J_0\ddot{x} + c_0\dot{x} = bu. \tag{6.3}$$

Thus, the corresponding transfer function for the SbW model is:

$$G(s) = \frac{X(s)}{U(s)} = \frac{b}{J_0 s^2 + c_0 s} \tag{6.4}$$

where $X(s)$ is the steering angle of front wheels which is the Laplace transformation of x, $U(s)$ is the steering motor input voltage which is the Laplace transformation of u. Then, using the values of the parameters of J_0 and c_0 in (2.24), the transfer function of the SbW system in (6.4) can be obtained:

$$G(s) = \frac{273.5}{s(85.5s + 218.8)} = \frac{3.2}{s(s + 2.56)}, \tag{6.5}$$

based on which an iterative learning controller will be designed.

In order to design a discrete-time iterative learning controller for the SbW system with a periodic reference, we need to discretize the original plant model $G(s)$ in (6.5) by utilizing a sampling mechanism composed of the sampling interval T_s and a zero-order hold. Then the plant model $G(z)$ can be obtained and the task in-

terval $[0, T]$ can be discretized in a set N made up of sampled instances $0, 1, \ldots, N$, where $T = NT_s$ [160].

The architecture of the iterative learning controller used in this chapter is shown in Figure 6.1, where $Q(z)$ is a low-pass filter and $L(z)$ is a learning filter; $C(z)$ is a discrete-time PD controller; $P(z) = C(z)G(z)/[C(z)G(z) + 1]$ is the transfer function of the inner closed-loop system; μ is the learning gain; $r(z)$ is the reference; $u_i(z)$ is the control input signal at the ith trial in the iteration domain; $e_{i+1}(z) = r(z) - y_{i+1}(z)$ is the tracking error; $y_{i+1}(z) = P(z)u_{i+1}(z)$ is the output, namely, the steering angle of the front wheels of the SbW system. According to Figure 6.1, the discrete-time ILC algorithm can be written as [160]:

$$u_{i+1}(z) = Q(z)[u_i(z) + \mu L(z)e_i(z)]. \tag{6.6}$$

From (6.6) we can see that the ILC is a feedforward control algorithm because the control input $u_{i+1}(z)$ at the $(i + 1)$th trial is related to the control input and the tracking error of the previous trial, $u_i(z)$ and $e_i(z)$.

Now, we shall analyze the convergence property of ILC. Since we have $e_{i+1}(z) = r(z) - y_{i+1}(z) = r(z) - P(z)u_{i+1}(z)$, then the following equation is obtained:

$$-P(z)u_{i+1}(z) = e_{i+1}(z) - r(z). \tag{6.7}$$

Substituting (6.6) in (6.7) yields

$$\begin{aligned} & - P(z)u_{i+1}(z) \\ & = -P(z)Q(z)[u_i(z) + \mu L(z)e_i(z)] \\ & = Q(z)[-P(z)u_i(z) - \mu P(z)L(z)e_i(z)]. \end{aligned} \tag{6.8}$$

Combining (6.7) and (6.8), we obtain

$$\begin{aligned} & e_{i+1}(z) - r(z) \\ & = Q(z)[-P(z)u_i(z) - \mu P(z)L(z)e_i(z)]. \end{aligned} \tag{6.9}$$

Re-arranging (6.9) yields

$$\begin{aligned} & e_{i+1}(z) \\ =& r(z) + Q(z)[-P(z)u_i(z) - \mu P(z)L(z)e_i(z)] \\ =& Q(z)[r(z) - P(z)u_i(z) \\ & - \mu P(z)L(z)e_i(z)] + [1 - Q(z)]r(z) \\ =& Q(z)[e_i(z) - \mu P(z)L(z)e_i(z)] \\ & + [1 - Q(z)]r(z) \\ =& Q(z)[1 - \mu P(z)L(z)]e_i(z) + [1 - Q(z)]r(z). \end{aligned} \tag{6.10}$$

It is clear that the learning convergence property can be guaranteed if the norm of $1 - \mu P(z)L(z)$ is less than 1 [160]–[162], which can be stated as follows:

$$\sup_{\theta \in [-\omega_s T_s, \omega_s T_s]} \left| Q(e^{j\theta})[1 - \mu P(e^{j\theta})L(e^{j\theta})] \right| < 1 \tag{6.11}$$

where $\theta \triangleq \omega T_s$, $\omega \leq \omega_s$, and ω_s is the Nyquist frequency in rad/s. This condition

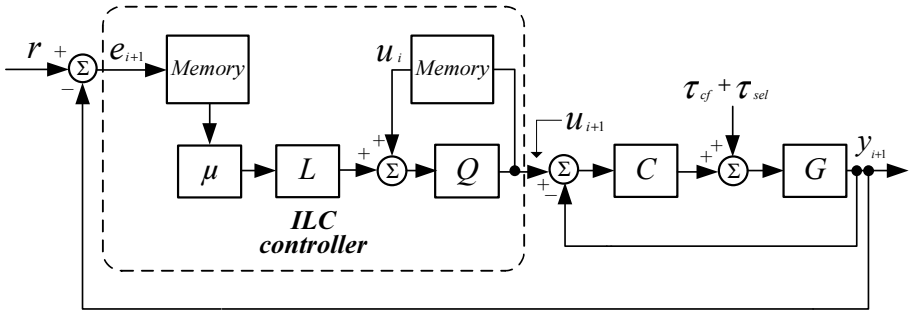

Figure 6.1: Discrete ILC architecture.

can be equivalently explained as that the Nyquist plot of $Q(z)[1 - \mu P(z)L(z)]$ should be within a unit circle centered at the origin of the complex plane.

Rearranging (6.5) yields

$$G(s) = \frac{273.5}{85.5s + 218.8} \cdot \frac{1}{s} \tag{6.12}$$

which is separated into two multipliers in order to add the external disturbances τ_{sel} and τ_{cf} in the simulation by constructing the block diagram of Simulink. By using a sampling mechanism composed of the sampling interval $T_s = 0.01$ sec and a zero-order hold, we get

$$\begin{aligned} G(z) =& \frac{0.03158}{z - 0.9747} \cdot \frac{0.01}{z - 1} \\ =& \frac{0.00032}{z^2 - 1.9747z + 0.9747}. \end{aligned} \tag{6.13}$$

To guarantee the robustness of the control system, a PD controller is designed to constitute an inner closed-loop system, which has a transfer function in $S-$domain as [165]:

$$C(s) = s + 6. \tag{6.14}$$

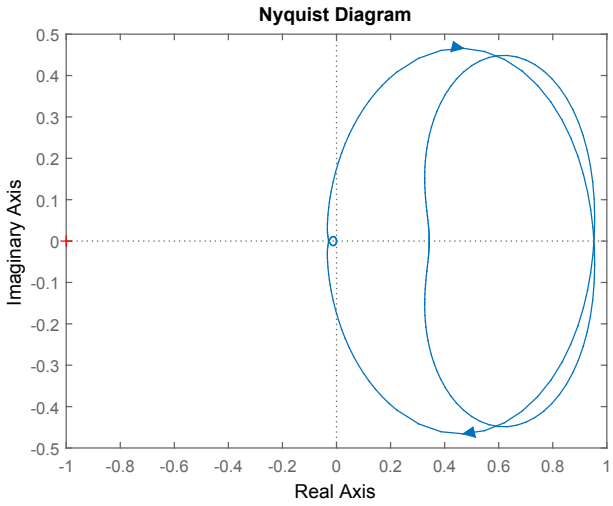

Figure 6.2: Nyquist plot of $P(z)$ which is within the unit circle centered at the origin of the complex plane indicating that the learning convergence property is guaranteed.

Then the transfer function of the PD controller in $Z-$domain is given by:

$$C(z) = \frac{206z - 194}{z + 1}. \tag{6.15}$$

Here, the basic design requirement is to ensure the Nyquist plot of $Q(z)[1 - \mu L(z)P(z)]$ being within a unit circle centered at the origin of the complex plane such that stability of the ILC control system can be guaranteed. For this goal, the low-pass filter $Q(s)$ can be selected with its cut-off frequency of 15 Hz, that is,

$$Q(s) = \frac{1}{\frac{1}{2\pi \cdot 15}s + 1}. \tag{6.16}$$

Its discretized version is given by:

$$Q(z) = \frac{0.3202z + 0.3202}{z - 0.3596}. \tag{6.17}$$

The transfer function $P(z)$ of the inner closed-loop system would be

$$\begin{aligned} P(z) =& \frac{C(z)G(z)}{1 + C(z)G(z)} \\ =& \frac{0.06592z - 0.06208}{z^3 - 0.9747z^2 - 0.9341z + 0.9126}. \end{aligned} \tag{6.18}$$

The learning filter $L(z)$ is designed as

$$L(z) = \frac{z - 0.75}{0.25z} \tag{6.19}$$

and the learning gain is selected as

$$\mu = 0.65. \tag{6.20}$$

As such, we can draw the Nyquist plot of $Q(z)[1 - \mu L(z)P(z)]$ as shown in Figure 6.2, which clearly shows that it is within a unit circle centered at the origin of the complex plane, indicating that the designed iterative learning controller achieves the convergence property.

As we know, in reality, it is not always the case that the road curves evenly and periodically. Sometimes, the curve of the road seems to be random and non-periodic. So the reference signal which the steering angle of front wheels tries to track is not a periodic signal. In this case, the iterative learning controller can not play its role well. To guarantee that the designed controller can adapt to different scenarios we confront in reality, we have a switch strategy, which is made up of two cases described as follows.

Case 1: When the driver perceives that the reference signal of the controller is a periodic signal, namely, the road has a repeated curve, then the iterative learning

controller in (6.6) will be switched on and added to the PD controller. As a result, the tracking errors will converge based on the aforementioned analysis.

Case 2: When the road that the driver confronts does not contain repeated curves, the iterative learning controller will be switched off and the control input $u_{i+1}(z)$ equals to the reference $r(z)$. As such, only the PD controller is in action.

The simulation results of Case 1 with a sinusoidal reference signal and Case 2 with a more general non-periodic reference signal are shown in Figures 6.3–6.5, respectively.

6.3 Simulation results

We study the simulation results to learn the characteristics, merits and drawbacks of the proposed iterative learning controller. Experimental verification will be conducted in future work. The simulation results are shown in Figures 6.3–6.5.

From Figure 6.3, we can see that during the first period of the sinusoidal reference signal r, the control input is totally 0 V because the iterative learning controller we designed is trying to "learn" and "memorize" the reference signal r during the first period. That is why the tracking error of the first period is extremely large with the maximum peak-to-peak value of 0.6. But the tracking error attenuates promptly with the increment of the iteration trials of the iterative learning controller. As shown in Figure 6.4, during 20 s to 25 s, the tracking performance is excellent with an extremely small maximum peak-to-peak tracking error of 0.03 rad approximately. From Figure 6.3 we can see that the iterative learning controller also presents strong robustness against the change of the self-aligning

torque τ_{sel} because the tracking error at the moment after 14 s stays almost the same as the one at the moment before 14 s and further converges to smaller values rapidly with just two iteration trials. It is also proved that the switch design of the iterative learning controller takes effect from Figure 6.5. When the reference signal is a more general non-periodic signal, the ILC skips the feedforward learning procedure and the inner PD controller starts to work. The steering angle of front wheels tracks the non-periodic reference signal well with the maximum peak-to-peak tracking error of approximate 0.045 rad. Therefore, the simulation results have clearly shown the convergence of the tracking errors in both cases.

The best merit of ILC is that it provides an optimal performance benchmark in the presence of periodic steering command such that we could use it to evaluate other controller performance. However, the method of ILC may not be practical because the steering commands may not be periodic all the time in reality. In addition, the robustness of ILC is much less than that of the sliding mode-based control methods as addressed in previous chapters. We will study these issues in the future.

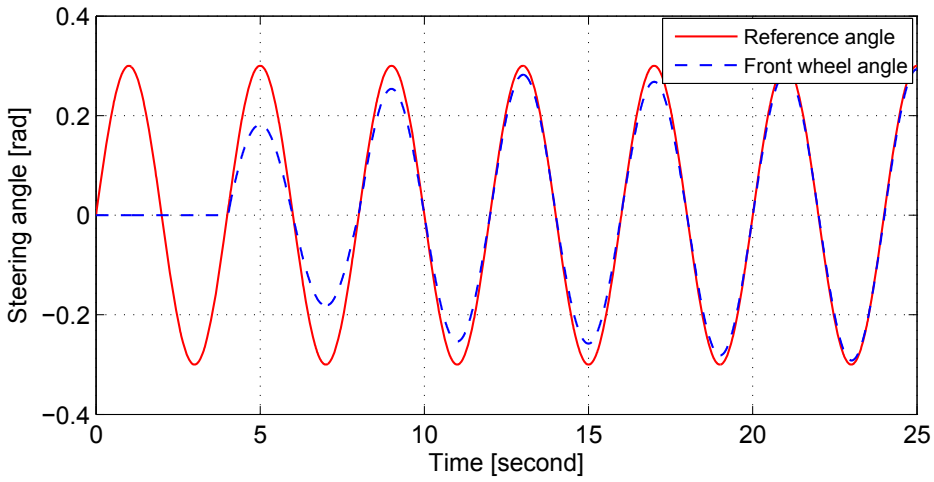

(a) Tracking performance

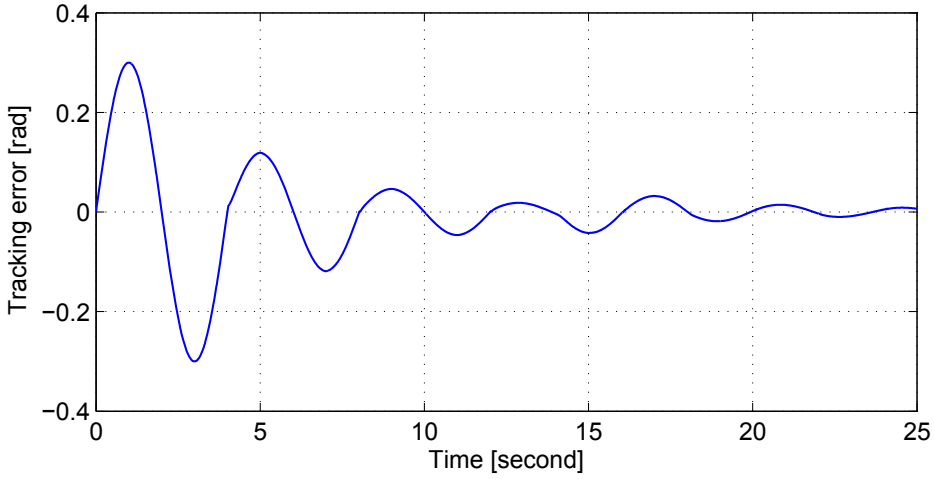

(b) Tracking error

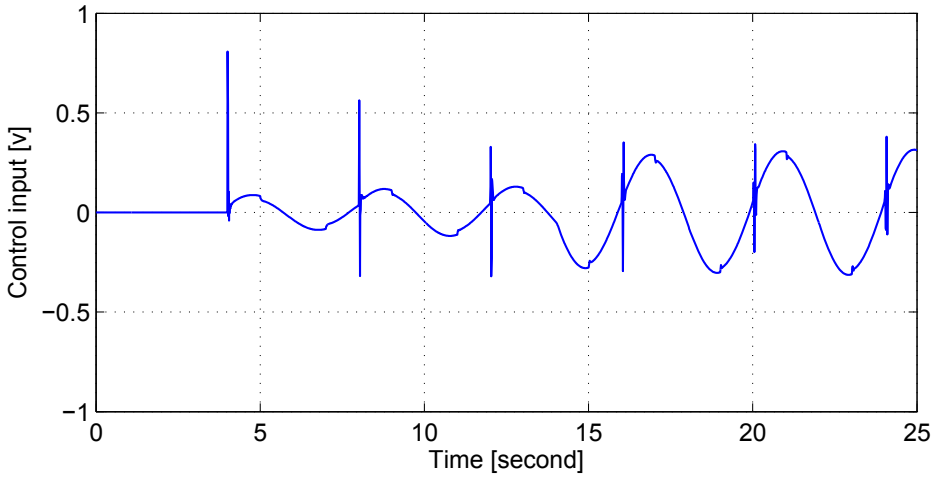

(c) Control input

Figure 6.3: Simulation results of the iterative learning controller in Case 1 during 0s to 25s.

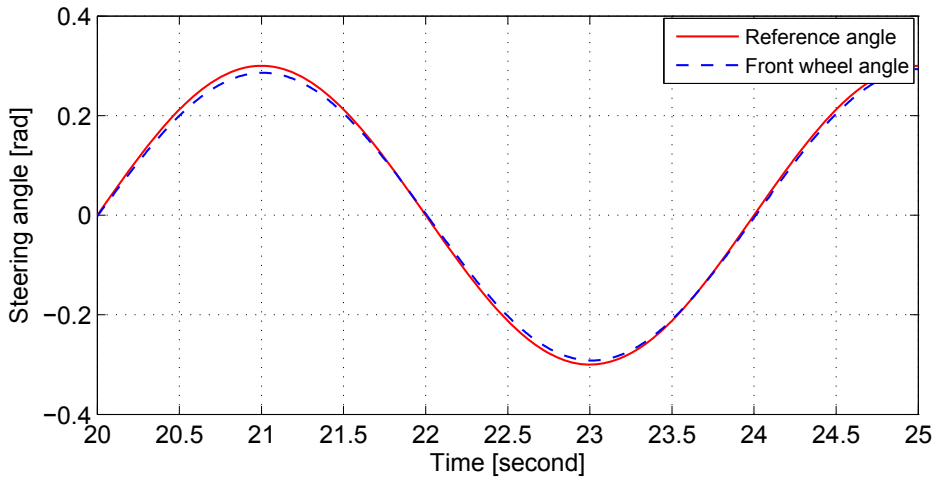

(a) Tracking performance

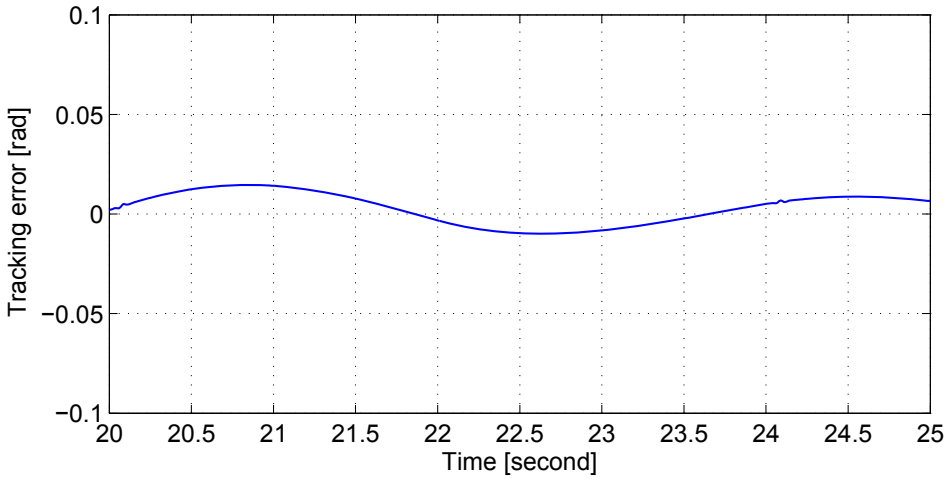

(b) Tracking error

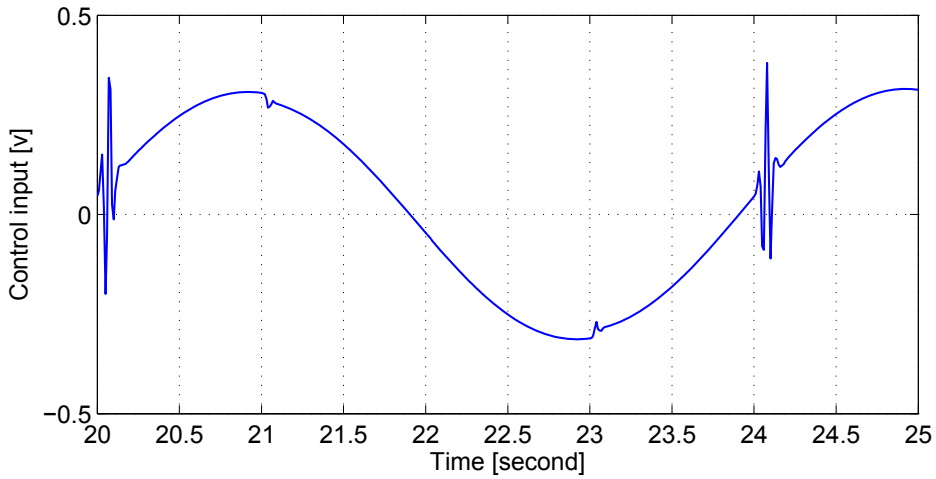

(c) Control input

Figure 6.4: Simulation results of the iterative learning controller in Case 1 during 20s to 25s.

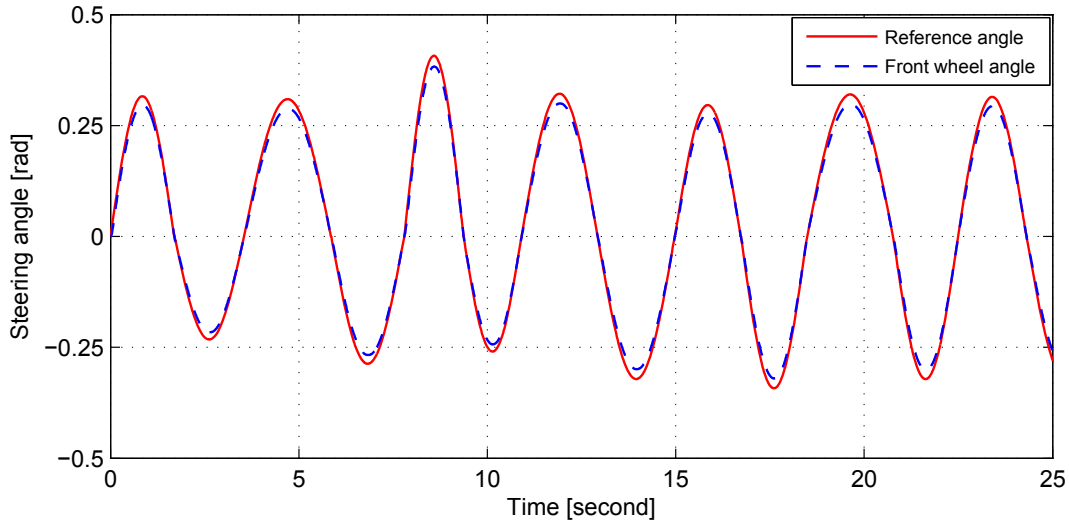

(a) Tracking performance

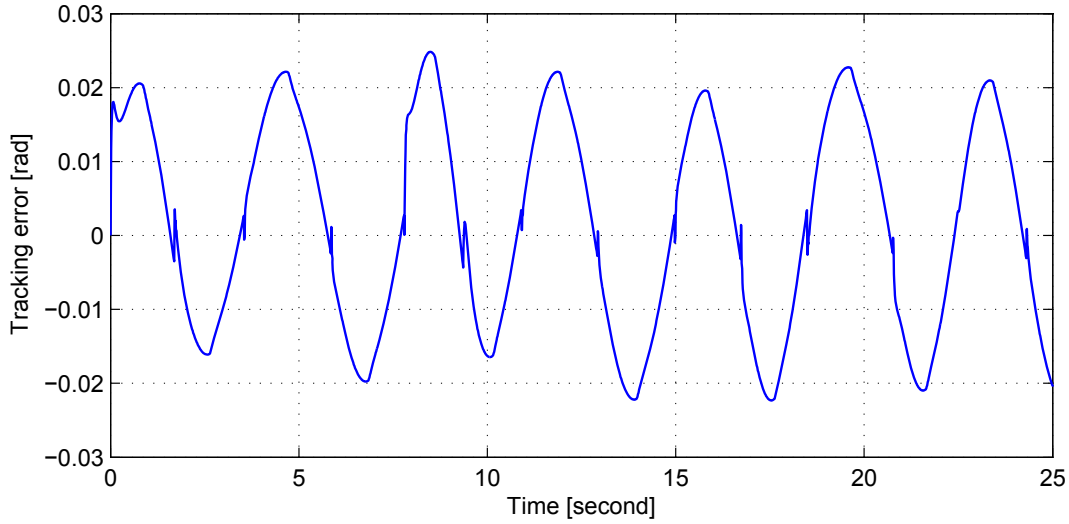

(b) Tracking error

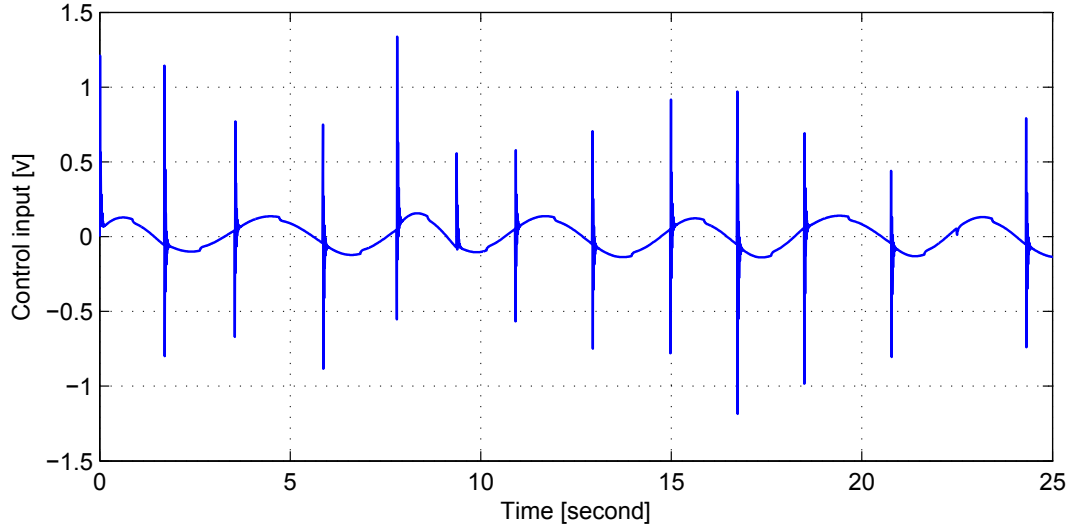

(c) Control input

Figure 6.5: Simulation results of the iterative learning controller in Case 2.

6.4 Summary

In this chapter, we design an iterative learning controller for the SbW system. The proposed iterative learning control can utilize the repetitive nature of the process and the past control information to change the control input iteratively from trial to trial such that the high-precision motion tracking can be achieved. From the simulation results we can see that after several iteration trials, the designed iterative learning controller can achieve a high tracking precision with rather small tracking errors. However, it should also be noted that the reference command for the iterative learning control must be periodic and even, which is unrealistic in the SbW control application due to the uneven and non-periodic road curves existing in real world. Hence, we will only use the performance achieved by iterative learning control to evaluate other control performance. The experimental work and other relevant issues will be conducted in our future work.

Chapter 7

Conclusion and Future Work

7.1 Conclusions

In this thesis, the experimental platform of the SbW system is shown, the mathematical model of the SbW system from the steering motor to the front wheels and the model of the self-aligning torque imposed on the steering system are described. With the control-oriented model of the SbW system, we have designed four different controllers, namely, an adaptive sliding mode controller, an adaptive fast non-singular terminal sliding mode controller, a sliding mode-based active disturbance rejection controller and an iterative learning controller, respectively. Through MATLAB Simulink, the simulation results of the adaptive sliding mode controller, the adaptive fast non-singular terminal sliding mode controller, the sliding mode-based active disturbance rejection controller and the iterative learning controller are obtained and analyzed. Besides, experiments of the adaptive sliding mode controller, the adaptive fast non-singular terminal sliding mode controller and the sliding mode-based active disturbance rejection controller are carried out

in the SbW experimental platform, and the experimental results are compared and analyzed based on the simulation results. Hence, advantages and disadvantages of the proposed controllers are analyzed based on the simulation results and experimental results.

The conventional sliding mode controller is experimentally verified to possess good tracking accuracy and strong robustness against not only the parametric uncertainties existing in the plant model but also varying road conditions. However, there is still the phenomenon of conservative control in the conventional sliding mode controller since it can only compensate for the self-aligning torque based on the upper bound. On the other hand, the proposed adaptive sliding mode controller is superior to the conventional one because it can not only guarantee the robustness against the parametric uncertainties via the sliding mode control algorithm, but also estimate the coefficient of the self-aligning torque. Thus the tracking accuracy is improved to a large extent because the self-aligning torque is compensated by the controller more accurately.

Compared with the conventional sliding mode controller, the performance of the adaptive sliding mode control is superior. However, the convergence rate of the tracking error under the adaptive sliding mode control is still slow, especially in the case of disturbance rejection during vehicle driving. This motivates us to combine the fast non-singular terminal sliding mode control with the adaptive estimation law such that the controller can possess good tracking accuracy by utilizing the adaptive estimation law to effectively estimate the self-aligning torque and strong robustness and fast convergence rate by the fast non-singular terminal sliding mode control law. The experimental results have obviously verified that the

designed adaptive fast non-singular terminal sliding mode controller can achieve the performance as we desire.

On this basis, we note that all these controllers need accurate mathematical models of the SbW system. However, the actual dynamical model may be very complicated with respect to many factors. For easy implementation, the mathematical model we adopted is a simplified one under the assumption of a small side-slip angle. Due to the restrictions of our experimental setup, there is no actual self-aligning torque acting on the steering wheels. Thus, the model of the self-aligning torque is also a simplified one. This motivates us to develop a controller with stronger robustness which is less dependent on accurate mathematical models. Hence, a sliding mode-based active disturbance rejection controller is designed for the SbW system. The simulation and experimental results indicate that the sliding mode-based active disturbance rejection controller is able to achieve good control performance without knowing the accurate mathematical model of the self-aligning torque. The nonlinear extended state observer can effectively estimate and compensate for the self-aligning torque disturbance to improve the tracking accuracy. Thus, the design and implementation of the sliding mode-based active disturbance rejection controller for the SbW system are proved to be innovative and successful.

When the reference signal is periodic, the tracking performance of the iterative learning controller after the 4th or the 5th iteration trial is extremely excellent which can be proved by the extraordinarily small maximum peak-to-peak tracking error regardless of the variation of external disturbances imposed on the steering system. But the tracking performance before the 3rd iteration trial is inferior to the ones of the adaptive sliding mode controller, the adaptive fast non-singular

terminal sliding mode controller and the sliding mode-based active disturbance rejection controller, especially the tracking performance in the 1st iteration due to the "learning" of the ILC. But we should also note that the proposed iterative learning controller turns out to be just a PD controller when the reference signal is non-periodic. Thus, its tracking performance is inferior to the other controllers. However, the iterative learning controller can still be used as a benchmark to evaluate other controller performance in the presence of periodic steering commands.

7.2 Future works

To this end, there are still several future works to be carried out. They are listed as follows.

1. Improvement of experimental setup

As shown in Figure 2.1, the current experimental setup of the SbW system is not a real vehicle, which leads to many restrictions, such as the lack of forward velocity of front wheels and the deficiency of the specific vehicle weight distributed on the front wheels. These restrictions result in the difficulty of generating actual frictions and self-aligning torques in experiments. Therefore, the first future work is to improve the experimental setup. We consider to implement an SbW system to a real ground vehicle such that the dynamics of the SbW systems can be thoroughly reflected in experiments, and more effective control schemes can be experimentally implemented to the SbW equipped vehicles.

2. Neural network control design for SbW systems

As one of the newly developed intelligent control methodologies, neural network control is pretty effective and widely utilized in the control of complex, nonlinear and uncertain systems. Hence, our next future work is to design an effective neural network controller for the vehicle SbW system, and implement the newly designed neural network controller to our new SbW equipped experimental ground vehicle.

3. Rollover preventing control for SbW equipped vehicles

When an SbW equipped vehicle is steering, the vehicle may be led outside of the curve it is trying to follow by the centrifugal force acting on it. Specifically, when the speed of the vehicle is high, the vehicle becomes pretty sensitive to

the steering input and the variation of system parameters, which can affect the vehicle's roll behavior severely. Hence, the design and implementation of control schemes for SbW equipped vehicle to predict and prevent rollover accident and improve vehicle's stability is of great importance. Many researches have been carried out in rollover preventing control for heavy vehicles and heavy trucks [163]–[166]. However, the investigation of rollover preventing control for SbW equipped vehicles is still very rare, which motivates us to investigate effective control schemes for SbW equipped vehicles to prevent rollover accident in the future.

4. Vehicle brake-by-wire systems control design

Brake-by-Wire (BbW) technology is also an important part of the Drive-by-Wire technology in automobile industry. The BbW system utilizes electromechanical actuators and communication networks to replace conventional mechanical or hydraulic devices such that enhanced safety and comfort can be achieved, cost related to manufacturing and maintenance can be cut off, and environmental concerns caused by hydraulic systems can be eliminated [167]. Since a real ground vehicle will be adopted as the experimental setup in the next stage, a BbW system will be installed on the vehicle and the control schemes for the BbW system will also be investigated in the future work.

Bibliography

[1] J. W. Post, "Modelling, simulation and testing of automobile power steering system for the evaluation of on-centre handling," PhD. dissertation, Graduate School Clemson University, Clemson, SC, 1995.

[2] Y. Xue and J. Watton, "Modelling of a hydraulic powering steering system," *International Journal of Vehicle Design*, vol. 38, no. 2, 2005.

[3] Y. Inaguma, K. Suzuki and K. Haga, "An energy saving technique in an electro-hydraulic power steering ehps system," in *SAE International Congress and Exposition*, no. 960934, Detroit, Michigan, USA, March, 1996.

[4] A. B. Proca and A. Keyhani, "Identification of power steering system dynamic models," *Mechatronics*, vol. 8, no. 3, pp. 255-270, April, 1998.

[5] J. Hur, "Characteristics analysis of interior permanent-magnet synchronous motor in electrohydraulic power steering systems," *IEEE Transactions on Industrial Electronics*, vol. 55, no. 6, pp. 2316-2323, June, 2008.

[6] D. Ammon, M. Borner, and J. Rauh, "Simulation of the perceptible feed-forward and feed-back properties of hydraulic power-steering systems on the

vehicle's handling behavior using simple physical models," *Vehicle System Dynamics*, vol. 44, Supplement, pp. 158-170, April, 2007.

[7] M. Rosth, "Hydraulic power steering system design in road vehicles," PhD. dissertation, Department of Mechanical Engineering, Linkoping University, Linkoping, Sweden, 2007.

[8] T. Wong, "Hydraulic power steering system design and optimization simulation," in *SAE 2001 World Congress*, no. 2001-01-0479, Detroit, Michigan, USA, March, 2001.

[9] V. Kokotovic, J. Grabowski, V. Amin and J. Lee, "Electro hydraulic power steering system," in *SAE International Congress and Exposition*, no. 1999-01-0404, Detroit, Michigan, USA, March, 1999.

[10] M. Parmar and J. Y. Yung, "A sensorless optimal control system for an automotive electric power assist steering system," *IEEE Transactions on Industrial Electronics*, vol. 51, no. 2, pp. 290-298, April, 2004.

[11] A. Marouf, M. Djemai, C. Sentouh and P. Pudlo, "A new control strategy of an electric-power-assisted steering system," *IEEE Transactions on Vehicular Technology*, vol. 61, no. 8, pp. 3574-3589, October, 2012.

[12] Y. G. Liao and H. I. Du, "Modelling and analysis of electric power steering system and its effect on vehicle dynamic behaviour," *International Journal of Vehicle Autonomous Systems*, vol. 1, no. 2, pp. 153-166, 2003.

[13] J. H. Kim and J. B. Song, "Control logic for an electric power steering system using assist motor," *Mechatronics*, vol. 12, no. 3, pp. 447-459, October, 2000.

[14] X. Chen, T. Yang, X. Chen and K. Zhou, "A generic model-based advanced control of electric power-assisted steering systems," *IEEE Transactions on Control Systems Technology*, vol. 16, no. 6, pp. 1289-1300, November, 2008.

[15] P. Zhao, X. Lin, J. Chen and J. Men, "Parametric design and application of steering characteristic curve in control for electric power steering," *Mechatronics*, vol. 19, no. 6, pp. 905-911, September, 2009.

[16] A. Marouf, M. Djemai, C. Sentouh and P. Pudlo, "Sensorless control of electric power assisted steering system," in *Proceedings of 20th Mediterranean Conference on Control and Automation*, Barcelona, pp. 909-914, July, 2012.

[17] D. Peter and R. Gerhard, "Electric power steering-the first step on the way to steer-by-wire," in *SAE International Congress and Exposition*, no. 1999-01-0401, Detroit, Michigan, USA, March, 1999.

[18] A. W. Burton, "Innovation drivers for electric power-assisted steering," *IEEE Control Systems Magazine*, vol. 23, no. 6, pp. 30-39, December, 2003.

[19] A. T. Zaremba, M. K. Liubakka and R. M. Stuntz, "Control and steering feel issues in the design of an electric power steering system," in *Proceedings of American Control Conference*, Philadelphia, PA, pp. 36-40, June, 1998.

[20] R. Isermann, R. Schwarz and S. Stolzl, "Fault-tolerant drive-by-wire systems," *IEEE Control Systems*, vol. 22, no. 5, pp. 64-81, October, 2002.

[21] Y-J. Pan, C. Canudas-de-Wit and O. Sename, "A new predictive approach for bilateral teleoperation with applications to drive-by-wire systems," *IEEE Transactions on Robotics*, vol. 22, no. 6, pp. 1146-1162, December, 2006.

[22] R. Hoseinnezhad and A. Bab-Hadiashar, "Missing data compensation for safety-critical components in a drive-by-wire system," *IEEE Transactions on Vehicular Technology*, vol. 54, no. 4, pp. 1304-1311, July, 2005.

[23] C. Rossi, A. Tilli and A. Tonielli, "Robust control of a throttle body for drive by wire operation of automotive engines," *IEEE Transactions on Control Systems Technology*, vol. 8, no. 6, pp. 993-1002, November, 2000.

[24] S. Haggag, D. Alstrom, S. Cetinkunt and A. Egelja, "Modeling, control, and validation of an electro-hydraulic steer-by-wire system for articulated vehicle applications," *IEEE/ASME Transactions on Mechatronics*, vol. 10, no. 6, pp. 688-692, December, 2005.

[25] S. Anwar and L. Chen, "An analytical redundancy-based fault detection and isolation algorithm for a road-wheel control subsystem in a steer-by-wire system," *IEEE Transactions on Vehicular Technology*, vol. 56, no. 5, pp. 2859-2869, September, 2007.

[26] M. B. N. Shah, A. R. Husain, H. Aysan, S. Punnekkat, R. Dobrin and F. A. Bender, "Error handling algorithm and probabilistic analysis under fault for CAN-based steer-by-wire system," *IEEE Transactions on Industrial Informatics*, vol. 12, no. 3, pp. 1017-1034, June, 2016.

[27] M. Bertoluzzo, G. Buja and R. Menis, "Control schemes for steer-by-wire systems," *IEEE Industrial Electronics Magazine*, vol. 1, no. 1, pp. 20-27, May, 2007.

[28] C. D. Gadda, S. M. Laws and J. C. Gerdes, "Generating diagnostic residuals for Steer-by-Wire Vehicles," *IEEE Transactions on Control Systems Technology*, vol. 15, no. 3, pp. 529-540, May, 2007.

[29] A. Balachandran and J. C. Gerdes, "Designing steering feel for steer-by-wire vehicles using objective measures," *IEEE/ASME Transactions on Mechatronics*, vol. 20, no. 1, pp. 373-383, June, 2014.

[30] H. E. B. Russell and J. C. Gerdes, "Design of variable vehicle handling characteristics using four-wheel steer-by-wire," *IEEE Transactions on Control Systems Technology*, vol. 24, no. 5, pp. 1529-1540, December, 2015.

[31] S. Anwar and B. Zheng, "An antilock-braking algorithm for an eddy-current-based brake-by-wire system," *IEEE Transactions on Vehicular Technology*, vol. 56, no. 3, pp. 1100-1107, May, 2007.

[32] W. Xiang, P. C. Richardson, C. Zhao and S. Mohammad, "Automobile brake-by-wire control system design and analysis," *IEEE Transactions on Vehicular Technology*, vol. 57, no. 1, pp. 138-145, January, 2008.

[33] M. Tanelli, A. Astolfi and S. M. Savaresi, "Robust nonlinear output feedback control for brake by wire control systems," *Automatica*, vol. 44, pp. 1078-1087, April, 2008.

[34] S. Anwar, "Generalized predictive control of yaw dynamics of a hybrid brake-by-wire equipped vehicles," *Mechatronics*, vol. 15, pp. 1089-1108, November, 2005.

[35] S. Haggag, D. Alstron, S. Cetinkunt and A. Egelja, "Modeling, control and validation of an electro-hydraulic steer-by-wire system for articulated vehicle applications," *IEEE/ASME Transactions on Mechatronics*, vol. 10, no. 6, pp. 688-692, December, 2005.

[36] M. Lindner and T. Tille, "Design of highly integrated mechatronic gear selector levers for automotive shift-by-wire systems," *IEEE/ASME Transactions on Mechatronics*, vol. 15, no. 6, pp. 961-968, December, 2010.

[37] S. Burkhardt, R. Ehrmaier, S. Furst and J. Neuner, "Shift-by-wire system gear changes in the new BMW 7 series (Meeting on Transmissions in Automotive Vehicles)," VDI Berichte, vol. 1610, pp. 497-518, June, 2001.

[38] H. P. Buchs, H. Versmold and I. Neunzig, "Shift-by-wire system gear changes simplified shifting with electronic implementation of safety features (Meeting on Transmissions in Automotive Vehicles)," VDI Berichte, vol. 1610, pp. 481-495, June 2001.

[39] S. A. Zulkifli, V. S. Asirvadam, N. Saad, A. R. A. Aziz and A. A. M. Mohideen, "Implementation of electronic throttle-by-wire for a hybrid electric vehicle using national instruments' compactRIO and labview real-time," in *Proceedings of the International Conference on Intelligent and Advanced Systems*, pp. 1-6, June, 2014.

[40] S. A. Zulkifli, V. S. Asirvadam, N. Saad and A. R. A. Aziz, "Implementation of electronic throttle-by-wire for a hybrid electric vehicle using national instruments' compactRIO and Labview real-time," in *Proceedings of 5th In-*

ternational Conference on Intelligent and Advanced Systems, pp. 1-6, June, 2014.

[41] R. Rajamani, *Vehicle Dynamics and Control*. Minneapolis, MN, USA: Springer, 2012.

[42] Y-H. J. Hsu, S. M. Laws and J. C. Gerdes, "Estimation of tire slip angle and friction limits using steering torque," *IEEE Transactions on Control Systems Technology*, vol. 18, no. 4, pp. 896-907, July, 2010.

[43] F. Wilhelm, T. Tamura, R. Fuchs and P. Mullhaupt, "Friction compensation control for power steering," *IEEE Transactions on Control Systems Technology*, vol. 24, no. 4, pp. 1354-1367, July, 2016.

[44] M. S. Mahmoud and M. F. Emzir, "Unknown-input estimator-based controller design of electric power-assisted steering system," *IET Control Theory & Applications*, vol. 6, no. 16, pp. 2485-2492, November, 2012.

[45] J. Choi, K. Yi, J. Suh and B. Ko, "Coordinated control of motor-driven power steering torque overlay and differential braking for emergency driving support," *IEEE Transactions on Vehicular Technology*, vol. 63, no. 2, pp. 566-579, February, 2014.

[46] M. Parmar and J. Y. Hung, "A sensorless optimal control system for an automobile electric power assist steering system," *IEEE Transactions on Industrial Electronics*, vol. 51, no. 2, pp. 290-298, April, 2004.

[47] N. Matsunaga, J. Im and S. Kawaji, "Control of steering-by-wire system of electric vehicle using bilateral control designed by passivity approach," *Journal of System Design and Dynamics*, vol. 4, no. 1, pp. 50-60, 2010.

[48] P. Yih and J. C. Gerdes, "Modification of vehicle handling characteristics via steer-by-wire," *IEEE Transactions on Control Systems Technology*, vol. 13, no. 6, pp. 965-976, November, 2005.

[49] H. Wang, H. Kong, Z. Man, D. M. Tuan, Z. Cao and W. Shen, "Sliding mode control for steer-by-wire systems with ac motors in road vehicles," *IEEE Transactions on Industrial Electronics*, vol. 61, no. 3, pp. 1596-1611, March, 2014.

[50] A. Baviskar, J. R. Wagner and D. M. Dawson, "An adjustable steer-by-wire haptic-interface tracking controller for ground vehicles," *IEEE Transactions on Vehicular Technology*, vol. 58, no. 2, pp. 546-554, February, 2009.

[51] S. Haggag, D. Alstrom, S. Cetinkunt and A. Egelja, "Modeling, control, and validation of an electro-hydraulic steer-by-wire system for articulated vehicle applications," *IEEE/ASME Transactions on Mechatronics*, vol. 10, no. 6, pp. 688-692, December, 2005.

[52] P. Setlur, J. R. Wagner, D. M. Dawson and D. Braganza, "A trajectory tracking steer-by-wire control system for ground vehicles," *IEEE Transactions on Vehicular Technology*, vol. 55, no. 1, pp. 76-85, January, 2006.

[53] S. Anwar and L. Chen, "An analytical redundancy-based fault detection and isolation algorithm for a road-wheel control subsystem in a steer-by-wire

system," *IEEE Transactions on Vehicular Technology*, vol. 56, no. 5, pp. 2859-2869, September, 2007.

[54] K. H. Ang, G. Chong and Y. Li, "Pid control system analysis, design, and technology," *IEEE Transactions on Control Systems Technology*, vol. 13, no. 4, pp. 559-576, July, 2005.

[55] T. L. Lam, H. Qian and Y. Xu, "Omnidirectional steering interface and control for a four-wheel independent steering vehicle," *IEEE/ASME Transactions on Mechatronics*, vol. 15, no. 3, pp. 329-338, June, 2007.

[56] N. C. Shieh, "Robust output tracking control of a linear brushless dc motor with time-varying disturbances," *IEE Proceedings-Electric Power Applications*, vol. 149, no. 1, pp. 39-45, January, 2002.

[57] N. C. Shieh and P. C. Tung, "Robust output tracking control of a linear dc brushless motor for transportation in manufacturing system," *IEE Proceedings-Electric Power Applications*, vol. 148, no. 2, pp. 119-124, March, 2001.

[58] M. Boccadoro, F. Martinelli and P. Valigi, "Supply chain management by H-infinity control," *IEEE Transactions on Automation Science and Engineering*, vol. 5, no. 4, pp. 703-707, March, 2008.

[59] R. B.-Quintero and M. J. Pont, "Implementation of H-infinity control algorithms for sensor-constrained mechatronic systems using low-cost microcontrollers," *IEEE Transactions on Industrial Informatics*, vol. 4, no. 3, pp. 175-184, August, 2008.

[60] G. Willmann, D. F. Coutinho, L. F. A. Pereira and F. B. Libano, "Multiple-loop H-infinity control design for uninterruptable power supplies," *IEEE Transactions on Industrial Electronics*, vol. 54, no. 3, pp. 1591-1602, April, 2007.

[61] D. Lefebvre, P. Chevrel and S. Richard, "An H-infinity-based control design methodology dedicated to the active control of vehicle longitudinal oscillations," *IEEE Transactions on Control Systems Technology*, vol. 11, no. 6, pp. 948-956, January, 2004.

[62] H. Imanari, Y. Morimatsu, K. Sekiguchi, H. Ezure, R. Matuoka, A. Tokuda and H. Otobe, "Looper H-infinity control for hot-strip mills," *IEEE Transactions on Industry Applications*, vol. 33, no. 3, pp. 790-796, August, 2002.

[63] R. A. Nichols, R. T. Reichert and W. J. Rugh, "Gain scheduling for H-infinity controllers: a flight control example," *IEEE Transactions on Control Systems Technology*, vol. 1, no. 2, pp. 69-79, August, 2002.

[64] Z. Du, D. Yue and S. Hu, "H-infinity stabilization for singular networked cascade control systems with state delay and disturbance," *IEEE Transactions on Industrial Informatics*, vol. 10, no. 2, pp. 882-894, May, 2014.

[65] M. Alma, J. J. Martinez, L. D. Landau and G. Buche, "Design and tuning of reduced order H-infinity feedforward compensators for active vibration control," *IEEE Transactions on Control Systems Technology*, vol. 20, no. 2, pp. 554-561, March, 2012.

[66] C. Huang, Y. Bai and X. Liu, "H-infinity state feedback control for a class of networked cascade control systems with uncertain delay," *IEEE Transactions on Industrial Informatics*, vol. 6, no. 1, pp. 62-72, February, 2010.

[67] M. Makarov, M. Grossard, P. R.-Ayerbe and D. Dumur, "Modeling and preview H_∞ control design for motion control of elastic-joint robots with uncertainties," *IEEE Transactions on Industrial Electronics*, vol. 63, no. 10, pp. 6429-6438, October, 2016.

[68] F. Chee, A. V. Savkin, T. L. Fernando and S. Nahavandi, "Optimal H_∞ insulin injection control for blood glucose regulation in diabetic patients," *IEEE Transactions on Biomedical Engineering*, vol. 52, no. 10, pp. 1625-1631, October, 2005.

[69] J. P. Ortiz, L. I. Minchala and M. J. Reinoso, "Nonlinear robust H-infinity PID controller for the multivariable system quadrotor," *IEEE Latin America Transactions*, vol. 14, no. 3, pp. 1176-1183, March, 2016.

[70] X. Huang, H. Zhang, G. Zhang and J. Wang, "Robust weighted gain-scheduling H_∞ vehicle lateral motion control with considerations of steering system backlash-type hysteresis," *IEEE Transactions on Control Systems Technology*, vol. 22, no. 5, pp. 1740-1753, September, 2014.

[71] K. Liao, Z. He, Y. Xu, G. Chen, Z. Y. Dong and K. P. Wong, "A sliding mode based damping control of DFIG for interarea power oscillations," *IEEE Transactions on Sustainable Energy*, vol. 8, no. 1, pp. 258-267, January, 2017.

[72] C. A. Evangelista, A. Pisano, P. Puleston and E. Usai, "Receding horizon adaptive second-order sliding mode control for doubly-fed induction genera-

tor based wind turbine.," *IEEE Transactions on Control Systems Technology*, vol. 25, no. 1, pp. 73-84, March, 2016.

[73] M. Rezkallah, S. K. Sharma, A. Chandra, B. Singh and D. R. Rousse, "Lyapunov function and sliding mode control approach for the solar-PV grid interface system," *IEEE Transactions on Industrial Electronics*, vol. 64, no. 1, pp. 785-795, January, 2017.

[74] J. Liu, S. Vazquez, L. Wu, A. Marquez, H. Gao, L. G. Franquelo, "Extended state observer-based sliding-mode control for three-phase power converters," *IEEE Transactions on Industrial Electronics*, vol. 64, no. 1, pp. 22-31, January, 2017.

[75] H. Li, J. Wang, H-K. Lam, Q. Zhou and H. Du, "Adaptive sliding mode control for interval type-2 fuzzy systems," *IEEE Transactions on Systems, Man, and Cybernetics: Systems*, vol. 46, no. 12, pp. 1654-1663, April, 2016.

[76] V. Repecho, D. Biel, J. M. Olm and E. F. Colet, "Switching frequency regulation in sliding mode control by a hysteresis band controller," *IEEE Transactions on Power Electronics*, vol. 32, no. 2, pp. 1557-1569, March, 2016.

[77] M. H. Choi, B. Shirinzadeh and R. Porter, "System identification-based sliding mode control for small-scaled autonomous aerial vehicles with unknown aerodynamics derivatives," *IEEE/ASME Transactions on Mechatronics*, vol. 21, no. 6, pp. 2944-2952, June, 2016.

[78] F. Sebaaly, H. Vahedi, H. Y. Kanaan, N. Moubayed and K. Al-Haddad, "Design and implementation of space vector modulation-based sliding mode con-

trol for grid-connected 3L-NPC inverter," *IEEE Transactions on Industrial Electronics*, vol. 63, no. 12, pp. 7854-7863, May, 2016.

[79] J. Zhang, X. Liu, Y. Xia, Z. Zuo and Y. Wang, "Disturbance observer-based integral sliding-mode control for systems with mismatched disturbance," *IEEE Transactions on Industrial Electronics*, vol. 63, no. 11, pp. 7040-7048, June, 2016.

[80] S. Wen, T. Huang, X. Yu, M. Z. Q. Chen and Z. Zeng, "Aperiodic sampled-data sliding-mode control of fuzzy systems with communication delays via the event-triggered method," *IEEE Transactions on Fuzzy Systems*, vol. 24, no. 5, pp. 1048-1057, November, 2015.

[81] J. Yang, S. Li and X. Yu, "Sliding-mode control for systems with mismatched uncertainties via a disturbance observer," *IEEE Transactions on industrial electronics*, vol. 60, no. 1, pp. 160-169, January, 2013.

[82] E. Bianconi, J. Calvente, R. Giral, E. Mamarelis, G. Petrone, C. A. Ramos-Paja, G. Spagnuolo and M. Vitelli, "A fast current-based MPPT technique employing sliding mode control," *IEEE Transactions on Industrial Electronics*, vol. 60, no. 3, pp. 1168-1178, March, 2013.

[83] H. Wang, Z. Man, W. Shen, Z. Cao, J. Zheng, J. Jin and D. M. Tuan, "Robust control for steer-by-wire systems with partially known dynamics," *IEEE Transactions on Industrial Informatics*, vol. 10, no. 4, pp. 2003-2015, November, 2014.

[84] G. Lai, Z. Liu, Y. Zhang and C. L. P. Chen, "Adaptive fuzzy tracking control of nonlinear systems with asymmetric actuator backlash based on a new

smooth inverse," *IEEE Transactions on Cybernetics*, vol. 46, no. 6, pp. 1250-1262, June, 2015.

[85] X. Zhao, P. Shi and X. Zheng, "Fuzzy adaptive control design and discretization for a class of nonlinear uncertain systems," *IEEE Transactions on Cybernetics*, vol. 46, no. 6, pp. 1476-1483, July, 2015.

[86] J. Baek, M. Jin and S. Han, "A new adaptive sliding-mode control scheme for application to robot manipulators," *IEEE Transactions on Industrial Electronics*, vol. 63, no. 6, pp. 3628-3637, January, 2016.

[87] L. Sun and W. Huo, "Adaptive fuzzy control of spacecraft proximity operations using hierarchical fuzzy systems," *IEEE/ASME Transactions on Mechatronics*, vol. 21, no. 3, pp. 1629-1640, October, 2015.

[88] P. Yadmellat and M. R. Kermani, "Adaptive control of a hysteretic magnetorheological robot actuator," *IEEE/ASME Transactions on Mechatronics*, vol. 21, no. 3, pp. 1336-1344, February, 2016.

[89] H. M. Hasanien, "An adaptive control strategy for low voltage ride through capability enhancement of grid-connected photovoltaic power plants," *IEEE Transactions on Power Systems*, vol. 31, no. 4, pp. 3230-3237, September, 2015.

[90] S. P. Nageshrao, G. A. D. Lopes, D. Jeltsema and R. Babuska, "Port-hamiltonian systems in adaptive and learning control: a survey," *IEEE Transactions on Automatic Control*, vol. 61, no. 5, pp. 1223-1238, July, 2015.

[91] C. Chen, Z. Liu, Y. Zhang and C. L. P. Chen, "Modeling and adaptive compensation of unknown multiple frequency vibrations for the stabilization and control of an active isolation system," *IEEE Transactions on Control Systems Technology*, vol. 24, no. 3, pp. 900-911, August, 2015.

[92] J. L. Fleck, C. G. Cassandras and Y. Geng, "Adaptive quasi-dynamic traffic light control," *IEEE Transactions on Control Systems Technology*, vol. 24, no. 3, pp. 830-842, August, 2015.

[93] S. Dominic, Y. A. W. Shardt, S. X. Ding and H. Luo, "An adaptive, advanced control strategy for KPI-based optimization of industrial processes," *IEEE Transactions on Industrial Electronics*, vol. 63, no. 5, pp. 3252-3260, December, 2015.

[94] Q-Y. Fan and G-H. Yang, "Adaptive fault-tolerant control for affine nonlinear systems based on approximate dynamic programming," *IET Control Theory & Applications*, vol. 10, no. 6, pp. 655-663, March, 2016.

[95] X. Zhang, Q-C. Zhong and W-L. Ming, "Stabilization of cascaded DC/DC converters via adaptive series-virtual-impedance control of the load converter," *IEEE Transactions on Power Electronics*, vol. 31, no. 9, pp. 6057-6063, February, 2016.

[96] D. Zhai, L. An, J. Li and Q. Zhang, "Simplified filtering-based adaptive fuzzy dynamic surface control approach for non-linear strict-feedback systems," *IET Control Theory & Applications* vol. 10, no. 5, pp. 493-503, March, 2016.

[97] D.-Y. Koh, Y. K. Kim, K.-S. Kim and S. Kim, "Bioinspired image stabilization control using the adaptive gain adjustment scheme of vestibulo-ocular

reflex," *IEEE/ASME Transactions on Mechatronics*, vol. 21, no. 2, pp. 922-930, October, 2015.

[98] B. Liu and A. E. Kamel, "V2X-based decentralized cooperated adaptive cruise control in the vicinity of intersections," *IEEE Transactions on Intelligent Transportation Systems*, vol. 17, no. 3, pp. 644-658, November, 2015.

[99] J. Yao, W. Deng and Z. Jiao, "Adaptive control of hydraulic actuators with LuGre model-based friction compensation," *IEEE Transactions on Industrial Electronics*, vol. 62, no. 10, pp. 6469-6477, October, 2015.

[100] S-K. Kim, K-G. Lee and K-B. Lee, "Singularity-free adaptive speed tracking control for uncertain permanent magnet synchronous motor," *IEEE Transactions on Power Electronics*, vol. 31, no. 2, pp. 1692-1701, February, 2016.

[101] Y. Yamaguchi and T. Murakami, "Adaptive control for virtual steering characteristics on electric vehicle using steer-by-wire system," *IEEE Transactions on Industrial Electronics*, vol. 56, no. 5, pp. 1585-1594, May, 2009.

[102] A. E. Cetin, M. A. Adli, D. E. Barkana and H. Kucuk, "Implementation and development of an adaptive steering-control system," *IEEE Transactions on Vehicular Technology*, vol. 59, no. 1, pp. 75-83, January, 2010.

[103] M. J. Jensen, A. M. Tolbert, J. R. Wagner, F. S. Switzer and J. W. Finn, "A customizable automotive steering system with a haptic feedback control strategy for obstacle avoidance notification," *IEEE Transactions on Vehicular Technology*, vol. 60, no. 9, pp. 4208-4216, November, 2011.

[104] K. Ma and M. N. G.-Nejhad, "Adaptive control of flexible active composite manipulators driven by piezoelectric patches and active struts with dead zones," *IEEE Transactions on Control Systems Technology*, vol. 16, no. 5, pp. 897-907, September, 2008.

[105] X.-G. Yan and C. Edwards, "Adaptive sliding-mode-observer-based fault reconstruction for nonlinear systems with parametric uncertainties," *IEEE Transactions on Industrial Electronics*, vol. 55, no. 11, pp. 4029-4036, November, 2008.

[106] Z. Zhu, Y. Xia and M. Fu, "Adaptive sliding mode control for attitude stabilization with actuator saturation," *IEEE Transactions on Industrial Electronics*, vol. 58, no. 10, pp. 4898-4907, October, 2011.

[107] B. Xiao, Q. Hu and Y. Zhang, "Adaptive sliding mode fault tolerant attitude tracking control for flexible spacecraft under actuator saturation," *IEEE Transactions on Control Systems Technology*, vol. 20, no. 6, pp. 1605-1612, November, 2012.

[108] E. D. Engeberg and S. G. Meek, "Adaptive sliding mode control for prosthetic hands to simultaneously prevent slip and minimize deformation of grasped objects," *IEEE/ASME Transactions on Mechatronics*, vol. 18, no. 1, pp. 376-385, February, 2013.

[109] F. F. M. E.-Sousy, "Adaptive dynamic sliding-mode control system using recurrent RBFN for high-performance induction motor servo drive," *IEEE Transactions on Industrial Informatics*, vol. 9, no. 4, pp. 1922-1936, November, 2013.

[110] L. Sun, S. Tong and Y. Liu, "Adaptive backstepping sliding mode H_∞ control of static var compensator," *IEEE Transactions on Control Systems Technology*, vol. 19, no. 5, pp. 1178-1185, September, 2011.

[111] X. Li and C. C. Cheah, "Adaptive neural network control of robot based on a unified objective bound," *IEEE Transactions on Control Systems Technology*, vol. 22, no. 3, pp. 1032-1043, May, 2014.

[112] B. Sencer and E. Shamoto, "Effective torque ripple compensation in feed drive systems based on the adaptive sliding-mode controller," *IEEE/ASME Transactions on Mechatronics*, vol. 19, no. 6, pp. 1764-1772, December, 2014.

[113] S. Yu, X. Yu, B. Shirinzadeh and Z. Man, "Continuous finite-time control for robotic manipulators with terminal sliding mode," *Automatica*, vol. 41, no. 11, pp. 1957-1964, November, 2005.

[114] X. Yu and Z. Man, "Fast terminal sliding-mode control design for nonlinear dynamical systems," *IEEE Transactions on Circuits and System-I: Fundamental Theory and Applications*, vol. 49, no. 2, pp. 261-264, February, 2002.

[115] J. Zheng, H. Wang, Z. Man, J. Jin and M. Fu, "Robust motion control of a linear motor positioner using fast nonsingular terminal sliding mode," *IEEE/ASME Transactions on Mechatronics*, vol. 20, no. 4, pp. 1743-1752, August, 2015.

[116] L. Zhao, Y. Yang, Y. Xia and Z. Liu, "Active disturbance rejection position control for a magnetic rodless pneumatic cylinder," *IEEE Transactions on Industrial Electronics*, vol. 62, no. 9, pp. 5838-5846, September, 2015.

[117] H-L. Xing, J-H. Jeon, K. C. Park and I-K. Oh, "Active disturbance rejection control precise position tracking of ionic polymer-metal composite actuators," *IEEE/ASME Transactions on Mechatronics*, vol. 18, no. 1, pp. 86-95, February, 2013.

[118] J. M.-Valenzuela, C. A.-Avelar, S. A. P.-Guzman and V. Santibanez, "Adaptive neural network control for the trajectory tracking of the furuta pendulum," *IEEE Transactions on Cybernetics*, vol. 46, no. 12, pp. 3439-3452, December, 2016.

[119] Y.-J. Liu, J. Li, S. Tong and C. L. P. Chen, "Neural network control-based adaptive learning design for nonlinear systems with full-state constraints," *IEEE Transactions on Neural Networks and Learning Systems*, vol. 27, no. 7, pp. 1562-1571, July, 2016.

[120] W. He, A. O. David, Z. Yin and C. Sun, "Neural network control of a robotic manipulator with input deadzone and output constraint," *IEEE Transactions on Systems, Man, and Cybernetics: Systems*, vol. 46, no. 6, pp. 759-770, August, 2015.

[121] A. L. Edelen, S. G. Biedron, B. E. Chase, D. Edstrom, S. V. Milton and P. Stabile, "Neural networks for modeling and control of particle accelerators," *IEEE Transactions on Nuclear Science*, vol. 63, no. 2, pp. 878-897, April, 2016.

[122] T. Li, S. Duan, J. Liu, L. Wang and T. Huang, "A spintronic memristor-based neural network with radial basis function for robotic manipulator control

implementation," *IEEE Transactions on Systems, Man, and Cybernetics: Systems*, vol. 46, no. 4, pp. 582-588, April, 2016.

[123] W. He, Y. Chen and Z. Yin, "Adaptive neural network control of an uncertain robot with full-state constraints," *IEEE Transactions on Cybernetics*, vol. 46, no. 3, pp. 620-629, March, 2016.

[124] X. Fu and S. Li, "Control of single-phase grid-connected converters with LCL filters using recurrent neural network and conventional control methods," *IEEE Transactions on Power Electronics*, vol. 31, no. 7, pp. 5354-5364, July, 2016.

[125] T. Wang, H. Gao and J. Qiu, "A combined adaptive neural network and nonlinear model predictive control for multirate networked industrial process control," *IEEE Transactions on Neural Networks and Learning Systems*, vol. 27, no. 2, pp. 416-425, February, 2016.

[126] B. Chen, H. Zhang and C. Lin, "Observer-based adaptive neural network control for nonlinear systems in constrict-feedback form," *IEEE Transactions on Neural Networks and Learning Systems*, vol. 27, no. 1, pp. 89-98, January, 2016.

[127] A. Melingui, O. Lakhal, B. Daachi, J. B. Mbede and R. Merzouki, "Adaptive neural network control of a compact bionic handling arm," *IEEE/ASME Transactions on Mechatronics*, vol. 20, no. 6, pp. 2862-2875, December, 2015.

[128] G. Chen and Y.-D. Song, "Cooperative tracking control of nonlinear multiagent systems using self-structuring neural networks," *IEEE Transactions on*

Neural Networks and Learning Systems, vol. 25, no. 8, pp. 1496-1507, August, 2014.

[129] C. L. P. Chen, G.-X. Wen, Y.-J. Liu and F.-Y. Wang, "Adaptive consensus control for a class of nonlinear multiagent time-delay systems using neural networks," *IEEE Transactions on Neural Networks and Learning Systems*, vol. 25, no. 6, pp. 1217-1226, June, 2014.

[130] S. Arimoto, S. Kawamura, and F. Miyazaki, "Bettering operation of dynamic systems by learning: a new control theory for servomechanism or mechatronic systems," in *Proceedings of the IEEE Conference on Decision and Control*, pp. 1064-1069, December, 1984.

[131] T. Kuc, K. Nam, and J. S. Lee, "An iterative learning control of robot manipulators," *IEEE Transactions on Automatic Control*, vol. 7, no. 6, pp. 835-841, December, 1991.

[132] D.-I. Kim and S. Kim, "An iterative learning control method with application for cnc machine tools," *IEEE Transactions on Industry Applications*, vol. 32, no. 1, pp. 66-72, January, 1996.

[133] A. D. Barton, P. L. Lewin and D. J. Brown, "Practical implementation of a real-time iterative learning position controller," *International Journal of Control*, vol. 73, no. 10, pp. 992-999, November, 2000.

[134] N. Liu and A. Alleyne, "Iterative learning identification for an automated off-highway vehicle," in *Proceedings of the 2011 American Control Conference*, pp. 4299-4304, July, 2011.

[135] C. Mi, H. Lin and Y. Zhang, "Iterative learning control of antilock braking of electric and hybrid vehicles," *IEEE Transactions on Vehicular Technology*, vol. 54, no. 2, pp. 486-494, March, 2005.

[136] Y. Fujimoto, "Robust servo-system based on two-degree-of-freedom control with sliding mode," *IEEE Transactions on Industrial Electronics*, vol. 42, no. 3, pp. 272-280, June, 1995.

[137] M. Gopal, *Control Systems: Principles and Design*. New Delhi, India: McGraw-Hill, 2002.

[138] J. E. Slotine and W. Li, *Applied Nonlinear Control*. Englewood Cliffs, NJ, USA: Prentice-Hall, 1991.

[139] K. Ma and M. N. G.-Nejhad, "Adaptive control of flexible active composite manipulators driven by piezoelectric patches and active struts with dead zones," *IEEE Transactions on Control Systems Technology*, vol. 16, no. 5, pp. 897-907, September, 2008.

[140] M. Hojati and S. Gazor, "Hybrid adaptive fuzzy identification and control of nonlinear systems," *IEEE Transactions on Fuzzy Systems*, vol. 10, no. 2, pp. 198-210, April, 2002.

[141] A. Fazeli, M. Zeinali and A. Khajepour, "Application of adaptive sliding mode control for regenerative braking torque control," *IEEE/ASME Transactions on Mechatronics*, vol. 17, no. 4, pp. 745-755, August, 2012.

[142] S. Huang, K. K. Tan and T. H. Lee, "Adaptive sliding-mode control of piezoelectric actuators," *IEEE Transactions on Industrial Electronics*, vol. 56, no. 9, pp. 3514-3522, September, 2009.

[143] B. Sencer and E. Shamoto, "Effective torque ripple compensation in feed drive systems based on the adaptive sliding-mode controller," *IEEE/ASME Transactions on Mechatronics*, vol. 19, no. 6, pp. 1764-1772, December, 2014.

[144] V. Utkin, *Sliding Mode Control in Electro-Mechanical Systems*. New York, NY, USA: Taylor & Francis, 2009.

[145] C. Edwards and S. Spurgeon, *Sliding Mode Control: Theory and Applications*. New York, NY, USA: Taylor & Francis, 1998.

[146] K. Zhou and J. C. Doyle, *Essentials of Robust Control*, New Jersey, USA: Prentice Hall, 1999.

[147] A. Al-Ghanimi, J. Zheng and Z. Man, "Robust and fast non-singular terminal sliding mode control for piezoelectric actuators," *IET Control Theory & Applications*, vol. 9, no. 18, pp. 2678-2687, December, 2015.

[148] V. T. Haimo, "Finite time controllers," *SIAM J. Control Optim.*, vol. 24, no. 4, pp. 760-770, Jul. 1986.

[149] Y. Feng, X. Yu and Z. Man, "Non-singular terminal sliding control of rigid manipulators," *Automatica*, vol. 38, no. 12, pp. 2159-2167, December, 2002.

[150] Y. Hong, J. Huang, Y. Xu, "On an output finite-time stabilization problem," *IEEE Transactions on Automatic Control*, vol. 46, no. 2, pp. 305-309, February, 2001.

[151] Z. Sun, J. Zheng, Z. Man and H. Wang, "Robust control of a vehicle steer-by-wire system using adaptive sliding mode," *IEEE Transactions on Industrial Electronics*, vol. 63, no. 4, pp. 2251-2262, April, 2016.

[152] W. Tan and C. Fu, "Linear active disturbance-rejection control: analysis and tuning via IMC," *IEEE Transactions on Industrial Electronics*, vol. 63, no. 4, pp. 2350-2359, April, 2016.

[153] X. Chang, Y. Li, W. Zhang, N. Wang and W. Xue, "Active disturbance rejection control for a flywheel energy storage system," *IEEE Transactions on Industrial Electronics*, vol. 62, no. 2, pp. 991-1001, February, 2015.

[154] B. Du, S. Wu, S. Han and S. Cui, "Application of linear active disturbance rejection controller for sensorless control of internal permanent-magnet synchronous motor," *IEEE Transactions on Industrial Electronics*, vol. 63, no. 5, pp. 3019-3027, May, 2016.

[155] L. Zhao, Y. Yang, Y. Xia and Z. Liu, "Active disturbance rejection position control for a magnetic rodless pneumatic cylinder," *IEEE Transactions on Industrial Electronics*, vol. 62, no. 9, pp. 5838-5846, September, 2015.

[156] Z. Gao, "Active disturbance rejection control: a paradigm shift in feedback control system design," in *Proceedings of the 2016 American Control Conference*, June, 2016.

[157] B. Bukkems, D. Kostic, B. d. Jager and M. Steinbuch, "Learning-based identification and iterative learning control of direct-drive robots," *IEEE Transactions on Control Systems Technology*, vol. 13, no. 4, pp. 537-549, July, 2005.

[158] Y. Wang, E. Dassau and F. J. Doyle, "Closed-loop control of artificial pancreatic β-cell in type 1 diabetes mellitus using model predictive iterative learning control," *IEEE Transactions on Biomedical Engineering*, vol. 57, no. 2, pp. 211-219, February, 2010.

[159] M.-B. Radac, R.-E. Precup and E. M. Petriu, "Model-free primitive-based iterative learning control approach to trajectory tracking of MIMO systems with experimental validation," *IEEE Transactions on Neural Networks and Learning Systems*, vol. 26, no. 11, pp. 2925-2938, November, 2015.

[160] J.-X. Xu, D. Huang, V. Venkataramanan and H. T. C. Tuong, "Extreme precise motion tracking of piezoelectric positioning stage using sampled-data iterative learning control," *IEEE Transactions on Control Systems Technology*, vol. 21, no. 4, pp. 1432-1439, July, 2013.

[161] K. Abidi and J.-X. Xu, "Iterative learning control for sampled-data systems: from theory to practice," *IEEE Transactions on Industrial Electronics*, vol. 58, no. 7, pp. 3002-3015, July, 2011.

[162] M. Norrlof and S. Gunnarsson, "Time and frequency domain convergence properties in iterative learning control," *International Journal of Control*, vol. 75, no. 14, pp. 1114-1126, September, 2002.

[163] T. Acarman and U. Özgüner, "Rollover prevention for heavy trucks using frequency shaped sliding mode control," *Vehicle System Dynamics*, vol. 44, no. 10, pp. 737-762, 2006.

[164] B. Chen and H. Peng, "Differential-braking-based rollover prevention for sport utility vehicle with human-in-the-loop evaluations," *Vehicle System Dynamics*, vol. 36, pp. 359-389, 2001.

[165] A. Visioli, *Practical PID Control*, Brescia, Italy: Springer, 2006.

[166] B. Chen and H. Peng, "Rollover warning for articulated heavy vehicles based on a time-to-rollover metric," *Journal of Dynamic Systems, Measurement, and Control*, vol. 127, no. 3, pp. 406-414, October, 2004.

[167] W. Xiang, P. C. Richardson, C. Zhao and S. Mohammad, "Automobile brake-by-wire control system design and analysis," *IEEE Transactions on Vehicular Technology*, vol. 57, no. 1, pp. 138-145, January, 2008.

Author's Publications

The research work related to this thesis resulted in the following publications

Journal papers

[1] Z. Sun, J. Zheng, Z. Man and H. Wang, "Robust control of a vehicle steer-by-wire system using adaptive sliding mode," *IEEE Transactions on Industrial Electronics*, vol. 63, no. 4, pp. 2251-2262, April, 2016.

[2] Z. Sun, J. Zheng, H. Wang and Z. Man, "Adaptive fast non-singular terminal sliding mode control for a vehicle steer-by-wire system," *IET Control Theory & Applications*, vol. 11, no. 8, pp. 1245-1254, May, 2017.

[3] Z. Sun, J. Zheng, Z. Man and H. Wang, "Sliding mode-based active disturbance rejection control for vehicle steer-by-wire systems," *IET Cyber-Physical Systems: Theory & Applications*, major revision.

Conference papers

[1] Z. Sun, J. Zheng, Z. Man and J. Jin, "Discrete-time iterative learning control for vehicle steer-by-wire systems," in *Proceedings of IEEE Conference on Industrial Electronics and Applications*, pp. 462-467, June, 2014.

[2] Z. Sun, J. Zheng and Z. Man, "Adaptive sliding mode control for a vehicle steer-by-wire system," in *Proceedings of IEEE Conference on Control Science and System Engineering*, pp. 77-81, July, 2016.

[3] Z. Sun, J. Zheng and Z. Man, "Advanced control design for a vehicle steer-by-wire system by using adaptive fast nonsingular terminal sliding mode," in

Proceedings of IEEE Conference on Advanced Mechatronic Systems, pp. 212-217, December, 2016.